

Added Value and regional effects in the
multidecadal trends of a very high-
resolution regional climate long-term
model simulation at the coasts of
Northern Germany

Dissertation zur Erlangung des Doktorgrades
an der Fakultät für Mathematik, Informatik und
Naturwissenschaften
im Fachbereich Geowissenschaften der Universität
Hamburg

vorgelegt von
Benjamin Schaaf
aus Bobingen

Hamburg, März 2018

Tag der Disputation: 19.06.2018

Gutachter: Prof. Dr. Dr. h.c. Hans von Storch

Dr. Frauke Feser

Abstract

Wind speed is a very important atmospheric variable, because it may cause storm surges, damages and high economic losses. Therefore, particularly for coastal areas and preventive protection measures, it is essential to learn more about changes in storminess, wherefore a long, homogeneous meteorological time series is needed. A consistent, gridded data set was computed with a regional climate model with a very high convection-permitting resolution. This is one of the very first atmospheric model simulations with such high resolution covering several decades.

This thesis aims to extend the knowledge of the added value and regional effects in the multidecadal trends with the focus on wind speed in a very high-resolution hindcast. Firstly, the effect of spectral nudging on the simulation with a small model domain size of about 700 x 500 km was examined. Subsequently it was investigated if the high-resolution regional climate model adds value in terms of high wind speeds in comparison to the driving regional climate model data set with a coarser grid distance. Furthermore, the question is answered whether the variability and long-term changes of different variables have any crucial regional effects, which justify such expensive high-resolution and long-term simulations.

In the first part of the thesis, it is shown that spectral nudging has only little effect on the simulation when the model region is relatively small and that it is not necessary for regional climate model domain sizes of only several hundred kilometers in diameter and over flat and homogeneous terrain.

Concerning the added value of the high-resolution simulation, it was found that the convection-permitting resolution simulation has, in most cases, a better agreement with observational data than the coarse grid resolution simulation. The added value is more distinct for the synoptic comparisons than for the multiple storm studies analyzed with statistical measures like the Brier Skill Score. This is mainly a result of the convection, which was not

parameterized in this simulation. The high-resolution model simulation is also able to capture small-scale features, which indicates an added value for atmospheric phenomena such as convective precipitation or post-frontal cloud cover. However, the added value strongly depends on region, time period and variable.

Findings related to the long term changes show the most clear and significant positive trends in temperature and wind speed. Spatial structures in the trends are weak. The strongest regional details were found in the precipitation and 10 m wind speed like the city effects with lower trends in the mean wind.

Zusammenfassung

Die Windgeschwindigkeit ist eine sehr wichtige atmosphärische Variable, weil hohe Windgeschwindigkeiten Sturmfluten, Schäden und hohe wirtschaftliche Verluste verursachen können. Gerade für Schutzmaßnahmen der Küstengebiete ist es wichtig, mehr über Veränderungen in der Sturmaktivität zu erfahren. Dafür wird aber eine lange, homogene Zeitreihe meteorologischer Variablen benötigt. Ein konsistenter, gegitterter Datensatz wurde mit einem regionalen Klimamodell mit einer sehr hohen Auflösung berechnet, bei der es möglich ist konvektive Prozesse explizit zu simulieren. Dies ist eine der ersten atmosphärischen Modellsimulationen mit einer solch hohen Auflösung, die mehrere Jahrzehnte umfasst.

Diese Arbeit zielt darauf ab, das Wissen über den Mehrwert und multidekadische Trends mit dem Fokus auf Windgeschwindigkeit in einer sehr hochauflösenden Simulation der vergangenen sieben Dekaden zu erweitern. Zunächst wurde der Effekt des spektralen Nudging auf die Simulation mit einer kleinen Modelldomänengröße von etwa 700 x 500 km untersucht. Anschließend wurde untersucht, ob das hochauflösende regionale Klimamodell im Vergleich zum regionalen Klimamodell mit einem größeren Gitterabstand, das zum Antrieb verwendet wurde, einen Mehrwert in Bezug auf hohe Windgeschwindigkeiten liefert. Darüber hinaus wird die Frage beantwortet, ob die Variabilität und die langfristigen Veränderungen verschiedener meteorologischer Variablen entscheidende regionale Auswirkungen haben.

Im ersten Teil der Arbeit wird gezeigt, dass das spektrale Nudging nur wenig Einfluss auf die Simulation hat, wenn die Modellregion relativ klein ist und dass es für regionale Klimamodellgebietsgrößen von wenigen hundert Kilometern Ausdehnung über flachem und homogenem Gelände nicht benötigt wird.

In Bezug auf den Mehrwert der hochauflösenden Simulation wurde festgestellt, dass die konvektionsauflösende Simulation in den meisten Fällen

eine bessere Übereinstimmung mit Beobachtungsdaten aufweist als die Simulation mit größerem Abstand der Gitterpunkte. Der Mehrwert ist für die synoptischen Vergleiche deutlicher als für die Sturmstudien, die mit statistischen Maßen wie dem Brier Skill Score analysiert wurden. Dies ist hauptsächlich auf Grund der Konvektion, die in dieser Simulation nicht parametrisiert wurde, sondern explizit berechnet wird. Die hochauflösende Modellsimulation ist auch in der Lage, kleinskalige Phänomene zu erfassen, was einen Mehrwert für atmosphärische Prozesse wie Konvektionsniederschlag oder postfrontale Bewölkung ist. Der Mehrwert hängt jedoch stark von der Region, dem Zeitraum und der Variable ab.

Die langfristigen Veränderungen zeigen die deutlichsten und signifikantesten positiven Trends bei der Temperatur und Windgeschwindigkeit. Räumliche Strukturen in den Trends sind schwach. Die stärksten regionalen Details wurden im Niederschlag und in der 10 m Windgeschwindigkeit gefunden, wie beispielsweise der Stadteffekt, aus dem niedrigere Trends im Mittelwind resultieren.

Contents

Abstract	i
Zusammenfassung	iii
Contents	v
1 Introduction	1
1.1 Motivation	1
1.2 Thesis objectives	4
1.3 Thesis structure	5
2 Data sets	5
2.1 Regional Climate Model COSMO-CLM	5
2.1.1 Model description	5
2.1.2 Parameterizations	7
2.1.3 Spectral nudging	8
2.2 Reanalysis data	9
2.3 CoastDat II data	10
2.4 Observation data	11
2.4.1 Station measurements of the German weather service	11
2.4.2 Weather mast Hamburg	11
2.4.3 Satellite data	12
3 Sensitivity studies	13
3.1 Importance of the Wadden Sea	13
3.2 Influence of domain extension	16
3.3 Final model setup	20
4 Spectral nudging in the small regional model domain	21
4.1 Introduction	21
4.2 Experimental setup	22

4.2.1	Simulations	22
4.2.2	Evaluation strategy	24
4.3	Results	25
4.3.1	Ensemble-variability of the SN and NN runs.....	25
4.3.2	Differences between SN and NN simulations	26
4.3.3	Comparison with observations.....	31
4.4	Summary and discussion.....	32
5	Added value	34
5.1	Introduction.....	34
5.2	Model configuration, data, and methods	37
5.2.1	Model configuration	37
5.2.2	Data.....	39
5.2.3	Methods of added value determination	40
5.3	Case study Christian	43
5.3.1	Storm description and development	43
5.3.2	Added value of the high resolution simulation	44
5.3.3	Conclusion	50
5.4	Added value in multiple storm analysis	51
5.4.1	Determination of added value.....	51
5.4.2	Impact of the roughness length.....	57
5.4.3	Conclusion	58
6	Long-term analysis.....	60
6.1	Introduction.....	60
6.2	Model configuration and methods	63
6.3	Comparison with QuikSCAT data.....	64
6.4	Trend analysis over Northern Germany 1948-2014	66
6.4.1	Annual means	67

6.4.2	Extreme events.....	73
6.5	Summary and discussion	81
7	Summary and conclusions.....	83
	Bibliography	88
	List of Figures	103
	List of Tables.....	110
	List of publications.....	111
	Acknowledgements	112
	Eidesstattliche Versicherung.....	113

1 Introduction

1.1 Motivation

Storms are globally the most frequent natural disasters (IPCC, 2013; Munich RE). Severe storms generate storm surges, flooding, uprooted trees or damage to buildings with high economic losses. Therefore, they have a large impact on coastal populations (Klawe and Ulbrich, 2003; Pinto et al., 2007; Neumayer and Barthel, 2011). For the North Sea coast, Northern Germany and the city of Hamburg, which is located in close proximity to the coast, winter storms are of general interest since they typically represent the strongest storms in this region. Feser et al. (2015) reviewed a large number of different studies of winter storm activity over the North Atlantic and Northwestern Europe. They found that winter storm activity shows large decadal variability (including a decrease since the 1960s and a subsequent increase for more recent decades) which depends a lot on the analyzed region and time period. However, generally no systematic long-term trends were apparent when looking at the past 100 to 150 years using storm proxies (Alexandersson et al., 2000; Krueger and von Storch, 2011). There are also indications based on long climate model simulations covering the last millennium that the storm track variability in the North Atlantic region is mainly controlled by internal climate variations (Fischer-Bruns et al., 2005; Xia et al., 2016).

Wind measurements, which are often used to derive storm activity, in many cases suffer from inconsistencies, arising from changes in observation methods, surrounding buildings or trees, or station location. Reanalysis data sets take into account such inhomogeneities of observation data and convert measurements into relatively consistent gridded data sets, which may still be influenced by increasing station density over time and, e.g., the introduction of satellite data with equal grid spacing and time intervals. These have a relatively low resolution, ranging between about 200 km for reanalysis of the

last more than six decades, and 50 km mesh size for the more recent reanalysis, which usually start in 1979 after the introduction of satellite data. Weisse et al. (2005, 2009, 2014) analyzed the long-term change of storminess in Europe by dynamically downscaling reanalysis data with regional climate models (RCMs). The quality of the results of RCM simulations depends on the domain size, location and on the quality of the forcing data (Rummukainen, 2010). Kitoh et al. (2016) review a number of studies, which used an atmospheric general circulation model (AGCM) with 20 km grid distance to simulate future changes in tropical cyclones, extreme precipitation and associated wind systems. In a subsequent step, the simulations were dynamically downscaled with an RCM to a grid of 5 km to analyze local extreme rainfall events or heat waves from foehn and their future changes. A future increase in strong precipitation was found over Japan. Oouchi et al. (2006) used the same 20 km AGCM to investigate future tropical cyclone (TC) changes and report a decrease in TC numbers for future scenarios while the number of strong TCs becomes larger. Barcikowska et al. (2017) investigated the changes in TCs using the RCM Cosmo-CLM, which is the model used for this thesis, and found a strong increase of intense tropical cyclone activity. The usage of RCMs forced by reanalysis data at its lateral boundaries can also help to minimize potential inhomogeneities in reanalysis and achieve higher resolutions. This approach was also applied in the current study, by dynamically downscaling a RCM simulation forced by reanalysis data to a convective-permitting resolution.

High-resolution RCMs are usually nested into a coarser RCM simulation, which is driven either by general circulation models or by reanalysis data. Reanalysis data are also based on a comprehensive weather forecast model assimilating available observational data. Therefore, the reanalysis is no real observation but over regions with high station density, the similarity between reanalysis and observations is usually very large. These high-resolution RCMs are expected to show an added value over their large-scale forcing data at the regional scale. This may be a more realistic simulation of convection or of other meteorological small-scale effects like wind flow dominated by

topography (Cholette et al., 2015). RCM dynamical downscaling method is closer to observations than very-fine-resolution global climate model simulations in terms of regional precipitation simulation (Guo and Wang, 2016). The horizontal grid distance of a convection-permitting simulation should be smaller than 4 km to resolve explicitly convective processes like precipitation or convective gusts, so that parametrizations for subgrid processes are no longer necessary (Prein et al. 2015). Besides increasing the horizontal resolution, it is also important to consider the vertical resolution. Some issues could then be better simulated in terms of troposphere-stratosphere connection. Comprehensive studies of the current state of high-resolution climate models and their potential added value were carried out by Parker et al. (2015) and Prein et al. (2015). They found that convective-permitting RCMs show improvements for deep convection, mountain regions and extreme events. Most studies using convective-permitting RCMs currently concentrate on the added value of precipitation, as this variable is most promising with regard to providing a benefit at this high resolution. For instance, Prein et al. (2013) analyzed the added value of an ensemble of convective-permitting seasonal simulations in comparison to coarser grid RCM simulations over the European Alps for temperature, precipitation, relative humidity and radiation. They reported an added value for summertime precipitation diurnal cycles, extreme precipitation intensities, and a more accurate distribution of rain. Chan et al. (2014) compared a 1.5 km RCM to a 12 km simulation for the southern United Kingdom from 1990 to 2008. They presented added value for precipitation extremes for the 1.5 km RCM simulation, especially for summer. They also showed that the high-resolution simulation could also realistically simulate the dynamical structure and life cycle of convective storms (Chan et al., 2014). Leutwyler et al. (2017) found substantial improvements in terms of the diurnal cycles of precipitation for a 2 km simulation over Europe in a 10 years simulation. Also the soil type classification has an influence on the realistic simulation of precipitation (Anders and Rockel, 2009). The bias in extreme precipitation statistics can be reduced with a nested Cosmo-CLM simulation with 12 km resolution compared to a 50 km resolution simulation over West Africa

(Dieng et al., 2017). Generally, comparing model precipitation with observed precipitation always possess the problem that the observed meteorological station typically represents other quantitative and spatial means given to the simulated grid point co-located with the station.

For hindcast simulations, the RCM tends to deviate from the observed state. The meteorological statistics over a long time period would not be influenced too much, but individual storm and extreme events cannot be reproduced if the internal variability exists. Therefore, the spectral nudging technique was introduced (von Storch et al., 2000) to keep large spatial scales of the RCM close to the driving data (see Chapter 2.1.3). Park and Hwang (2017) applied spectral nudging with the RCM WRF over hilly terrain in South Korea and found more realistic air temperature, precipitation, and surface fluxes than without spectral nudging. Ma et al. (2016) investigated the performance of spectral nudging over China and summarized that the bias of conventional meteorological elements near the surface decreases with applying spectral nudging.

1.2 Thesis objectives

Based on the introduction presented in the preceding Chapter on storminess over Northwestern Europe and the downscaling of regional climate models the following research questions for this PhD thesis are formulated:

- Does spectral nudging have an effect on dynamical downscaling applied in geographically comparatively small regional climate model domains (such as the domain size of 500 km x 700 km used for this study)?
- Is there added value of very highly resolved convection-permitting regional climate model simulations for simulating storms over the German Bight and Northern Germany?
- Are there regional effects in the multidecadal trends of annual mean meteorological values and extreme events over Northern Germany and the German Bight?

1.3 Thesis structure

The thesis contains three main chapters (four to six), which answer the main research questions. In Chapter 2 an overview of the regional climate model CCLM is given and the data sets used for the investigations are introduced. Subsequently some sensitivity studies, which have been done to determine the optimal settings for the CCLM simulations, are pointed out in Chapter 3. In Chapter 4, the effect of spectral nudging and the necessity in small regional model domains was investigated. Chapter 5 deals with the determination of added value of the very high resolution model simulation. An evaluation of the long-term trends and regional effects over the last about seven decades is conducted in Chapter 6. Finally, a summary of the main findings and the answers of the research questions are presented in Chapter 6.

2 Data sets

2.1 Regional Climate Model COSMO-CLM

2.1.1 Model description

For the hindcast simulations, which were computed for this thesis, the non-hydrostatic limited-area atmospheric model COSMO-CLM (version 5.0) (Steppeler et al., 2003; Rockel et al., 2008) (CCLM), which is the climate version of the regional weather prediction model COSMO of the German weather service (DWD), is employed.

CCLM uses an Arakawa C-grid for the horizontal discretization and a Lorenz grid for the vertical discretization. Scalars are defined in the center of the grid box. For the vertical, a generalized terrain-following height coordinate is used with grid stretching in the vertical. The distance between two height levels increases with increasing height. This results in a better vertical resolution in

the boundary layer than in the free troposphere (Schaettler et al., 2008). A rotated geographical latitude-longitude coordinate system is used (Roeckner, 2003). The reason for this is that for conventional latitude-longitude grids a convergence of the meridians to the poles takes place, which means the grid distance becomes smaller (in km) using a grid distance in longitude. Consequently, the horizontal resolution varies. This feature becomes stronger the closer one gets to the poles. The rotated coordinate system takes into account these problems. The North Pole is rotated, so that the equator runs right through the middle of the model domain, which leads to less grid distortion.

The meteorological fields of the initial and boundary conditions for CCLM are provided by global climate model simulations or reanalyzes data sets. For high resolution regional climate model simulations often an intermediate nesting step is necessary, when spatial resolutions are degraded by more than a factor of 12 between the forcing data and the simulation result (Laprise et al., 2012). For this double nesting, a simulation with coarser horizontal resolutions is needed as forcing data. At the lateral boundaries in a sponge zone, the prognostic variables are adopted to the driving data, using a conventional sponge zone constraint after Davies (1976). At the top of the model domain, Rayleigh damping is applied. At the lower boundary, CCLM needs constant information from external datasets. These are e.g. orography, land use and land cover characteristics, soil type and roughness length. Over sea points, the roughness length is not an external parameter and not temporally constant but a variable computed on the basis of the Charnock-formula, using the wind speed of the last time step. Over ice-covered sea points, the roughness length is assigned a constant value of 0.001 m. Over land, the roughness length is constant in time and is composed of two parts: One part is derived from the variance of the subscale orography (hilly terrain) and the other part is dependent on the type of vegetation and buildings. The information about sea surface temperature is provided to CCLM by interpolating values of the forcing data. The forcing data of the lateral boundaries and over the ocean is updated every 6 hours throughout the

entire simulation period and interpolated in the times in between according to the modelling time step.

2.1.2 Parameterizations

If processes cannot be resolved by the model's grid size applied, but are important for the results of the model, the effects of these processes have to be covered by special approaches. This process is called parameterization. A parameterization is a simplification of the real process but is necessary for coarser models to mimic important processes. The added value of higher resolved simulations is avoiding those parameterizations by explicitly simulating the processes. A variety of physical processes are taken into account by parameterization schemes in the CCLM model (Schulz and Schaettler, 2009; Doms et al., 2011). The most important and these with the most computing time are radiation, clouds, precipitation, turbulent fluxes schemes and the soil model.

For this work, the question arises, which convection parameterization is most suitable? The model implies two convection types. One convection type is deep convection, which describes thermally driven turbulent mixing with vertical motion throughout large parts of the troposphere (above the 500 hPa level) producing precipitation. The other type is shallow convection with limited vertical mixing such as cumulus clouds, which does not generate precipitation. The shallow convection scheme is a simplified Tiedtke scheme (Tiedtke, 1989). It incorporates a number of simplified assumptions, e.g., on the convection vertical extent, and neglects dynamic entrainment, meaning that no precipitation is produced by the parameterization. Up to a grid distance of about 3 km, cumulus convection is a subscale process, which cannot be solved by the grid and therefore cannot be explicitly simulated. Therefore, the full Tiedtke scheme should be used for simulations with a grid distance of more than 3 km. Below this 3 km grid size, the shallow Tiedtke convection scheme parameterization is recommended, because the deep convection can be solved and calculated explicitly, without using the parameterization, which is prone for errors and precipitation underestimations.

For wind gusts, the standard parameterization of the DWD is used for this work. The wind gusts were derived from the wind speed in the lowest model layer and the friction velocity, which is parameterized after Schulz and Heise (2003) and Schulz (2008). This parametrization is based on a two-component approach that contains turbulent and convective gusts.

2.1.3 Spectral nudging

Spectral nudging was developed by Waldron et al. (1996) and was later extended by von Storch et al. (2000) who used it in climate simulations. Spectral nudging keeps large weather systems (about 100 – 1000 km, it depends on the extent of the model domain) close to the large-scale atmospheric conditions simulated by the forcing data, not only at the lateral boundaries but also within the entire model domain. Smaller spatial scales were not nudged; these were solely computed by the regional climate model. Only certain variables (usually the horizontal wind components) were spectrally nudged towards the reanalysis. The influence of spectral nudging increases exponentially from a pressure level of 850 hPa to the top of the model domain. Spectral nudging is strongest in the uppermost levels. Below this pressure level, no spectral nudging is applied, so that small weather phenomena, which often occur close to the surface, are not affected and the climate model can develop its own dynamics.

The RCM solution in grid-point space is transformed with a Fourier transformation into the spectral space. The same is done for the forcing data set. Through this transformation, the Fourier coefficients are determined. The spectral nudging term $\eta_{j,k}$ is then added to the RCM model equations for a certain range of wave numbers while the other wave numbers are left unchanged. The added nudging term depends on the difference of spatial scales between the simulation and forcing data:

$$\Psi(\lambda, \varphi, t) = \sum_{j=-J_a, k=-K_a}^{J_a, K_a} (\alpha_{j,k}^m(t) + \eta_{j,k} [\alpha_{j,k}^a(t) - \alpha_{j,k}^m(t)]) \exp\left(\frac{ij\lambda}{L_\lambda}\right) \exp\left(\frac{ik\varphi}{L_\varphi}\right)$$

with zonal coordinates λ , zonal wavenumbers j and zonal extension of the area L_λ . Meridional coordinates are denoted by φ , meridional wavenumbers by k , and the meridional extension by L_φ . For the forcing data, the number of zonal and meridional wavenumbers is J_a and K_a and $\alpha_{j,k}^a$ are the Fourier coefficients. The Fourier coefficients for the RCM are labeled $\alpha_{j,k}^m$. The zonal and meridional wavenumbers can be selected in the CCLM model. For $\eta_{j,k} = 0$ no spectral nudging takes place and for $\eta_{j,k} = 1$ the value of the respective sinusoidal component function of the RCM is identical to that of the reanalysis. The nudging coefficient increases with height to leave more room for the RCM at lower levels, where regional features become important, and is defined as:

$$\eta(p) = \begin{cases} \alpha \left(1 - p/850hPa\right)^2 & \text{for } p < 850hPa \\ 0 & \text{for } p > 850hPa \end{cases}$$

The coefficient α can also be set in the CCLM model to regulate the strength of the spectral nudging. After the addition of the nudging term, the RCM results are transformed back from spectral space to grid point space. Spectral nudging is relatively expensive if it is used every time step and increases the computing time. If spectral nudging is used every third time step, the computing time increases by about 15% in comparison to a simulation without spectral nudging.

2.2 Reanalysis data

The meteorological reanalysis method assimilates different historical meteorological observational data over an extended period into a weather model. This is used to produce to produce a homogeneous, gridded meteorological data set. Observations often suffer from inconsistencies, which arise from changes in observation methods, changing in the surrounding buildings or trees, or station location movements. Reanalysis data sets take into account such inhomogeneities of observation data and convert measurements into relatively consistent gridded data sets with equal grid spacing and time intervals. These have a relatively low resolution,

ranging between about 200 (for reanalysis of the last more than 6 decades) and 50 km mesh size (for the more recent reanalysis, which usually starts in 1979 after the introduction of satellite data). The homogeneity of the reanalysis data sets may still be influenced by increasing station density over time and, e.g., the introduction of satellite data in the late 1970s. The NCEP/NCAR Reanalysis 1 project is using a state-of-the-art analysis system to perform data assimilation using past data from 1948 to the present (Kalnay et al., 1996). A large subset of this data is available four times daily at 0Z, 6Z, 12Z, and 18Z. The NCEP1 reanalysis data set has a grid distance of 1.875° (about 210 km) and was used in this work as forcing data for the simulations. Recent reanalysis sets as ERA-Interim (Dee et al., 2011), starting in 1979, tend to be more homogeneous, but one focus of this work should be the long term analysis, where NCEP1 has a better coverage.

2.3 CoastDat II data

The coastDat II data set is an atmospheric re-analysis for Europe for the last 67 years, from 1948 to 2014 (Geyer and Rockel, 2013; Geyer, 2014). For the coastDat II re-analysis, NCEP/NCAR global re-analysis with a grid distance of 1.875° (Kalnay et al., 1996) was dynamically downscaled using the version 4.8 of the same, albeit hydrostatic regional CCLM model to a grid distance of 0.22 degrees (~ 24 km). Spectral nudging was applied for the horizontal wind components (U, V), beginning at a height of 850 hPa with exponentially increasing strength towards higher layers. Below 850 hPa, no spectral nudging is applied so that small weather phenomena, which often occur close to the surface, are not affected. The domain has 234×228 grid points, 40 layers up to 27.2 km height in the vertical, 10 soil levels down to 11.5 m depth, a rotated pole at 170.0°W and 35.0°N , and a time step of 150 seconds.

This data set was used as well for comparisons with other model simulations with higher resolution as forcing data for these high-resolution simulations.

2.4 Observation data

For comparison with the simulated model output data, a large number of observation data are used, which are described in the following section.

2.4.1 Station measurements of the German weather service

In this thesis comparisons and validations of different meteorological variables with station data were performed. Therefore, observation data from 115 observation stations of the German Weather Service¹ located in the model domain, which will be used for the studies and explained in Chapter 3.3, are used. They provide hourly data of wind speed and wind direction at a height of 10 m, precipitation, sea level pressure and total cloud cover and were compared to model data. The relocation of a station is treated as a new station. The strong influence of the environment on wind measurements leads to large inconsistencies even if the station is only moved several meters. A distance-weighted average of the four nearest neighbor grid point values was used for each model value, which means that not only the value of the grid box, which includes a certain station, is used, but also the surrounding grid boxes are considered.

2.4.2 Weather mast Hamburg

Additionally to the DWD stations, comparisons with observation data from the Wettermast (weather mast, Lange, 2014) weather station in Hamburg in Northern Germany was used. The weather mast is located in a suburb of Hamburg, since 1967 and is operated by the meteorological Institute of the University of Hamburg and the Max Planck Institute for Meteorology in Hamburg. The geographic coordinates are 53° 31' 09.0" N and 10° 06' 10.3" E. The mast at a height of 300 m measures the wind speed, wind direction, air temperature and humidity at its six platforms at height levels 50, 70, 110, 175, 250, and 280 m. On each platform, a south-oriented arm holds the measuring instruments. Additionally there is a separate 10 m mast, which is

¹ WebWerdis (<http://www.dwd.de/webwerdis>)

equipped with the same instruments in 10 m height as the 300 m mast at every height level. At a height of 2 m temperature and humidity is measured, too.

2.4.3 Satellite data

For visual comparison with model data, especially for cloud cover, satellite data are used which were taken from NOAA and METEOSAT². They are geostationary meteorological satellites, equipped with radiometers, which measure in the visible and infrared spectral channel. They provide pictures of the cloud cover every 30 minutes, so that continuous data are available.

Another satellite, which is used for model data comparisons, is QuikSCAT. It is a polar-orbiting satellite of the NASA, which means there is not continuous and gapless data coverage. The data product used in this work is the latest version 3 of the QuikSCAT Level 2B wind data (QuikSCAT L2V3). The wind speed and direction is measured over the ocean and is calculated based on the roughness of the sea. For this reason, only data over open water areas at a distance of at least 15 km from the coast and not over ice are available. In addition, no measurements below 3 m/s and above 25 m/s are considered, because of the limited quality and increased error rate during low and extreme wind speed situations. The satellite was launched in June 1999 and was operated until November 2009. Therefore, there are 10 years of wind data available with a spatial resolution of 12.5 km, which is the resolution provided by the NASA. Because the orbit surrounding time is 100 minutes and the track width of the measurements is 1800 km, there is ideally one overflight of the satellite per day at one grid point. The time resolution is lower compared to other measurement data sets, but it is the only possibility for comprehensive wind field measurements over the sea.

² NOAA / METEOSAT, Satellite data. <http://imkhp2.physik.uni-karlsruhe.de/~muehr/archive.html>

3 Sensitivity studies

In this section, the optimal setting for the long-term high-resolution simulation will be explored and investigated with specific sensitivity test studies.

3.1 Importance of the Wadden Sea

Non-hydrostatic climate models such as the COSMO model, can be used for simulations with spatially highly resolved setups (<10 km). There are numerous studies, which show added value (especially for precipitation) for these high-resolution convection-permitting simulations (Prein et al., 2013). However, such simulations pose new challenges since they have to take into account mesoscale features and processes in contrast to lower resolution simulations. The Wadden Sea is an intertidal zone in the southeastern part of the North Sea, which falls dry and is flooded twice daily, respectively. This sensitivity study deals with the question if it is necessary to consider the tidal cycle of the Wadden Sea in order to achieve realistic weather states at this high resolution.

For this reason two test simulations with the model COSMO-CLM (CCLM) was used (Steppeler et al., 2003; Rockel et al., 2008). The tide cycle and the related change of sea/land area are not implemented in CCLM. Two simulations were integrated with a horizontal grid distance of 1 km, corresponding to 86 x 82 grid points, and forced by the coastDat II data set (Geyer, 2014) with double nesting. Simulated is the year 1962, which is the year of the big storm surge in Hamburg. One simulation was carried out in the state “low tide” and one in the state “high tide” which were created by using different land-sea masks representing the respective states. The domain includes the Wadden Sea around the North Frisian Islands of Northern Germany (Figure 3.1).

In the following, 10 m wind speed, 2 m temperature, and precipitation were analyzed. Precipitation does not show any notable differences between low and high tide. In the low-tide state, the mean autumn and winter

temperatures are decreased by more than 3 K in the Wadden area in

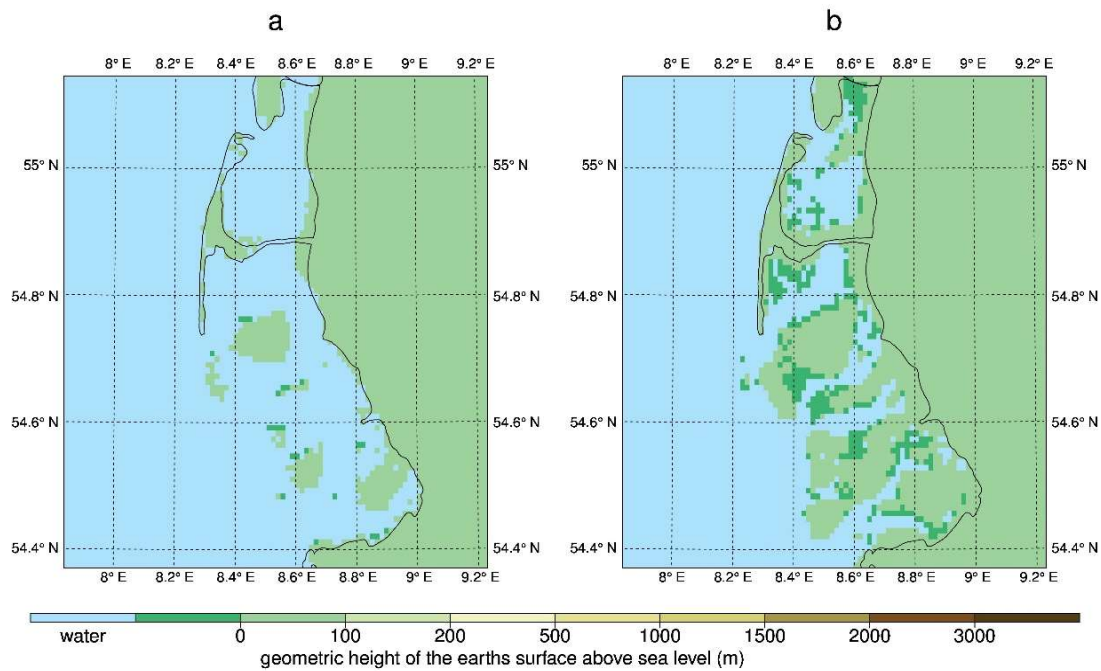


Figure 3.1: Model domain of the simulations and according topography of the a) “high tide” state and b) “low tide” state.

comparison to the high-tide state. In the wintertime, the North Sea is warmer than the air temperature and heats the near surface air. This heating does not apply if the sea area falls dry in the low tide state, which results in lower 2 m temperatures (Figure 3.2). This effect is most pronounced in the Wadden area, but also in the close surroundings a temperature decrease (especially in wintertime) is visible, which also extends to the lee side a few kilometers further inland. On the other hand, the roughness length increases for low tide. Therefore the 10 m wind speed is reduced in this area (up to 1.7 m/s for seasonal mean), especially in seasons with high wind speeds (winter and autumn). In contrast to the 2 m temperature, the effect is limited to the areas where the surface type changes from water to land (Figure 3.3). A validation with observation data is unfortunately not possible, because the mainly affected areas are over the sea, where no measurements take place. In this study, only the two extreme conditions - low and high tide - are examined and not the realistic conditions of continuous transient change from low to high tide for six hours and back.

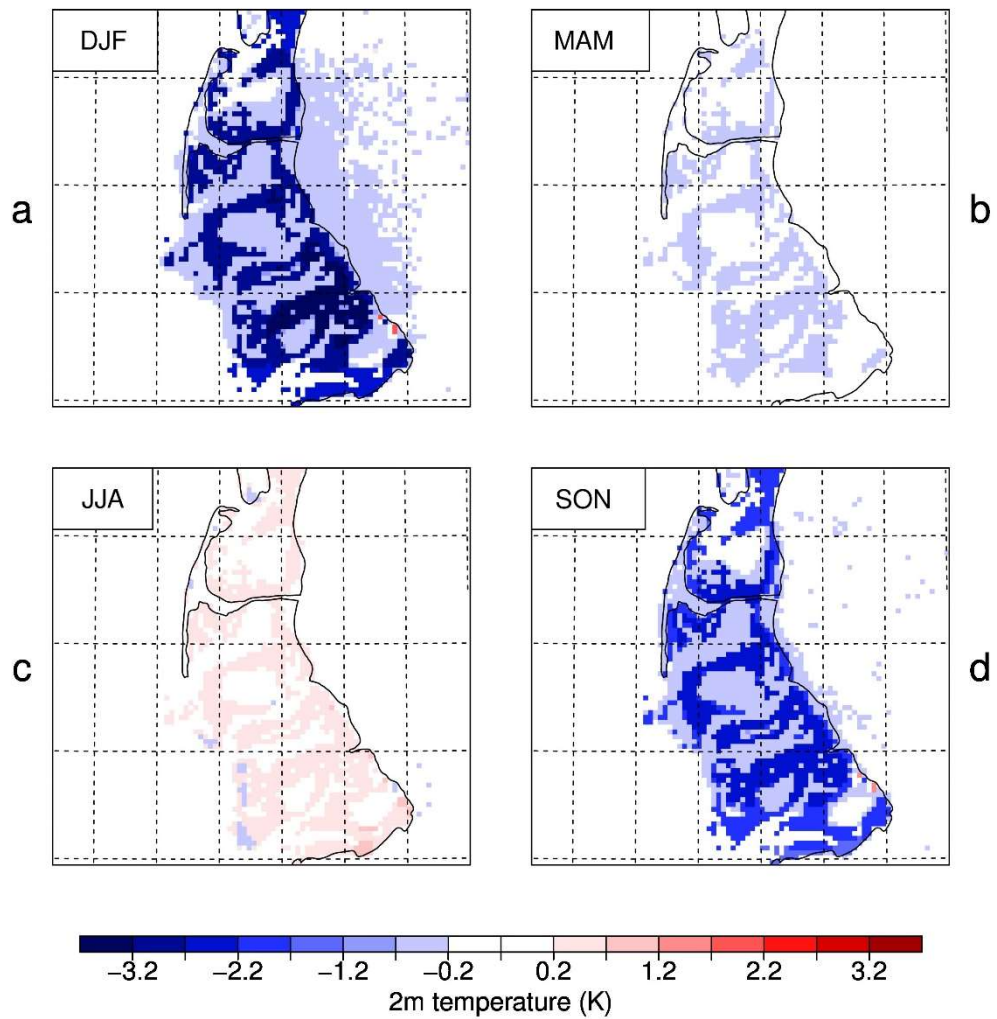


Figure 3.2: Difference of the seasonal mean 2 m temperature between low and high tide state for a) winter, b) spring, c) summer, and d) autumn.

Nevertheless, 20% of the grid points fall dry and become flooded in this model domain and should thus be taken into account for grid distances of 1 km and less, although the effect shown in this study is certainly overestimated. The temperature difference is quite large, because the sea surface temperature (SST) is taken from NCEP I reanalysis with a resolution of 1.875° (about 200 km). This means, that the whole model domain comprises only parts of a single NCEP grid point. Therefore, not only the changes between land and sea should be considered, but also the resolution of the SST should be improved when simulating the Wadden Sea area with this high resolution. The Wadden Sea seems to become more important for a resolution of 1 km and higher. For the resolution of 2.8 km the Wadden Sea

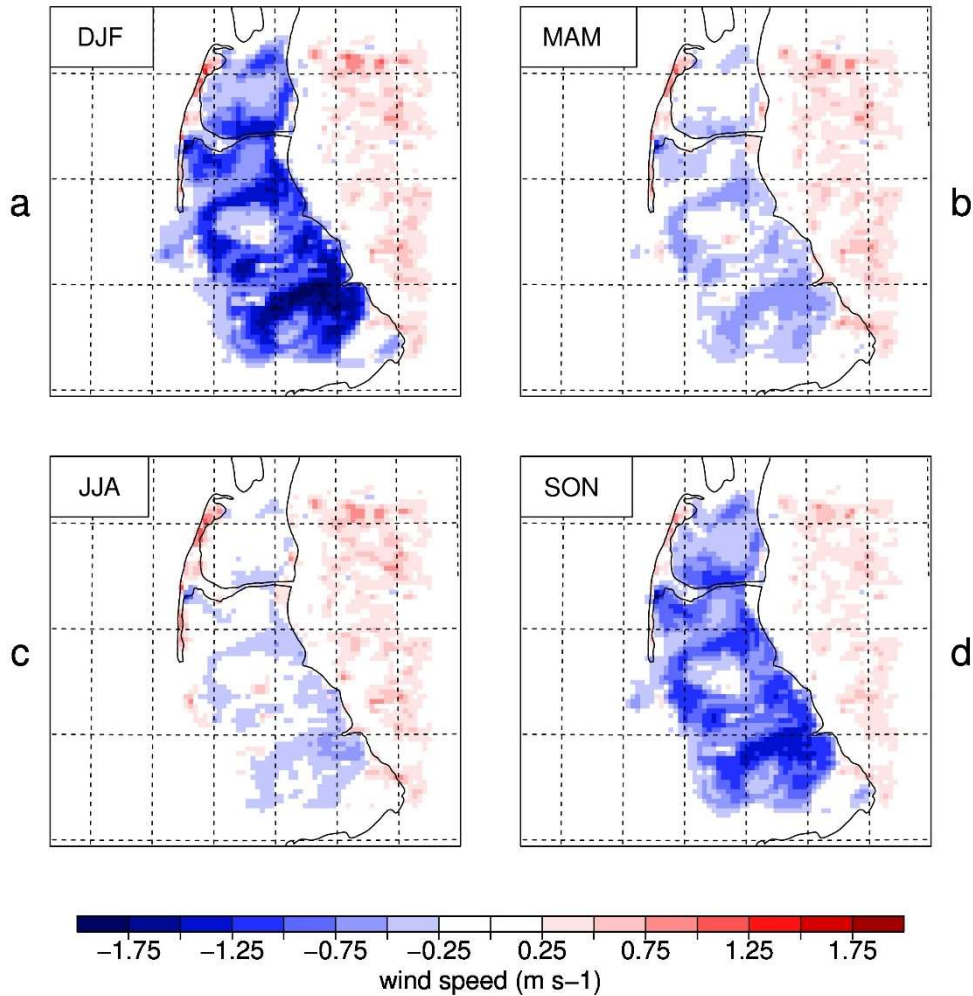


Figure 3.3: Difference of the seasonal mean 10 m wind speed between low and high tide state for a) winter, b) spring, c) summer, and d) autumn.

do not need to be considered, but for grid distances smaller than 1 km one should think about the consideration of the Wadden Sea.

3.2 Influence of domain extension

Increasing computer resources allow increasing the resolution of RCMs, but the domain size is the limiting factor. A doubling of the domain size means an eightfold increase in computing time, because the grid points are doubled in both horizontal directions and the time step of the model simulation must be halved. Optimally, also the vertical resolution is increased with an increase of the horizontal resolution, which leads to an even longer computing time. However, the expansion (in km, not in grid points) of the model domain could be essential for the development of extreme events such as cyclones. In

this section it is examined, how the domain size influences the model results in terms of high wind speeds and storms.

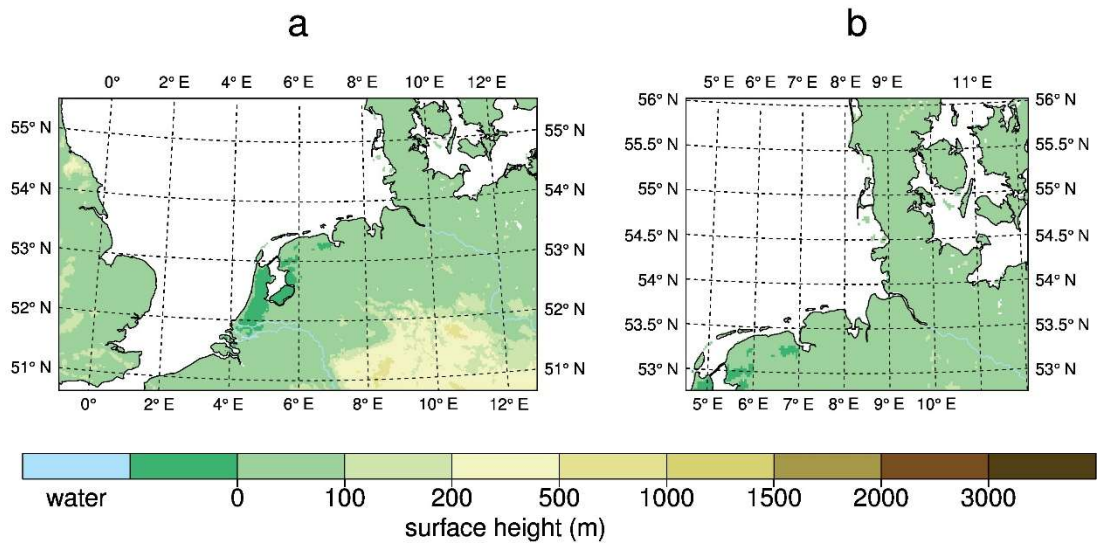


Figure 3.4: Model domain of the simulations and according topography of the a) CCLMo28large and b) CCLMo28small domain.

October 2013, a month with an extreme storm event (storm Christian) which affected Northern Germany and the German Bight, was simulated with the CCLM model (Steppeler et al., 2003; Rockel et al., 2008), using a horizontal grid distance of 2.8 km and with two different domain sizes (Figure 3.4). The domain of the first simulation covers the German Bight, Northern Germany and parts of the Baltic Sea (CCLMo28small). The second domain is expanded in the westerly and southerly direction to the British Channel (CCLMo28large). This means there is more time for extratropical cyclones to develop in this high convection-permitting resolution before reaching the German Bight. The domain is extended from 181x131 to 346x196 grid points, which results in an increase of the expansion from about 500x370 km to 970x550 km.

The 10 m wind speed, 10 m gust speed, sea level pressure and precipitation were analyzed. No crucial difference for the monthly mean wind speed was found (not shown), but in extreme situations like the storm event Christian up to 20 m/s stronger wind speeds occur in the simulation with the larger domain. These large differences at individual time steps during extreme

situations play no role for the long-term means. Figure 3.5 shows the difference fields of the analyzed variables for the area shared by of both model domains. Presented are the results for the time period of storm Christian, considering the 28th and 29th of October 2013. The measured

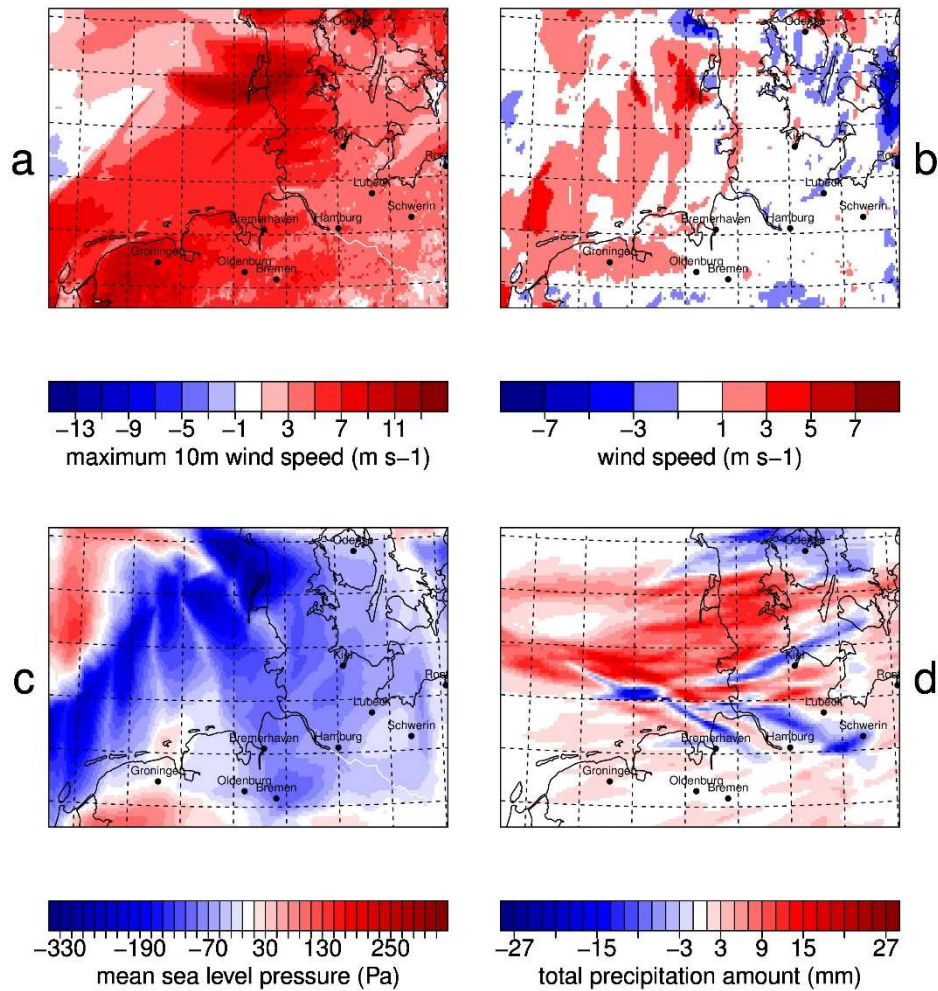


Figure 3.5: Difference of the a) maximum 10 m gust speed b) maximum 10 m wind speed c) lowest mean sea level pressure d) precipitation sum during storm Christian (28th – 29th of October 2013) between large and small domain (CCLMo28large – CCLMo28small) for the common domain area.

maximum wind gusts at the North Sea coast are largely between 40 and 50 m/s. At the coast of Denmark 53.3 m/s and in the city center of Hamburg 33.4 m/s were measured. In the CCLMo28large simulation, maximum gust speeds of up to 34 m/s were simulated at the coast and up to 18 m/ in Hamburg and in CCLMo28small up to 24 m/s at the coast and 16 m/s in Hamburg were simulated (not shown). This means that these extreme wind

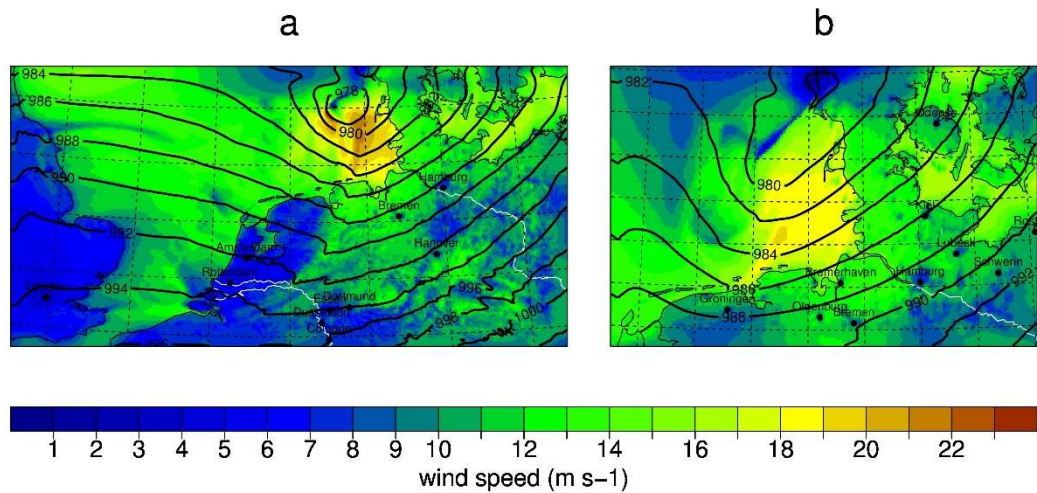


Figure 3.6: 10 m wind speed (shaded areas) in combination with isobars (black lines) for storm Christian on October 28, 2013, 11 UTC. a) large domain, b) small domain.

speeds are strongly underestimated in both simulations. However, the larger domain of CCLM028large simulates up to 12 m/s stronger gust speeds (Figure 3.5a) than CCLM028small. The underestimation of the 10 m mean wind speed is also reduced by up to 8 m/s, especially over the North Sea (Figure 3.5b). The mean sea level pressure reached a minimum core pressure of the cyclone of about 965 hPa in the DWD-analyses in the model domain, while CCLM028small simulates only a minimum core pressure of about 975 hPa. The core pressure, especially along the track of the cyclone was deepened in the CCLM028large simulation by about 3 hPa (Figure 3.5c). This fact increases the pressure gradient, which leads to the higher wind speeds and gust speeds in the CCLM028large simulation. The precipitation amount during storm Christian is about 10 to 15 mm higher in the CCLM028large simulation over the North Sea and Schleswig-Holstein (Figure 3.5d). The larger domain permits the development of convective precipitation at the cold front, whereas the precipitation in the small CCLM028small domain is dominated by the prescribed coarse forcing data, because of the missing time to develop heavy convective precipitation areas inside of the small domain.

Looking at the time, at which storm Christian had its highest intensity (Figure 3.6), the wind speed at the southeastern flank of the low-pressure system, which is usually the region with the highest wind speeds, is about 20% higher in the larger model domain. A maximum wind speed of 19 m/s is

shown in the small domain, but more than 23 m/s are simulated over the North Sea in the simulation with the larger domain.

Because of the strong dependency of the domain size, a domain size of 250x180 grid points for the simulation was chosen for the final simulation, which covers large parts of the North Sea, so the development can take place quite well. It is a compromise between both tested domain sizes and available computing time. A long-term simulation with a large domain size is impossible at the moment with the available computer resources. However, a large domain size like for example the coastDat II domain would probably improve the results.

3.3 Final model setup

In the last sections, different model setups were presented. According to these sensitivity experiments and test simulations with different settings and model domains, the final model setup is decided. In addition, the recommended settings of the operational configuration of the DWD at 2.8 km horizontal resolution in the domain of Germany were considered. This results in a model domain, which covers the German Bight and Northern Germany

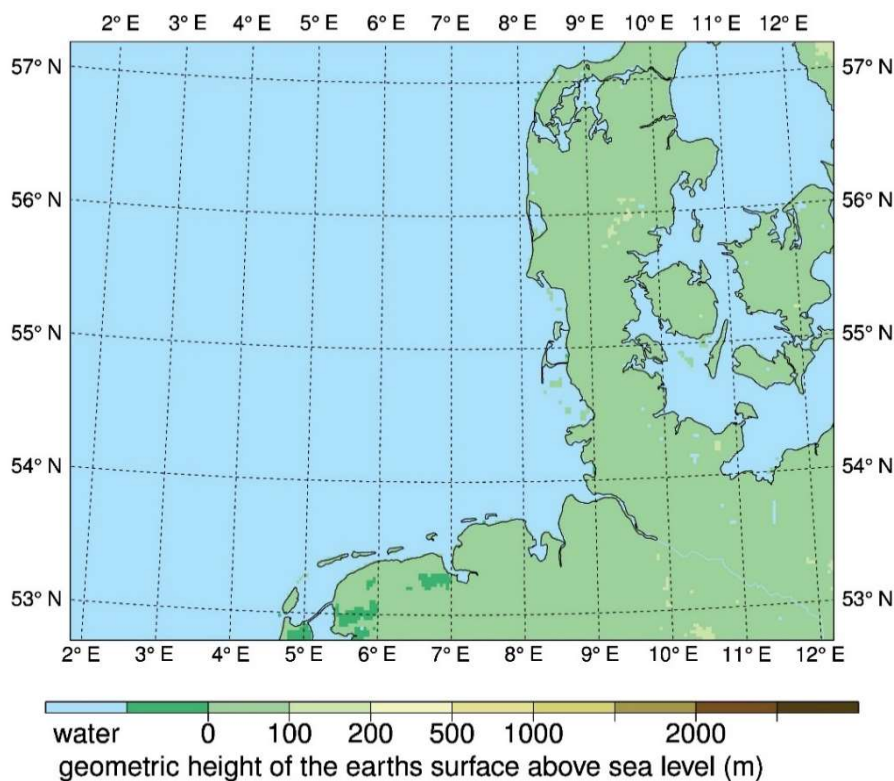


Figure 3.7: Model domain for the high-resolution simulations

(Figure 3.7).

As forcing data the coastDat II data set was applied, which used NCEP1 reanalyses as driving data. Furthermore, the convection parametrization was switched off, so only the shallow convection was parameterized and the convective precipitation was calculated explicitly. Spectral nudging was used for the sensitivity study in Chapter 4, but for the rest of the simulations in Chapter 5 and 6 it was switched off, because for this domain it is not necessary (see Chapter 4).

4 Spectral nudging in the small regional model domain

4.1 Introduction

After having observed that the traditional set-up of regional climate modelling, namely a relaxation only along a sponge zone at the lateral boundaries, plus a forcing at the lower boundary, exerts an insufficient steering of the large-scale dynamics in the interior of a region of 1000-8000 km, the concept of additionally constraining the large spatial scales of these fields in the interior and above a certain level was introduced. Without this so-called spectral nudging (von Storch et al., 2000; Castro et al., 2005; Rockel et al., 2008), in the interior different trajectories emerge intermittently in an ensemble of regional simulations (Giorgi and Xunqiang, 2000; Weisse et al., 2000; Christensen et al., 2001; Weisse and Feser, 2003; Caya and Biner, 2004; Lucas-Picher et al., 2008; Deque et al., 2012; Feser and Barcikowska, 2012; Laprise et al., 2012).

However, when such a constraint was implemented, the different trajectories stayed close to each other and also close to observations for the entire time.

Thus, the advantage of using spectral nudging in regional modeling was to enforce similarity of the large-scale state with a given state and the efficient reduction of ensemble variability. Separovic et al. (2015) showed that the internal variability at scales larger than 300 km could be reduced by using spectral nudging. Recently, such constraining was also used for improving the forecast of regional details (Zhao et al., 2016; Zhao et al., 2017). These results were based on simulations with grid sizes of about 20 and more kilometers and domains of 1000 km and more (Feser et al., 2011).

After computer resources further improved, more and more studies of regional models which explicitly resolve convective processes are used for dealing with small-scale atmospheric variability (Prein et al., 2015). For doing so, the grid resolution is significantly reduced to a few kilometers - and at the same time, the domain size is reduced to less than 1000 km, say 500 km and less due to high computing time costs for such small grids and time steps. These small regions are quickly flushed by horizontal transports, and it is plausible that in these small-domain cases the lateral boundary value constraints are much more efficient in determining the “large-scale” (large compared to the domain size) state within the domain. Therefore, the additional constraining by spectral nudging and related techniques in keeping the trajectory close to the prescribed state and the suppression of intermittent divergence in phase space may be of little significance. Here, this question is addressed if the spectral nudging technique does have an effect in small domains.

4.2 Experimental setup

4.2.1 Simulations

For the simulations, the COSMO-CLM model is employed using a model domain, which covers the North Sea and Northwestern Germany (Figure 4.1), with about 700 km in longitudinal direction and about 500 km in latitudinal direction. The grid sizes amount to about 2.8 km; the time step is 25s. The lateral sponge zone is 12 grid points wide. The simulations are forced by the

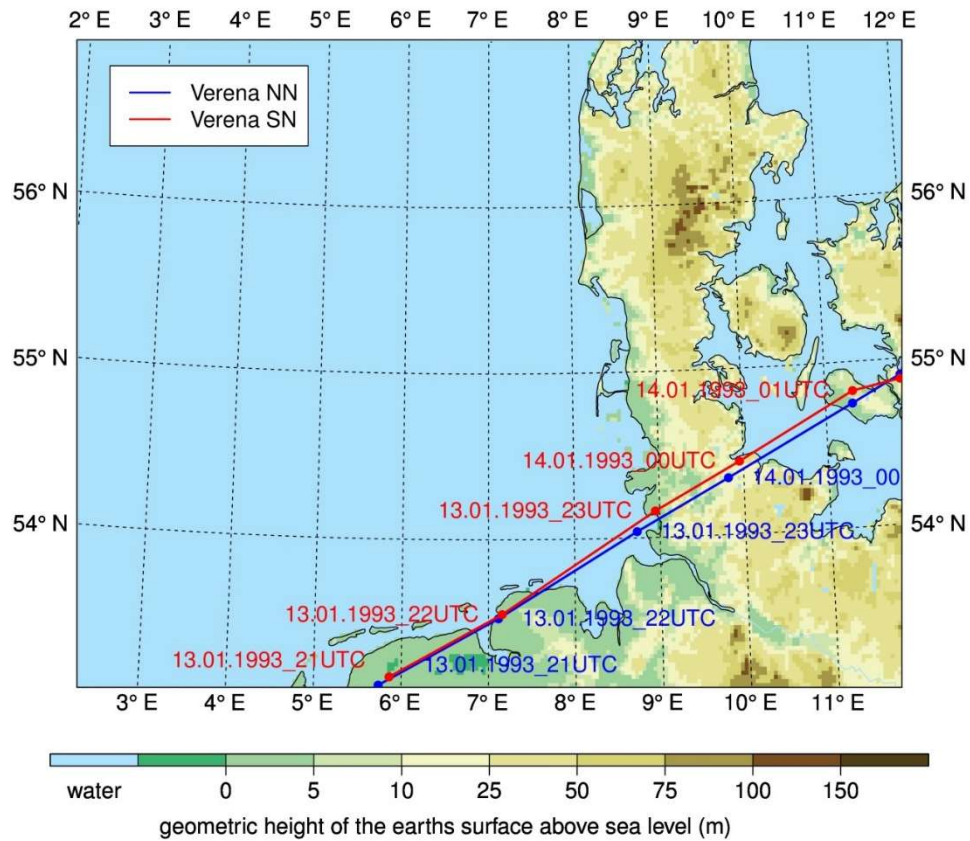


Figure 4.1: Model domain of the high-resolution simulation with tracks of storm Verena of January 1993 for SN (red) and NN (blue) simulations.

coastDat II data set, which is an atmospheric re-analysis for Europe for the last 67 years, from 1948 to 2014 (Geyer and Rockel, 2013; Geyer, 2014).

In total, four simulations were computed with this model, all for the year 1993. This year was chosen because larger deviations between the ensemble members were expected in this year due to a former study (von Storch et al., 2000). This von Storch et al. (2000) study analyzed the winter 1993 (January to March), during which a major phase of divergence was found. Differences in the large-scale patterns without spectral nudging arise between the non-nudged simulation and the forcing data. The study used a domain of about 5000 km x 4500 km and grid sizes of 53 km. Two simulations, which employed spectral nudging towards the coastDat II data set (SN₁ and SN₂), and two without spectral nudging (NN₁ and NN₂) were performed. In all four simulations, lateral boundary conditions were relaxed towards the coastDat II data set, using a conventional sponge zone constraint (Davies, 1976). One

of the spectrally nudged (SN) and one of the non-nudged (NN) simulations were initialized on 01.12.1992 (SN₁ and NN₁); the other two on 01.11.1992 (SN₂ and NN₂). Previous experiments showed that such a difference in the initial conditions is sufficient to generate intermittent differences between the individual ensemble members for various variables in the large domain set-up (Weisse et al., 2000; Weisse and Feser, 2003).

In the two SN-runs, only scales shorter than 80 km are unconstrained, i.e., wavenumbers 9 and above in zonal directions are subject to spectral nudging, and wavenumbers 6 and above in meridional directions. SN was applied every third time step with a nudging factor of 0.5.

4.2.2 Evaluation strategy

The data from the SN and NN simulations are available hourly, and are thus markedly correlated in time, and the tests become liberal (the null hypothesis is much more often rejected than stipulated by the normal risk level). To avoid this, all data were used to calculate the differences, but a critical value valid for 122 samples, corresponding to one value every three days, was used. This approach, mimicking the use of real degrees of freedom in t-tests (Zwiers and von Storch, 1995), is expected to overcome the problem of serial correlation.

Then a number of statistics of these difference fields were calculated, and three episodes were examined, when relatively large NN-SN differences in terms of synoptic similarity and regional detail were found. It turns out that there are hardly any differences at the synoptic scale, quite differently from the large-domain case of von Storch et al. (2000), but that the differences in precipitation are regionally large, in particular at the grid-point scale.

4.3 Results

4.3.1 Ensemble-variability of the SN and NN runs

In this section, the similarity of the SN₁ and SN₂ simulation as well as the similarity of the NN₁ and NN₂ simulation is investigated. Analyzed were 10 m and 500 hPa scalar wind speed (WSS), 2 m temperature (T_{2M}), precipitation (TOT_PREC) and sea level pressure (PMSL). In addition, the meridional and zonal 10 m wind speed is analyzed separately, but found that they behave just like the 10 m wind speed, so these variables are not shown separately. Figure 4.1 also shows the tracks of Storm Verena, which occurred in January 1993. The tracks were determined with a simple tracking algorithm (Feser and Storch, 2008a) on the basis of sea level pressure and near-surface wind speed. The tracks of the SN-runs are exactly identical, as well as the tracks of the NN-runs. The SN and NN tracks are almost identical and differ no more than 17 km.

The root mean square error (RMSE) is calculated spatially for every time step and is given by

$$RMSE = \sqrt{\frac{1}{n} \sum_{i=1}^n (x_i - y_i)^2}$$

where x and y are the modeled variables of simulation 1 and 2. The index n is the total number of grid points in the model domain. Subsequently the cumulated distribution function of the whole analyzed year (one dot for every time step) is plotted. These distribution functions of the RMSE between NN₁ and NN₂, and between SN₁ and SN₂ are again very similar for 10 m wind speed (Figure 4.2). Precipitation and 2 m temperature show the same behavior as the 10 m wind speed and the SN and NN curves do not differ (not shown). For sea level pressure and wind speed at 500 hPa, the NN runs show slightly higher variability (i.e., RMSEs) than the SN simulations (Figure 4.2). The reason for this behavior is that 500 hPa is a vertical level where spectral

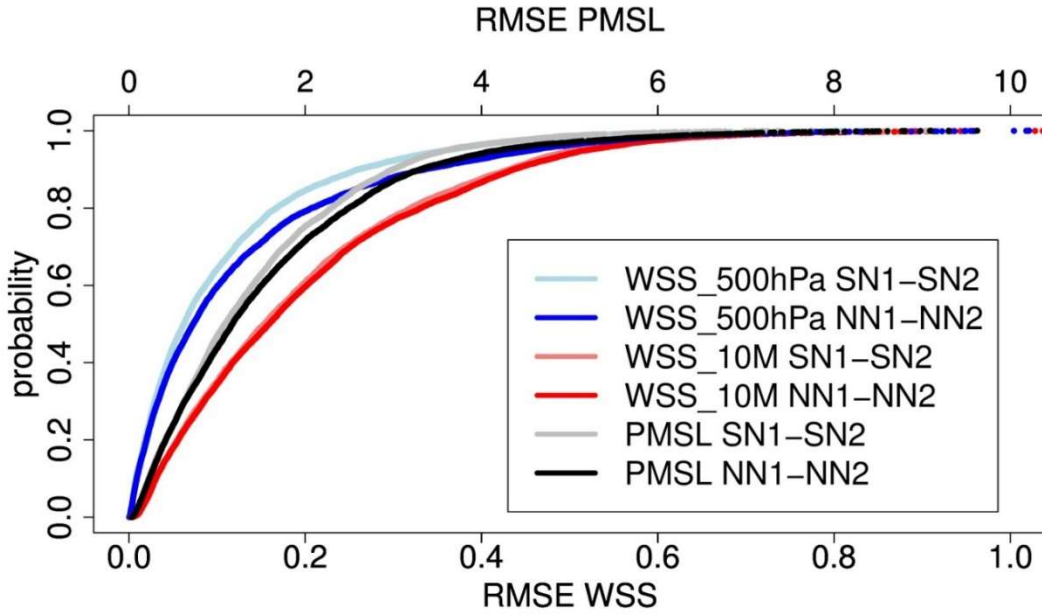


Figure 4.2: Distribution function of the RMSE between SN_1 and SN_2 (light color) and between NN_1 and NN_2 (dark color) for 10 m wind speed (red, WSS_10M), sea level pressure (black, PMSL), and wind speed in 500 hPa (blue, WSS_500hPa).

nudging takes place and sea level pressure is a height integrated variable and therefore influenced by spectral nudging at higher levels. The Kolmogorov-Smirnov-test (Conover, 1971) assesses the differences between NN and SN as not statistically significant. However, for sea level pressure and wind speed at 500 hPa, the two distribution functions support the hypothesis that the variability for SN is slightly smaller than for NN.

4.3.2 Differences between SN and NN simulations

For this comparison the SN_1 and NN_1 simulation is chosen, because in the previous section it was shown, that the differences between SN_1 and SN_2 are similar to the differences between NN_1 and NN_2 , so it doesn't matter if SN_1 and NN_1 or SN_2 and NN_2 is chosen (not shown). In Table 4.1 statistical values are presented for the $NN_1 - NN_2$, $SN_1 - SN_2$ and $SN_1 - NN_1$ difference distributions. The distributions are all centered around zero, except the $SN_1 - NN_1$ distribution for sea level pressure, which is shifted by 7 Pa. The absolute maximum values, 99th percentiles and standard deviation (SD) are higher in

Table 4.1: Statistical values of hourly data differences SN_1 - NN_1 (upper value), NN_1 - NN_2 (middle value) and SN_1 - SN_2 (lower value) for 1993 for 10 m wind speed (WSS_10M), total precipitation (TOT_PREC), sea level pressure (PMSL), wind speed in 500 hPa (WSS_500hPa) and 2 m temperature (T_2M). For precipitation only hourly precipitation sums are considered, which are different from zero. Shown is the absolute maximum difference, the mean difference, the standard deviation and the 99th percentile of the difference. In addition, the values and dates of the minimal pattern correlation between SN_1 and NN_1 (upper value), NN_1 and NN_2 (middle value) and SN_1 and SN_2 (lower value) are shown. Also the 10th percentiles of the pattern correlation and the values of the minimum time correlations are listed.

		WSS_10M [m/s]	TOT_PREC [mm]	PMSL [Pa]	WSS_500hPa [m/s]	T_2M [K]
Absolute maximum	SN_1 - NN_1	17.76	64.53	284	21.60	9.45
	NN_1 - NN_2	15.24	38.44	158	15.64	4.97
	SN_1 - SN_2	12.79	31.80	146	14.24	9.05
Mean	SN_1 - NN_1	-0.01	0	7.41	0.07	0
	NN_1 - NN_2	0	0	0	0	0
	SN_1 - SN_2	0	0	-0.01	0	0
Standard deviation	SN_1 - NN_1	0.54	0.42	12.13	1.11	0.21
	NN_1 - NN_2	0.26	0.21	2.07	0.20	0.09
	SN_1 - SN_2	0.25	0.21	1.83	0.16	0.11
99th percentile	SN_1 - NN_1	1.62	1.03	41.46	3.18	0.68
	NN_1 - NN_2	0.79	0.34	6.66	0.57	0.28
	SN_1 - SN_2	0.76	0.33	5.77	0.44	0.39
Minimum pattern correlation	SN_1 - NN_1	0.79	-0.01	0.92	0.39	0.79
	NN_1 - NN_2	0.90	0	0.99	0.95	0.91
	SN_1 - SN_2	0.92	0	0.99	0.96	0.94
Date of minimum pattern correlation	SN_1 - NN_1	11.07.1993 17UTC	26.04.1993 16UTC	11.03.1993 00UTC	13.04.1993 14UTC	16.10.1993 11UTC
	NN_1 - NN_2	24.11.1993 12UTC	19.10.1993 00UTC	18.09.1993 16UTC	11.09.1993 09UTC	06.08.1993 17UTC
	SN_1 - SN_2	13.08.1993 16UTC	21.11.1993 01UTC	18.09.1993 05UTC	11.09.1993 04UTC	16.10.1993 13UTC
10th percentile of pattern correlation	SN_1 - NN_1	0.94	0.29	0.997	0.91	0.98
	NN_1 - NN_2	0.98	0.68	0.9998	0.99	0.99
	SN_1 - SN_2	0.98	0.68	0.9999	0.997	0.99
Minimum time correlation	SN_1 - NN_1	0.96	0.62	0.9998	0.98	0.99
	NN_1 - NN_2	0.99	0.84	0.999	0.99	0.997
	SN_1 - SN_2	0.99	0.84	0.999	0.99	0.995

the SN_1 - NN_1 difference than in the other ones. The minimum pattern correlations during the whole year and the value of the grid point with the minimum time correlation are lower in the SN_1 - NN_1 difference. However, the correlations still show a very high similarity with values larger than 0.8 except for the precipitation in the time and pattern correlation and 500 hPa wind speed in the pattern correlation. The 10th percentile of the pattern correlation shows that the minimum values of the pattern correlation are rare exceptions.

The time series of the pattern correlation (Figure 4.3) confirms that for all variables, except for 500 hPa wind speed and precipitation, the correlation is larger than 0.8 at every time step. The pattern correlation of the 500 hPa wind speed shows a few cases with lower values between 0.8 and 0.4. The hourly precipitation pattern correlation (not shown) is close to zero in many situations, but only for regionally restricted small precipitation amounts. For

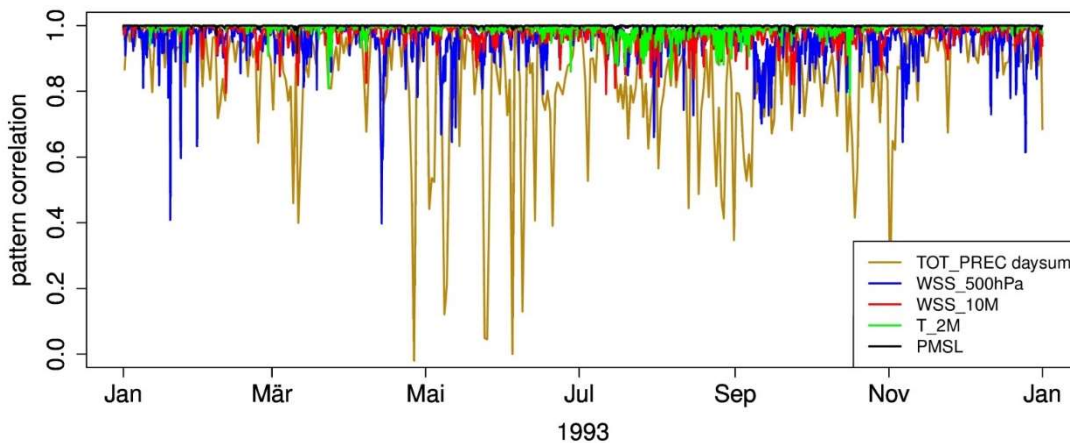


Figure 4.3: Time series of the hourly pattern correlation between SN_1 and NN_1 (except for “TOT_PREC day sum” daily values are shown) of sea level pressure (PMSL), 2 m temperature (T_2M), 10 m wind speed (WSS_10M), 500 hPa wind speed (WSS_500hPa), and the daily sum of precipitation (TOT_PREC day sum).

large precipitation areas, there is a minimum correlation of 0.8. If only daily sums of precipitation are analyzed, the small spatial shifts of precipitation and the low pattern correlations of certain time steps are reduced. This leads to an increase of the pattern correlation to more than 0.5 for nearly all days, except for some days especially in early summer. In Figure 4.4 (a and b) sea level pressure and the 10 m wind speed maps are shown for times of minimum pattern correlation between SN_1 and NN_1 for July 11, 1993, which featured a minimum for 10 m wind speed correlation and March 11, 1993, with a minimum sea level pressure correlation (see Table 4.1). The date of the minimal sea level pressure pattern correlation is the same as in the von Storch et al. (2000)-study. However, in this study there are only some small differences in the pressure field, but no large-scale deviations like the ones shown in the von Storch et al. (2000)-study (differences of more than 15 hPa). It is a stable high pressure situation, in which the air mass can remain longer in the model domain than for weather situations such as strong westerlies and thus there is more time for the RCM to develop large-scale variations, which cause smaller, but still very high, pattern correlations. The wind field at the date of the minimum pattern correlation of the 10 m wind speed shows some different structures, especially in regions with calm winds. As an example for low precipitation correlation, Figure 4.4c shows a situation with small isolated spots of precipitation. The pattern correlation

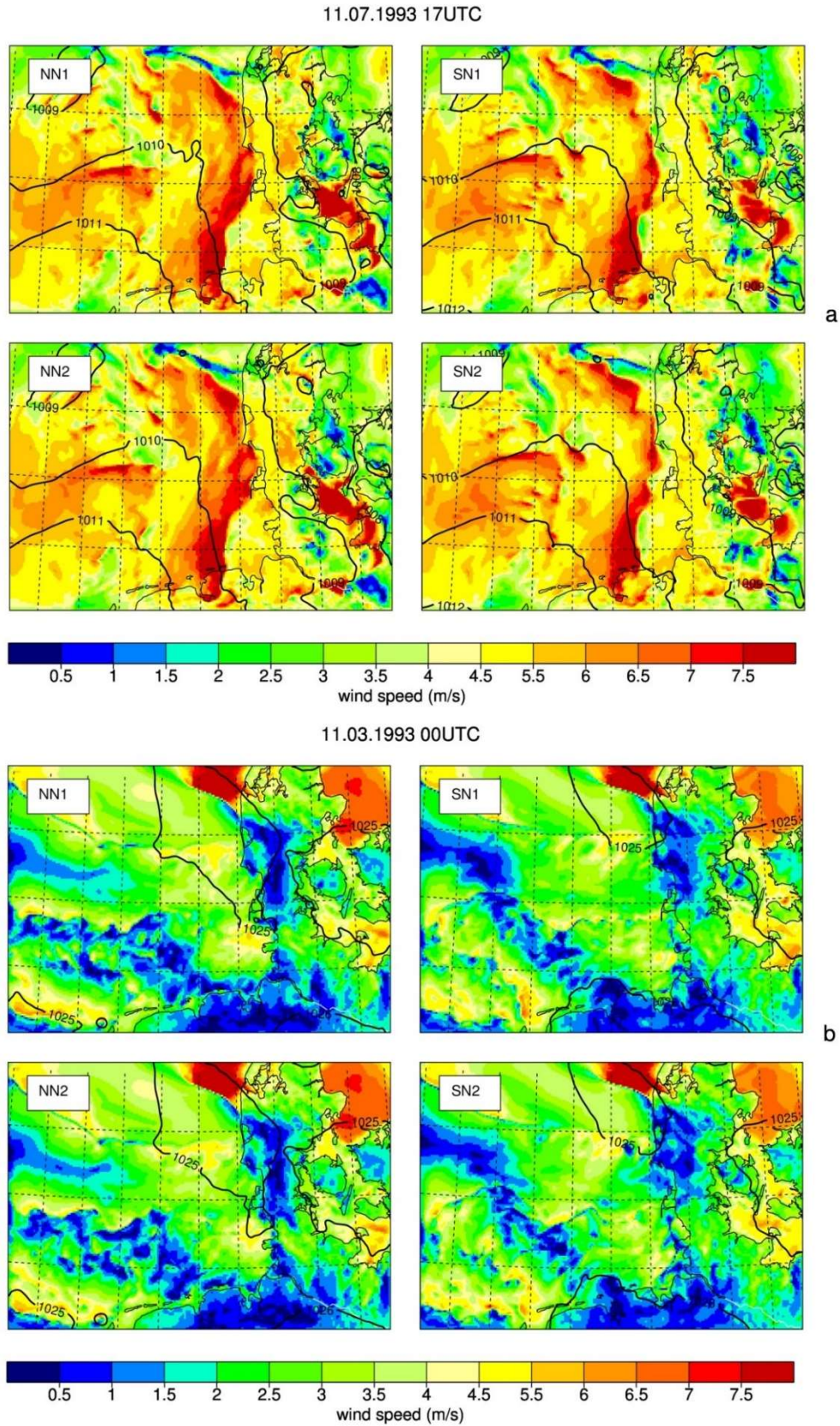


Figure 4.4: Pressure isobars (NN₁ (top left), NN₂ (bottom left), SN₁ (top right), SN₂ (bottom right)) for the (a) 11th of July 1993, 17UTC, (b) 11th of March 1993, 00UTC, with shaded wind speed fields; (c) 23rd of May 1993, 04UTC, with shaded precipitation fields.

23.05.1993 04UTC

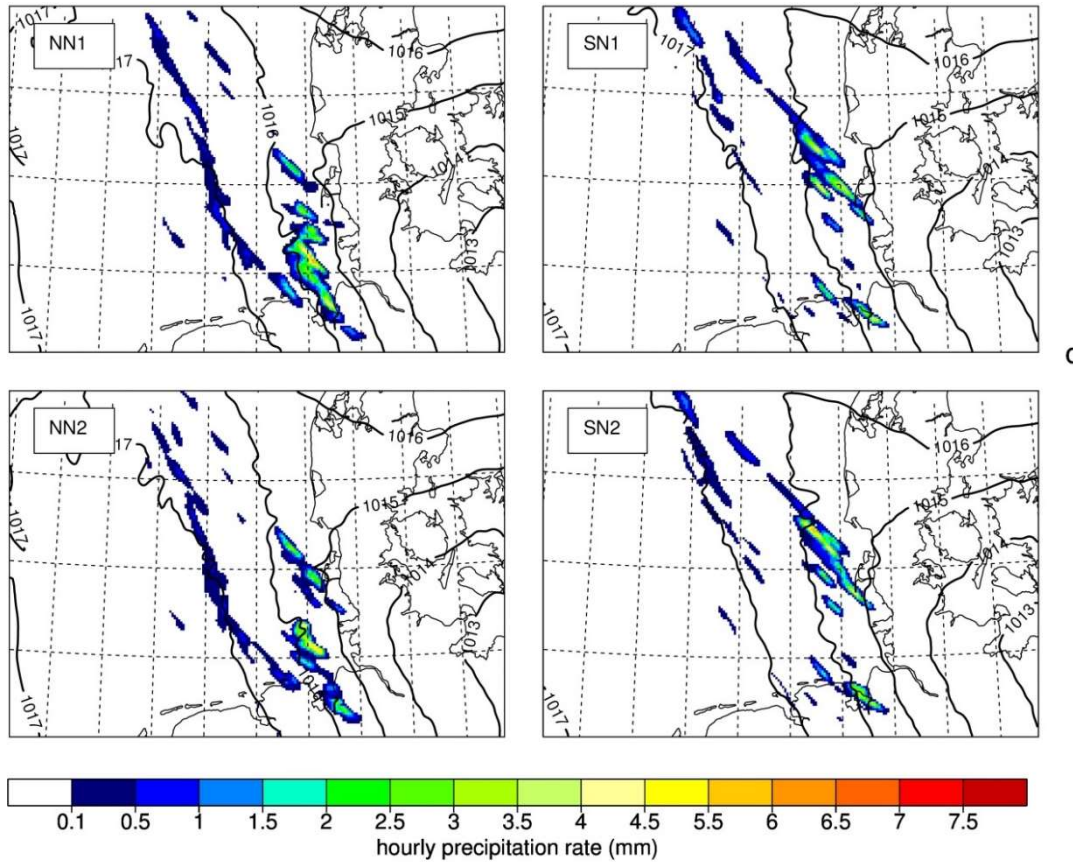


Figure 4.4: Pressure isobars (NN₁ (top left), NN₂ (bottom left), SN₁ (top right), SN₂ (bottom right)) for the (c) 23rd of May 1993, 04UTC, with shaded precipitation fields.

between SN₁ and NN₁ is 0.145. The location of the main precipitation is shifted southwards in the NN₁ simulation. The results show that precipitation is a very non-deterministic variable, as there are also larger differences between the precipitation fields of NN₁ and NN₂ than in the fields of the other investigated atmospheric variables. The two SN precipitation fields are moresimilar to each other. If only daily sums of precipitation are analyzed, the small spatial shifts of precipitation and the low pattern correlations of certain time steps are reduced. This leads to an increase of the pattern correlation to more than 0.7 for nearly all days.

The comparison between SN₁ and NN₁ shows larger differences than between SN₁ and SN₂ and between NN₁ and NN₂, especially for precipitation, but also for all other variables. It is supposed that the state, which is strived for by the model, is slightly different from the state of the RCM using spectral nudging.

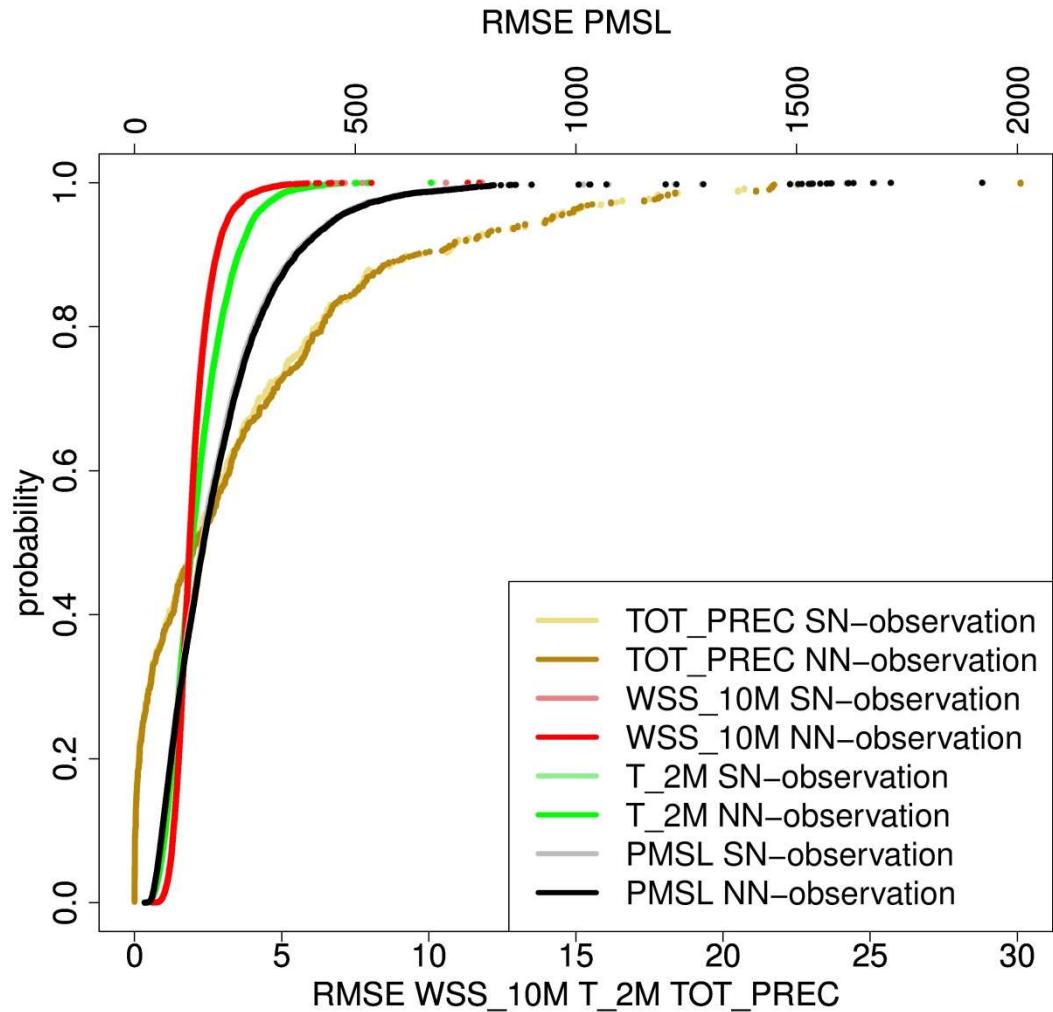


Figure 4.5: Distribution function of the RMSE between SN and observations (light colors) and between NN and observations (dark colors) for 10 m wind speed (WSS_10M), total precipitation (TOT_PREC), 2 m temperature (T_2M), and sea level pressure (PMSL).

4.3.3 Comparison with observations

A comparison with observation was performed in order to analyze the quality of the simulations with and without spectral nudging. Figure 4.5 shows the distribution function of the RMSE between the SN or NN simulations and observations of the German weather service. Wind speed, 2 m temperature and sea level pressure observations were available hourly; precipitation daily. Both distribution functions are nearly identical for all variables. The bias relative to observations is about as large for the NN runs as for the SN runs. The Kolmogorov-Smirnov-Test (5% error probability) cannot reject the

null-hypothesis, that the SN-RMSE is larger than or equal to the NN-RMSE, so the differences between the NN and SN are not statistically significant. This means that simulations computed with spectral nudging are not significantly closer to observations than simulations without spectral nudging.

4.4 Summary and discussion

The effect of spectral nudging on regional climate model results when using very small model domains, which are often used nowadays for very high convection-permitting resolutions due to high computing time costs, was examined. Both SN simulations show negligible differences for all analyzed variables. Even both NN simulations do not show noteworthy differences, though they lack the spectral nudging control within the model domain. The ensemble variability of spectral nudging for the surface variables 10 m wind speed and precipitation has the same negligible magnitude like the ensemble variability without spectral nudging for the domain size of about 700 km x 500 km. The ensemble variability of the runs without spectral nudging for wind speed at 500 hPa is higher, because at this pressure level spectral nudging takes place in the SN runs. A similar effect on sea level pressure, a height-integrated variable, is detected.

With spectral nudging nearly the same state is produced independently of the starting date, which is the initial idea of spectral nudging. However, also for the simulation without spectral nudging the model produces very similar states and fields at various starting dates, which is not the case for larger domain sizes (Alexandru et al., 2009). Even though the high-resolution RCM features a high number of model grid points, the region is still small in absolute dimensions. An air parcel will quickly cross the model domain and will be largely influenced by its values at the inflowing model boundaries. This implies that the size of the domain is too small to develop large-scale variations and the lateral boundary conditions are sufficient to force the atmospheric state into a similar state.

The temporal and spatial states of the two ensembles with and without spectral nudging are nearly identical. However, the state, which is developed by the model without spectral nudging, is slightly different from the state of the RCM using spectral nudging. All simulations employ the same lateral and lower boundary conditions, but the SN runs use in addition spectral nudging at higher model levels inside the model domain, which seems to lead to marginally different weather states. It is conceivable that these differences result from different model versions, which were used for the sensitivity study and for the simulation of the forcing data coastDat II, which is also used for the spectral nudging. In addition, different settings, which are necessary for different resolutions, could cause these discrepancies. However, generally the SN and NN simulations are very similar for most variables with correlations larger than 0.8. Only precipitation shows pattern correlations smaller than 0.3 at certain times. These small correlations usually occur in situations with very weak precipitation with an hourly precipitation rate smaller than 1 l/m^2 in the model domain (see Figure 4.4c, pattern correlation of only 0.145 between SN1 and NN1). When daily precipitation sums are taken into account, the pattern and time correlation increases to values of more than 0.7. Comparisons with observations showed that the simulations with spectral nudging are not closer to station data than the ones without spectral nudging.

It was demonstrated that spectral nudging is not necessary for small RCM domain sizes of only several hundred kilometers in diameter and over flat and homogeneous terrain. The experiment is limited because of the small number of simulations of only four simulations (two ensembles with spectral nudging and two ensembles without spectral nudging). The results suggest that a higher number of ensemble members would have given similar results, but this should be analyzed in more detail in the future. What remains to be done for the future are further systematic tests with various domain sizes over different orographic terrains and geographical regions in order to determine threshold domain sizes from which spectral nudging becomes essential.

5 Added value

5.1 Introduction

The added value of RCMs in comparison to coarser model data sets like reanalyses was determined in numerous studies in regional climate hindcasts. For instance, Feser et al. (2011) describe added value for several studies over Europe in numerous variables and areas. The potential for added value in RCMs and for dynamical downscaling was investigated by Di Luca et al. (2012) and Di Luca et al. (2015). The potential added value describes small spatial scale variability in regional climate statistics, which could not be simulated, on coarser grids as a prerequisite for added value. They found that a more meaningful added value may be found by exploring conditions conducive to particular weather and climate events than by focusing on simple statistics and that the potential added value of RCMs is much higher for short time scales (e.g. hourly data) than for long time scales (monthly mean). An RCM ensemble study by Di Luca et al. (2016) showed the strong dependence of added value on the type of driving data, the variable, and the region of interest. An added value for RCM simulations was found mainly due to a more detailed spatial variability of surface variables as, for instance, the 2 m temperature in coastal areas or regions with structured topography. Li et al. (2016) investigated the added value of an RCM using satellite and in situ observations as references for the region of the Bohai Sea and Yellow Sea and found an added value especially in coastal regions. Winterfeldt and Weisse (2009) discussed the added value of an RCM with a resolution of 50 km for a time period of 10 years (1994-2003) and showed an added value for RCM wind speed compared with reanalyses (they also used satellite data as a reference). They found an added value for areas with more structured orography and coastal regions, but not over the open sea and the German Bight. Von Storch et al. (2017a) discussed that regional dynamical downscaling simulations in midlatitude and subtropical regions of the world add value to observational data.

There have only been a few dynamical downscaling studies so far showing the added value for storms, and most of these cover tropical cyclones (TCs). Xue et al. (2013) analyzed the Atlantic hurricane season of 2010 with an RCM using a 4 km grid by means of 48 h TC forecasts. The high-resolution RCM showed benefits in comparison to its global forcing data for forecasted TC tracks and TC intensity, with the largest improvements for TCs that feature hurricane strengths. Gentry and Lackmann (2010) studied hurricane Ivan of 2004 in an RCM with varying grid sizes between 8 and 1 km. The higher resolutions resulted in an increase in storm intensity and a broader range of updraft and downdraft processes in the eye wall. Taraphdar et al. (2014) analyzed TCs over the Indian Ocean in high-resolution weather forecasts computed with RCMs at 10 and 1.1 km resolution. They found that the high-resolution simulations lead to modelled TC tracks and intensities, which were closer to observations than the simulations, which used parameterized convection. However, the higher resolution had no effect on the intrinsic predictability limit, which was the same for both simulations.

So far, there are only a small number of studies, which examine extra-tropical cyclones in high-resolution models. Most of these did not look into the added value of convection-permitting simulations in comparison to coarser RCM or GCM simulations. For instance, Gallagher et al. (2016) dynamically downscaled wind and waves from ERA-Interim reanalysis with a meso-scale model of 2.5 km grid size. The authors assessed the uncertainty regarding the wind and wave renewable energy potential in Irish coastal areas with this 14-year hindcast from 2000 to 2013. The data set's quality for wind and waves was found to be good in comparison to observations. Ludwig et al. (2015) analyzed the formation of a secondary cyclone along the occluded front and severe cold front of storm Kyrill of January 2007. The high-resolution RCM run realistically reproduced observed storm features and the gusts along the cold front were often close to observations and exceeded hurricane strength. Other extra-tropical winter storms were investigated in RCM studies, such as Anatol (Nilsson et al., 2007), Lothar and Vivian (Usbeck et al., 2012), and Xynthia (Liberato et al., 2013). These studies showed that an RCM with a

Table 5.1: Analysis period and number of hourly values used for the calculation of the BSS for each of the ten storm events investigated.

Storm name	Analysis period	Number of values for BSS
Anatol	03.12.-04.12.1999	48
Kyrill	18.01.-19.01.2007	48
Emma	29.02.-02.03.2008	72
Xynthia	28.02.-02.03.2010	72
Yoda	26.11.-28.11.2011	72
Christian	28.10.-29.10.2013	48
Xaver	04.12.-07.12.2013	96
Anne	03.01.-04.01.2014	48
Gonzalo	21.10.-22.10.2014	48
Niklas	31.03.-02.04.2015	72

high resolution of 2 km produces a realistic wind field compared with observations. Some case studies on the added value of RCMs running in numerical weather prediction mode have been published (Kain et al., 2006; Baldauf et al., 2011). The majority of these focused on precipitation, as this variable is most likely to add value in convection-permitting simulations.

In this work, the added value of high-resolution convection-permitting regional climate simulations for ten strong extra-tropical storm cases over the North Sea, the German Bight, and Northern Germany is analyzed. The storms of interest are listed in Table 5.1. This study is the first to analyze the added value of convection-permitting RCMs with a focus on very high wind and storm conditions. Two RCM simulations with different resolutions against reference measurement data using different statistical measures are compared here.

5.2 Model configuration, data, and methods

5.2.1 Model configuration

For this study, two different CCLM simulations will be compared to each other, one with a grid distance of about 24 km (CCLM240) and one with a grid distance of about 2.8 km (CCLM028). Both model domains are shown in Figure 5.1. The coarse simulation is the coastDat II data set (see Chapter 2.3; in this section referred to as CCLM240). In the following, the high-resolution storm simulations will be referred to as CCLM028. The model domain of the CCLM028 simulation covers the German Bight and the western part of the Baltic Sea (Figure 5.1) with a spatial grid distance of 0.025° (about 2.8 km), 250x180 grid points, 40 layers in the vertical, a rotated pole at 8.82° E and 54.45° N, and a time step of 25 seconds. The lateral sponge zone has a width of 12 grid points, so 226x156 grid points are analyzed in this study. The climate simulation is forced by CCLM240. The double nested hindcast simulation CCLM028 (from NCEP1 to CCLM240 and from CCLM240 to CCLM028) was computed for ten individual storm cases in climate mode, which means that the simulation is continuous for the whole storm event and no repeated initialization is carried out during the model run. For each storm, the preceding month was computed for the spin-up of the model, followed by the month the storm evolution took place. The most relevant atmospheric variables for this study, such as wind speed, pressure, or precipitation, are stored with hourly resolution.

The spectral nudging technique described by von Storch et al. (2000) was applied for the CCLM240 simulation to keep large weather systems (larger than about 1200 km) close to the large-scale atmospheric conditions simulated by the forcing reanalysis. Smaller spatial scales were not nudged; these were solely computed by the regional climate model. Only the horizontal wind components (U, V) were spectrally nudged towards the reanalysis. The influence of spectral nudging increases exponentially from

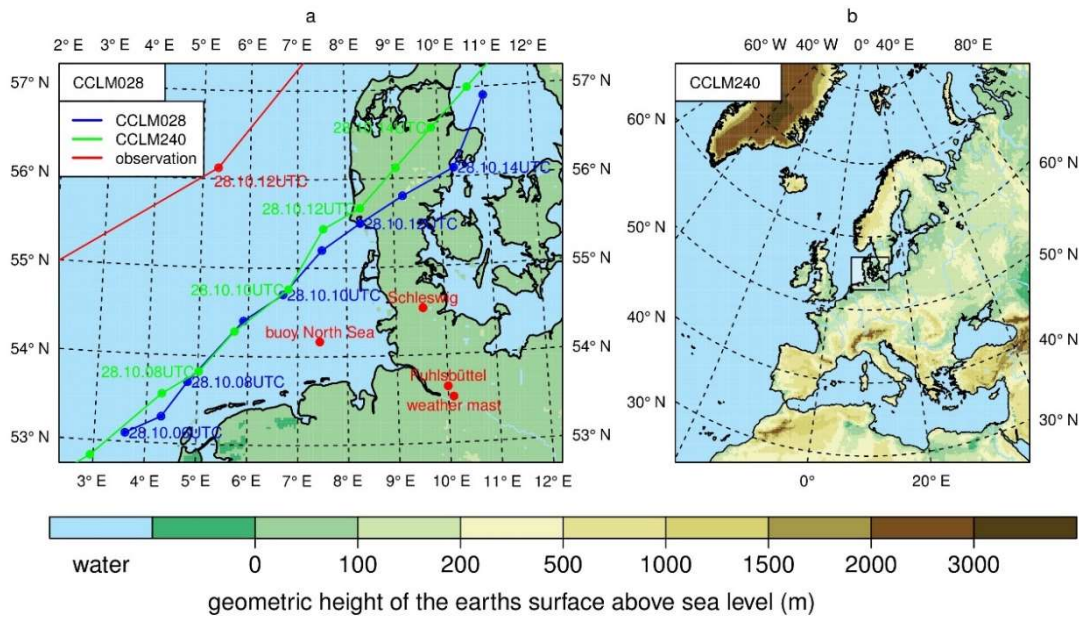


Figure 5.1: Model domain of a) the high-resolution simulation CCLM028 and b) CCLM240 and related topographies. The locations of the weather stations used for most comparisons in the study are shown as red dots. Storm tracks of storm Christian of CCLM028 (blue), CCLM240 (green) and the German Weather Service (DWD) analysis (red) are shown as well.

850 hPa to the top of the model domain. Below 850 hPa, no spectral nudging is applied, so that small weather phenomena, which often occur close to the surface, are not affected. Test simulations, which are referred to the 2.8 km simulation, with and without spectral nudging showed no significant differences and therefore lead to the conclusion that spectral nudging is not necessary for high-resolution simulation (Chapter 4). This is presumably a consequence of the relatively small model domain as spacious weather patterns, which deviate from observed large weather systems have no time to develop inside this domain. In addition, the area of the German Bight is topographically very flat and often dominated by strong westerlies and this prevailing exchange of air masses between the model boundaries and its interior leads to a smaller potential effect of spectral nudging. Due to the high resolution, many meteorological phenomena such as convective clouds can be simulated explicitly by the model. CCLM240 uses both convection parameterizations (deep and shallow convection). CCLM028 uses a grid point distance of 2.8 km and can thus simulate precipitating deep convection

explicitly (Prein et al., 2015). Therefore, the CCLM028 simulation only uses the shallow convection scheme.

The CCLM028 and CCLM240 simulations differ in their horizontal resolutions and their convection schemes, which leads to the following distinctions: The high-resolution CCLM028 simulations feature about 70 grid points in comparison to each coarser CCLM240 grid point and can thus simulate much more detail, e.g. small islands, as the North Frisian Islands of Amrum or Föhr can be resolved. In addition, the roughness length shows more detail for CCLM028, whereby the range of the roughness length is larger than in CCLM240, and places with higher roughness (e.g. cities) appear much more clearly. A further difference is the time step of the simulations, which decreases from about 5 minutes for CCLM240 to 25 seconds for CCLM028. The main dynamical difference between the two simulations is the ability of CCLM028 to resolve small convective clouds and associated weather features explicitly. The 2.8 km simulation can develop vertical dynamics, which cannot be developed by the coarser simulation. Hence, small-scale variables like precipitation or wind speed to show more details and thus potential added value are expected. In addition, the more detailed coastline in the high-resolution simulation may lead to results that are more realistic.

5.2.2 Data

For comparisons with the observations, data from the weather mast were used (Chapter 2.4.2). For all other comparisons with observational data from 115 observation stations of the German Weather Service³ located in the CCLM028 model domain are used. Wind speed and wind direction in 10 m, precipitation, sea level pressure and total cloud cover were compared to model data.

The analyzed track data for storm Christian were provided by the German weather service (von Storch et al., 2014). The satellite data used for

³ WebWerdis (<http://www.dwd.de/webwerdis>)

comparison were taken from NOAA and METEOSAT⁴. 12-hourly sounding measurements at the observation station Schleswig in Northern Germany served as a reference for simulated vertical wind profiles. The data were provided by the University of Wyoming⁵.

5.2.3 Methods of added value determination

This study focuses on the added value of very high-resolution RCM simulations for storm situations. Hereby, the added value of convective-permitting simulations in comparison to coarser RCM simulations is divided into potential added value (prerequisites for added value exist, but added value remains to be shown) and added value and can be demonstrated as described in the following:

Potential added value:

- higher spatial resolution and more complex roughness length
- more detailed coastlines or orography
- more abundant and varying vegetation and soil characteristics
- simulation of very small-scale dynamical atmospheric processes

Added value:

- more realistic high-resolution atmospheric features and patterns in comparison to e.g. satellite data or vertical sounding data
- smaller bias/RMSE compared to observations
- positive Brier Skill Score, which serves as a measure of simulation quality
- positive sign test over statistical measure at a station in comparison to observations
- percentile distributions closer to measurements

The Brier Skill Score (BSS; von Storch and Zwiers, 1999) was used to test which of the two RCM simulations provides a more realistic representation of

⁴ NOAA / METEOSAT, Satellite data. <http://imkhp2.physik.uni-karlsruhe.de/~muehr/archive.html>

⁵ Sounding data. <http://weather.uwyo.edu/upperair/sounding.html>

various meteorological variables in comparison to measurement data. It represents a measure of quality for comparing two simulations against each other with measurement data serving as a reference. In this study the modified BSS after Winterfeldt et al. (2010) was used, which is given by:

$$BSS = \begin{cases} 1 - \sigma_{SH028}^2 \sigma_{CoastDat}^{-2} & \sigma_{SH028}^2 \leq \sigma_{CoastDat}^2 \\ \sigma_{CoastDat}^2 \sigma_{SH028}^{-2} - 1 & \sigma_{SH028}^2 > \sigma_{CoastDat}^2 \end{cases}$$

where σ_{SH028}^2 and $\sigma_{CoastDat}^{-2}$ represent the error variance of the CCLM028 and the CCLM240 simulations. The error variance is the square error of the modelled variable compared to the observation. The BSS can vary between -1 and +1. Positive values represent a better performance of the high-resolution simulation CCLM028. Negative values represent a better performance of the coarse-resolution simulation CCLM240 in comparison to measurement data. The error variances for both RCM runs are computed with DWD measurement data serving as a reference.

To merge different BSSs, a sign test (von Storch and Zwiers, 1999) was used, in this case the two-sample problem was avoided. The sign test counts how often the BSS is positive or negative for a station, storm, or variable. Here, the sign test either to merge the BSSs for all available stations for each storm and variable individually or to merge the BSSs for all storms at each station and for all variables is used. Subsequently the probability P that the BSSs are positive in at least k cases at a certain station was calculated by

$$P = \sum_{n \geq k} \frac{m!}{n! (m-n)!} 0.5^m$$

where m represents the number of storm events, which are considered, n represents the number of storm events with positive BSSs, and k is the number of storm events with positive BSSs at the respective station. This probability determines the level of significance. The significance was calculated for all storm events merged at each station. The application of this test for all stations merged for each storm is not possible because the stations are not independent of one another.

Another index, which is used to show an added value, is the root mean square error (RMSE). The RMSE is given by:

$$RMSE = \sqrt{\frac{1}{n} \sum_{i=1}^n (x_i - y_i)^2}$$

where x and y are the observed and modelled variables. The BSS is the ratio of the RMSE of the CCLM028 and the CCLM240 simulations. For the calculation of the BSS and RMSE, hourly measurement data and RCM output data were used for the duration of each storm event.

For the investigation of the potential added value of the convective-permitting RCM simulations, ten important high-impact storms over Northern Germany of the last 20 years were examined. Table 5.1 lists all ten storm events and the time period the CCLM028 model domain was affected by the storm. The number of hourly values, which are used for the calculation of the BSS, varies between 48 and 96 for the different storm events. The model domain of the high-resolution simulation CCLM028 is not large enough to capture the entire development of all investigated storm cases. The incorporation of the storm origin regions may result in an improved storm representation as the storms would have more time to develop inside the model domain at high resolution, featuring presumably more realistic dynamical processes. However, to include all ten storm origins, which were analyzed in this study, the model domain would have been enlarged to a size about as large as the CCLM240 domain. This would increase the computing time enormously. In addition, such a large model domain would request the use of spectral nudging, which also increases the computing time by about 15%, to keep larger weather phenomena close to observations as the model would otherwise tend to simulate alternative weather states for certain weather situations (especially those with little exchange via the lateral boundaries, e.g., von Storch et al. (2000)). However, due to the limited model domain of CCLM028, the storm tracks are close to observations even though no spectral nudging was applied.

The simulated storms analyzed in this study were tracked with a simple tracking algorithm (Feser and Storch, 2008b) on the basis of sea level pressure and near-surface wind speed. For the tracking, the sea level pressure fields were digitally filtered (Feser and von Storch, 2005) so that only the spatial scales of interest (370 km to 100 km) remained. In the first step, sea level pressure minima were detected, which were then combined to tracks according to different selection criteria like minimum track length, wind speed threshold, or maximum storm travel distance between two time steps.

5.3 Case study Christian

In the following section, a single storm is evaluated in more detail in order to show differences in the regional-scale storm dynamics and associated atmospheric patterns between the coarse and the high-resolution RCM simulations.

5.3.1 Storm description and development

Storm Christian of October 2013 was chosen because it was a very fast moving low-pressure system and also a very intense storm. It led to large amounts of damage due to its early occurrence in the year, which meant that many still densely foliated trees were blown over (Haeseler and Lefebvre, 2013). The storm featured high wind gusts and caused a lot of damage, especially in the area of the model domain. Storm Christian formed on the 26th of October 2013 over the Western Atlantic of the Northeastern coast of the US. It moved along the southern coast of England and the North Sea, crossed Denmark where it reached its maximum intensity (von Storch et al., 2014), and then headed across Sweden and the Baltic Sea towards Finland and Russia. Christian was a low pressure system which proceeded with a forward speed of 1200 km in 12 hours (Haeseler and Lefebvre, 2013). It was a so-called Shapiro-Keyser-cyclone, named after the cyclone model of Shapiro and Keyser (1990). Such a cyclone does not show much of a classic occlusion like normal low-pressure systems. Instead, the cold front is weaker, intersects the warm front at a right angle, and the warm air is located close to the low-pressure center.

5.3.2 Added value of the high resolution simulation

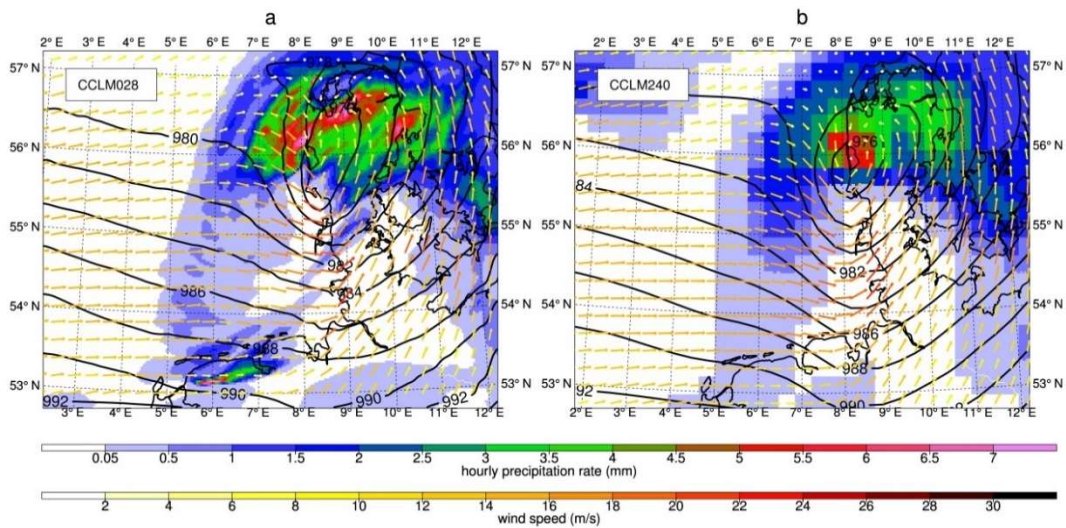


Figure 5.2: Precipitation rate (shaded areas) in combination with wind vectors and isobars (black lines) for storm Christian on October 28, 2013, 12 UTC. a) CCLM028, b) CCLM240.

Storm Christian was tracked as described in Chapter 5.2.3. The storm tracks represented in the CCLM240 and the CCLM028 simulations (Figure 5.1a, blue and green lines) show a more southerly position (about 150 km) than the track deduced from a sea level pressure analysis performed by the DWD (Figure 5.1a, red line). The modelled storms move slightly faster than the one derived from observations. Figure 5.2 shows the precipitation rate, pressure field and wind speed on October 28, 2013, at 12 UTC. The cold front passes the model area between 9 and 15 UTC. In the 2.8 km simulation (Figure 5.2a), the cold front can be detected by an increased precipitation rate and a ‘nose’ in the pressure field. This ‘nose’ is typical for a cold front, which results from a rapid increase in pressure behind the cold front. In the CCLM240 simulation (Figure 5.2b), these features cannot be seen. However, both simulations show a change in wind direction. Other high-resolution details of the CCLM028 simulation are clear weather spots behind the cold front caused by small-scale dynamical processes. The ceilometer backscatter intensity for storm Christian (Figure 5.3) at the Hamburg weather mast station (see Figure 5.1) shows clear patches behind the cold front (total cloud

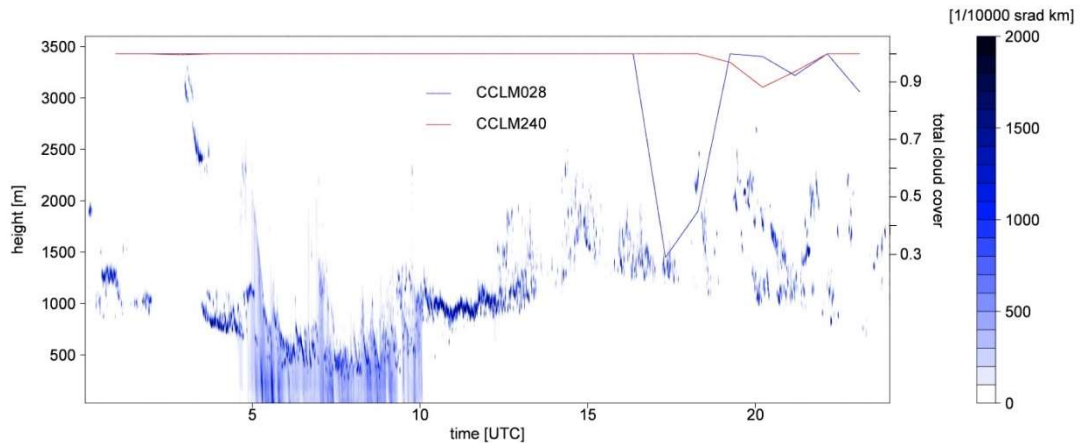


Figure 5.3: Ceilometer backscatter intensity at Hamburg weather mast (see Figure 5.1) for storm Christian on October 28, 2013, 00 UTC – October 29, 2013 00 UTC in $1/10000$ sr km. The lines represent the time series of total cloud cover at weather mast Hamburg (see Figure 5.1) for CCLM240 (red) and CCLM028 (blue).

cover of 30%). These are visible in the simulated total cloud cover of the CCLM028 simulation (Figure 5.4a, c), but not in the CCLM240 data set (Figure 5.4b, d). A satellite image⁶ (Figure 5.4e) of October 28, 2013, 13 UTC, confirms the cloud-free area behind the cold front. This feature can also be seen in Figure 5.4a-d, which show the total cloud cover for the entire model domain at 13 and 14 UTC. Again, the areas of clear and partly cloudy skies were only simulated by the 2.8 km simulation.

Another striking feature of the storm is the post-frontal subsidence. Directly behind the cold front strong downward motions dominate, before typical convective motions arise, which leads to cumulus clouds and some scattered showers. The area of the post-frontal subsidence moving eastwards is clearly visible in Figure 5.4a and c for CCLM028 as well as in the satellite images (Figure 5.4e). In Figure 5.4c there are cloud free areas at the North Sea coast and a clear sky band over the south east part of Hamburg (white colors) with a cloud cover between 0% and 20%, which are not present at the same time in the CCLM240 simulation (Figure 5.4d). In addition, the satellite image shows these spots with a quite similar structure. Cloud free spots over the North Sea and along the Coast and the clear sky band over Hamburg is visible

⁶ NOAA / METEOSAT, Satellite data. <http://imkhp2.physik.uni-karlsruhe.de/~muehr/archive.html>

in Figure 5.4e, which can be identified by green colors over land and blue colors over sea in this case. Since the low pressure system is slightly faster in the model simulations than in the analysis of the German weather service, the cold front and the highest wind speeds cross the city of Hamburg more than

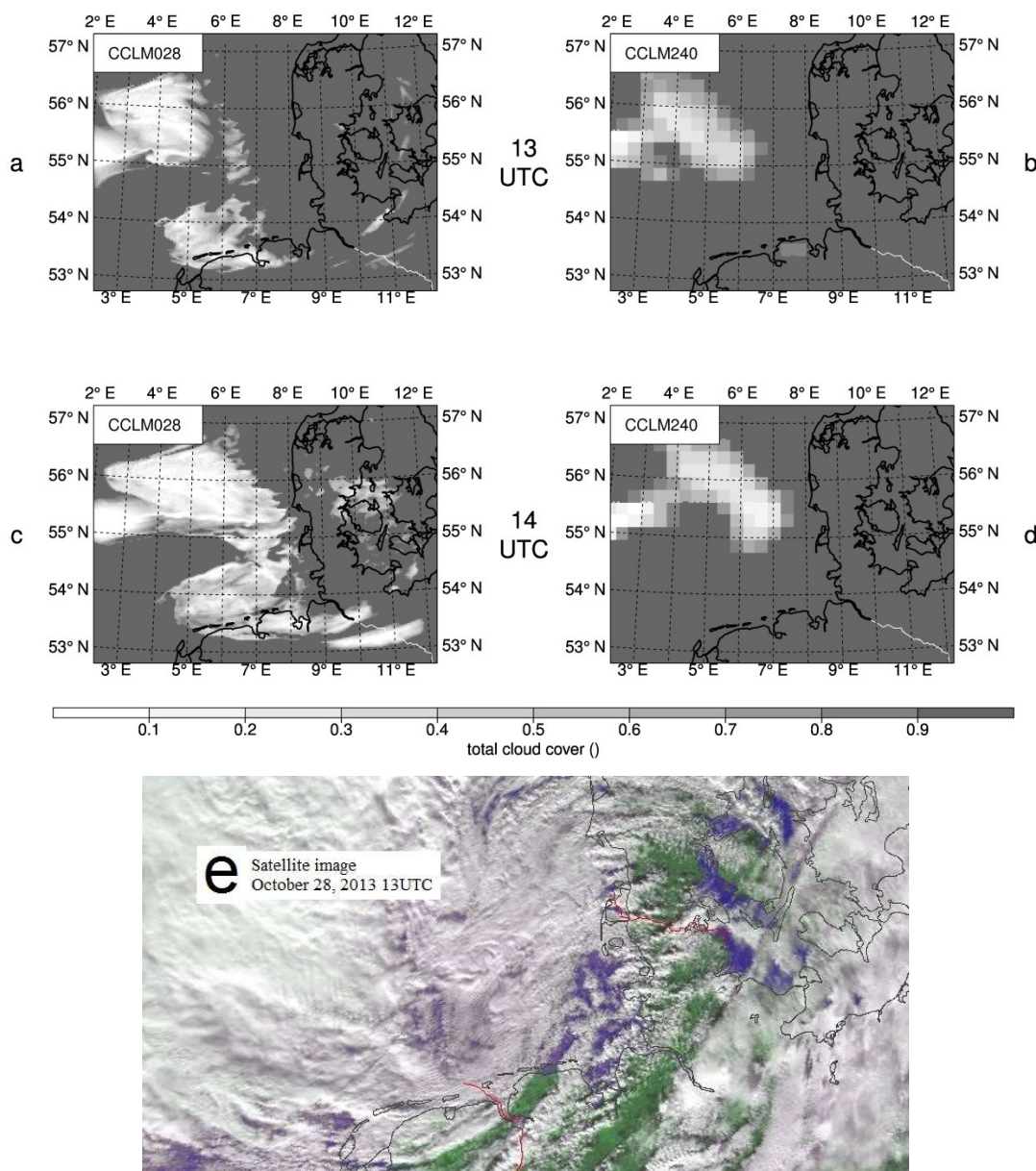


Figure 5.4: Total cloud cover for storm Christian on October 28, 2013, 13 and 14 UTC for CCLM028 (a, c) and CCLM240 (b, d) at 13 UTC (a, b), 14 UTC (c, d). Grey shows a high backscatter signal and consequently clouds or precipitation. White areas represent cloud-free skies. Satellite image of October 28, 2013, 13 UTC © DLR (e) White represents clouds, green represents visible land areas and blue represents visible sea areas. This means that areas with blue and green have cloud-free skies.

two hours earlier in the simulations compared to the observations. The vertical wind profile at the location of the Hamburg weather mast, depicted in Figure 5.5, shows the maximum wind speed during the intense phase of storm Christian on the 28th of October, 2013, which means that the values can come from different times between 00 UTC and 23 UTC. The simulated maximum wind speeds are underestimated in comparison to the measured ones in all heights, also in 10 m. On the contrary, for most time steps, the modelled 10 m wind speed of both simulations is overestimated in comparison to the 10 m Hamburg weather mast observations.

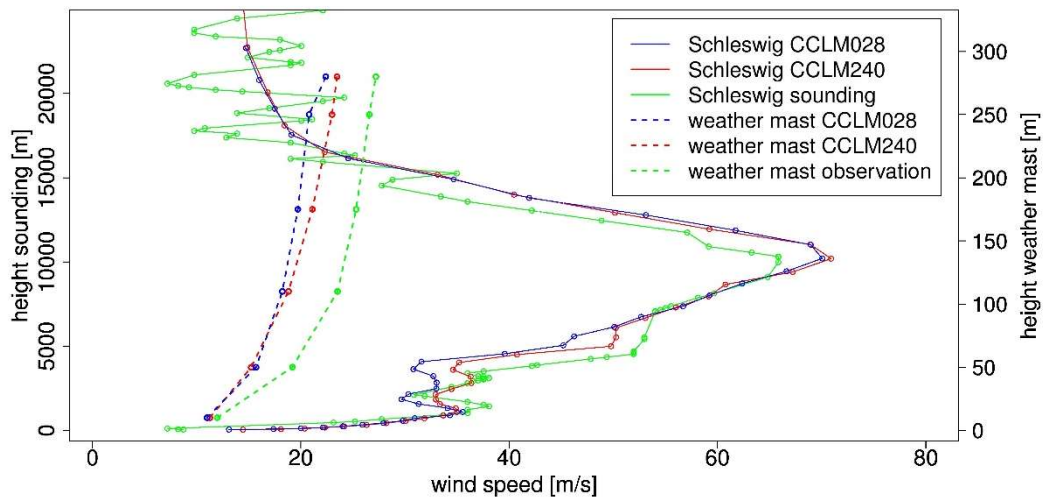


Figure 5.5: Vertical wind profile at the Schleswig station in Northern Germany (see Figure 5.1a) for CCLM240 (red) and CCLM028 (blue) compared with sounding measurements (green) on the 28th of October 2013 at 12 UTC (solid lines). Vertical wind profile at weather mast Hamburg in CCLM240 (red) and CCLM028 (blue) in comparison with the weather mast Hamburg measurements (green, for its location see Figure 5.1a) for the maximum mean wind speed during storm Christian on the 28th of October, 2013 (dashed lines).

Figure 5.5 represents the vertical wind profile at the station Schleswig on the 28th of October 2013, 12 UTC, for all model levels up to 22 km. Upper air sounding measurements serve as a comparison. The simulations are in good agreement with the vertical profiles of the sounding measurements. Figure 5.6 shows sea level pressure and 10 m wind speed at the Hamburg airport meteorological weather station. The measurements show lower pressure values than the simulations, but the temporal evolution is very similar. The highest wind speeds occur shortly after the cold front passage, which is

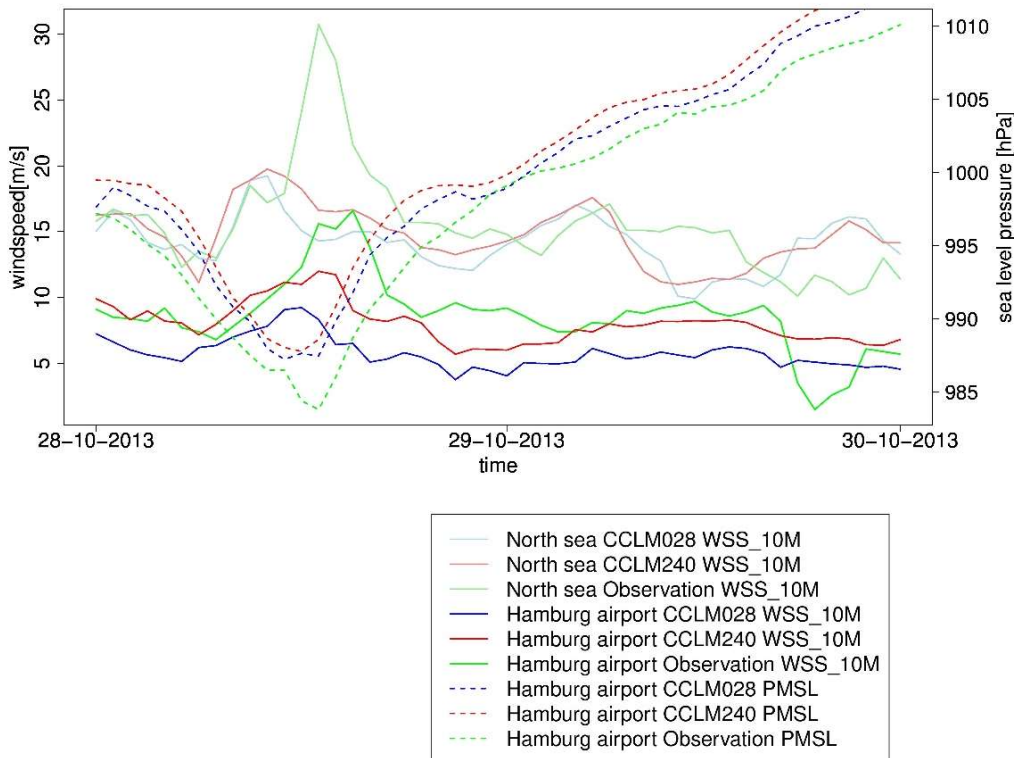


Figure 5.6: Time series of storm Christian in CCLM240 (red), CCLM028 (blue) and observations (green) for the Hamburg airport station (strong colors) in Northern Germany (see Figure 5.1a) and for a buoy in the North Sea (light colors). Shown is 10 m wind speed (solid lines) and sea level pressure (dotted lines).

marked by a sea level pressure minimum. The wind speed peaks on the 28th of October 2013 (12 UTC to 15 UTC) are visible in both simulations, but in the simulations the front passes Hamburg about 2 hours earlier than in the observations.

Finally, the BSS for storm Christian between CCLM028 and CCLM240 in comparison to DWD station data was computed at all available stations for the variables wind speed, wind direction, total cloud cover, mean sea level pressure, and total precipitation (Figure 5.7). Green indicates positive BSSs and thus an added value for CCLM028 compared with CCLM240. Negative BSS values (added value for CCLM240) are plotted in orange to red, white dots show BSS values around zero (indicating a similar quality for CCLM028 and CCLM240), and black dots represent missing values. The numbers of stations with positive, negative or zero value BSSs are given in Table 5.2. For storm Christian, the largest added value is found for mean sea level pressure

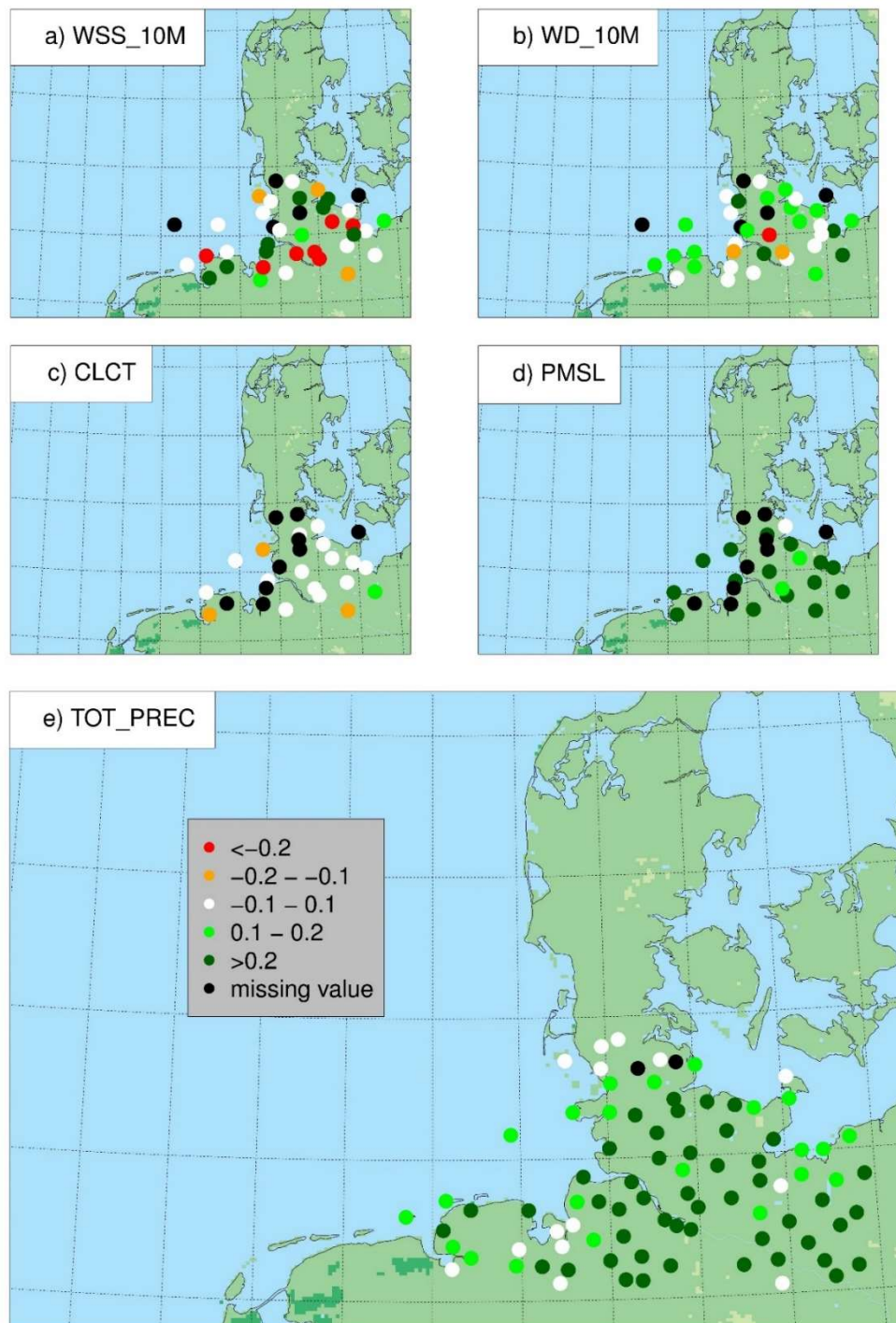


Figure 5.7: Brier Skill Score between CCLM028 and CCLM240 in comparison to DWD station data for storm Christian at all available DWD stations for the variables: a) wind speed (WSS), b) wind direction (WD), c) total cloud cover (CLCT), d) mean sea level pressure (PMSL), and e) total precipitation (TOT_PREC). BSS values larger than 0 (green) indicate an added value for CCLM028 compared with CCLM240. Negative BSS values (added value for CCLM240) are plotted in orange to red. White dots show BSS values around 0 (CCLM028 and CCLM240 have similar quality) and black dots represent missing values.

and precipitation. The BSS is positive at almost all stations (no negative values) and thus indicates an added value for CCLMo28 for these variables. A weak added value is apparent for wind direction, while for total cloud cover and wind speed both RCMs are of about the same quality. However, the values of the improvements described by the BSS are generally small. Therefore, the added value shown for the synoptic comparisons like the improved precipitation at the cold front or the improved postfrontal

Table 5.2: Number of stations, which show a positive or negative BSS, corresponding to Figure 5.7.

	Positive BSS	Negative BSS
WSS	15	18
WD	22	11
CLCT	7	11
PMSL	18	0
TOT_PREC	80	4

subsidence is more important.

5.3.3 Conclusion

This study was performed in order to analyze if very high-resolution RCM simulations would return an added value for extreme events like storms in comparison to coarser model runs. A very high-resolution simulation is carried out with the regional climate model COSMO-CLM for Northern Germany and the German Bight with a grid distance of 2.8 km.

Winter storm Christian of October 2013 was discussed in detail to show small-scale meteorological features of the high-resolution simulation. For this storm, the high-resolution CCLMo28 simulation shows more convective and more intense precipitation at its cold front in comparison to the CCLM240 simulation, which could not resolve these small-scale patterns. The convective precipitation is produced by deep convective cumulus cloud, which is produced explicitly with CCLMo28. The precipitation is not so intense if it is produced with the deep convective parameterization used in

CCLM240. Behind the cold front, post-frontal subsidence and partly clear skies were simulated by CCLMo28 in contrast to the coarser simulation. The grid distance of CCLM240 is too small to show this small band of cloud-free area because the descending motion of the air mass is restricted too locally. The regionally simulated wind speeds for storm Christian are lower than the observed ones. A Brier Skill Score analysis for storm Christian between the regional simulations and DWD station data as a reference was computed at all stations. The largest added value for CCLMo28 was found for mean sea level pressure and precipitation, followed by wind direction, but generally, the BSS values were small. For wind speed and total cloud cover, both RCM data sets are of about the same quality.

5.4 Added value in multiple storm analysis

5.4.1 Determination of added value

In this chapter, the added value of the high-resolution RCM simulations in comparison to measurement data for ten storm cases described above is analyzed. BSSs were computed between CCLMo28 and CCLM240 in comparison to DWD station data for all storm cases at each station available for five variables: wind speed, wind direction, total cloud cover, mean sea level pressure, and total precipitation. Further, a sign test (see Chapter 5.2.3) was computed which counts how often the BSS is positive or negative for all storms available at each station. Figure 5.8 shows the percentage of storm cases with a BSS larger than zero, which indicates – as green dots – an overall added value of CCLMo28 compared with CCLM240. White dots represent a value of 50% for the sign test (the same quality for CCLMo28 and CCLM240), while red dots show values smaller than 50% (CCLM240 performs better in comparison to observations). The numbers in the dots give the percentage of positive BSS values. For several storm events and variables, station measurements were not available, so the total number of stations varies between the individual sign tests.

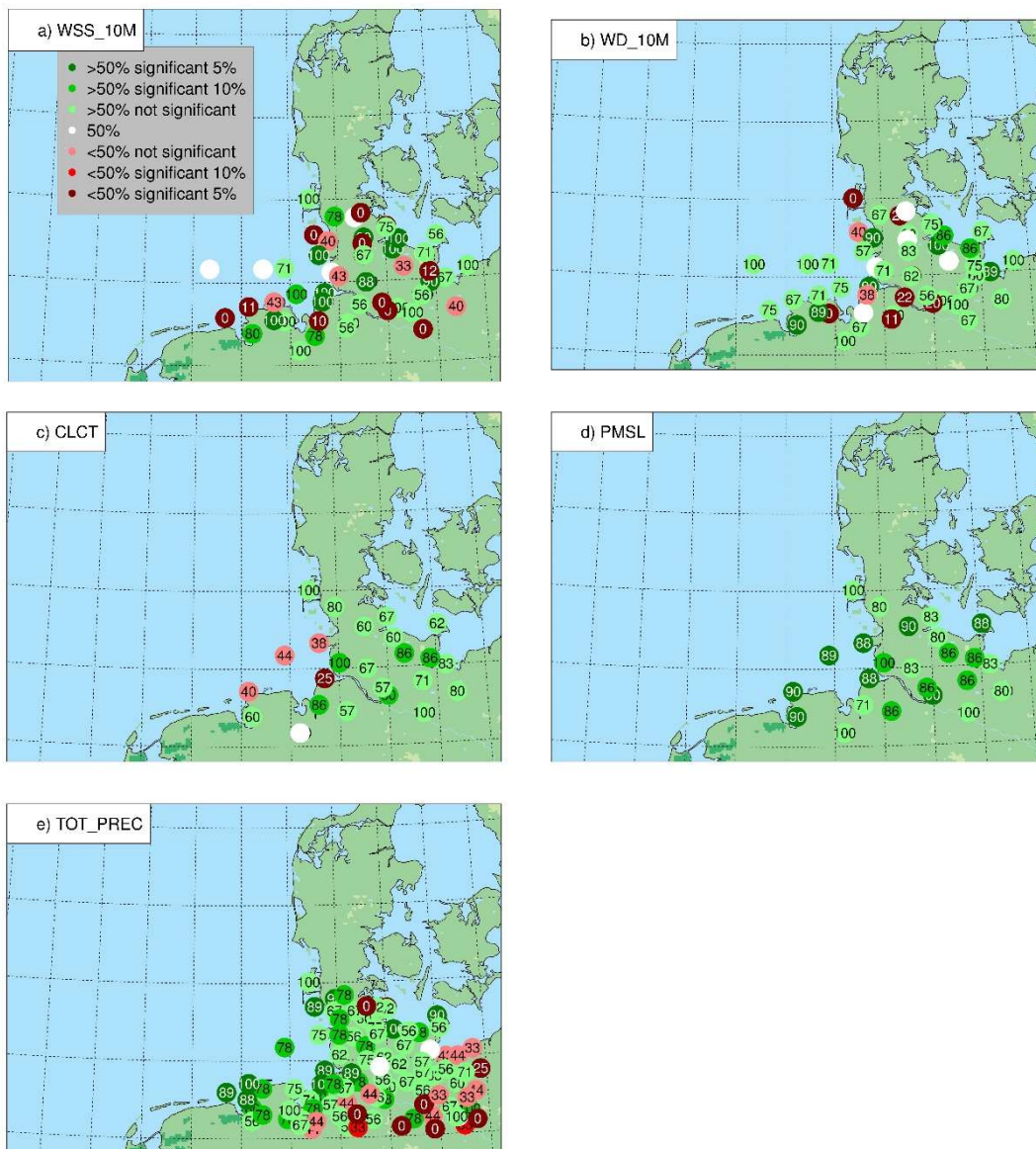


Figure 5.8: Sign test for BSS between CCLMo28 and CCLM240 in comparison to DWD station data for all 10 storms at all available DWD stations for the variables: a) wind speed (WSS), b) wind direction (WD), c) total cloud cover (CLCT), d) mean sea level pressure (PMSL), and e) total precipitation (TOT_PREC). Shown is the percentage of storm cases with a BSS larger than 0, which indicates an added value of CCLMo28 compared with CCLM240. Green dots show that more than 50% of all storm cases, which were measured at an individual station, have a positive BSS, white dots illustrate that 50% of the storm cases have a positive BSS, and red dots represent values of less than 50%. The numbers in the dots give the percentage of positive BSS values. Light colors indicate that the sign test at a station is not significant according to a significance test. Thereby very light colors represent stations where the sign test was not significant at the 10% significance level. Medium-light colors show stations where the sign test was significant at the 10% level, but not at the 5% significance level.

In addition, a significance test was performed. It tested at each station if the number of storms that did add value for either CCLM028 or CCLM240 was significant or not. Such a test of significance may be problematic, as the individual stations taken into account cannot be regarded as being independent due to their close proximity. In Figure 5.8 very light colors show stations where the sign test was not significant at the 10% significance level (SL) according to the significance test. Medium-light colors represent results, which are significant at the 10% SL, but not at the 5% SL. Dark colors show a SL of 5%. In addition to the usual 5% SL, the 10% SL was introduced because even with 10 different storm events it is hard to achieve an SL of 5%. It is quite rare that a station can provide hourly measurements for the entire duration of all storm cases. Even if this is the case, to reach the 5% SL, 9 out of 10 cases have to achieve a positive sign test. If a certain station can only provide measurements for, say, 7 storm cases, then a positive sign test is needed for every single storm in order to reach the 5% SL. Table 5.3 shows the number of stations which feature either a positive, negative, or neutral sign test.

Table 5.3: Number of stations which show a positive, neutral, or negative sign test (with 5%, 10%, or no significance), corresponding to Figure 5.8. The positive/negative sign test is defined as a positive BSS for more/less than 50% of all storm cases available at a station. Neutral sign test means that 50% of all storm cases show a negative BSS and 50% a positive BSS.

Significance	Positive sign test			Neutral sign test	Negative sign test		
	5%	10%	none	none	5%	10%	none
WSS	9	4	24	5	6	0	12
WD	7	2	31	9	3	0	8
CLCT	0	5	15	3	3	0	1
PMSL	8	6	13	0	0	0	0
TOT_PREC	11	17	44	6	13	2	10

For wind speed, the sign test is positive for most stations and thus shows an added value for CCLM028. However, the values are all small. For wind

direction, most stations do show a positive sign test, but the majority of these are not significant. The total cloud cover again features a positive sign test at most stations, with many of these not being significant. Here, only few stations right at the coast and the station on the island of Heligoland show a negative sign test. For mean sea level pressure, the sign test is positive for all stations, but again the values are small. For precipitation, which has the highest station data coverage, most coastal stations return a positive sign test, while many stations located further inland show negative values. The reason for this result is unknown, but most stations with a negative sign are located close to the lateral boundaries and are right next to the model's sponge zone, which may have had an effect, although the sponge zone was already cut off for the analysis. Even though the large majority of stations did show added value for CCLM028 precipitation, the overall values are small and most of these are not significant, thus only for the significant ones an added value for CCLM240 results. In short, sea level pressure and 10 m wind speed show the added value with the highest significance rate. Total precipitation, total cloud cover and wind direction also show an added value for the high-resolution simulation, but the SL is lower than 10% for most of the stations.

After comparing all storms at each station, now atmospheric variables at all stations for each individual storm event are analyzed. Figure 5.9 shows a bar plot of the ratio of stations with a positive BSS and smaller RMSE for CCLM028 for all storm cases and the variables of wind speed, wind direction, precipitation, mean sea level pressure, and total cloud cover. For all variables, the BSS returns an overall added value for CCLM028. Similar to the sign test at the different stations, the mean sea level pressure shows the most positive result, followed by wind direction, and then wind speed, total cloud cover, and precipitation. The RMSE shows similar results for sea level pressure and wind direction, but for precipitation, wind speed and cloud cover there is no clear added value.

Figure 5.10 shows the mean percentile-percentile distribution of 10 m wind speed at all DWD stations for all ten storm cases. The 99 dots per color represent the wind speed percentiles in steps of 1 percent from the first to the

99th percentile. Both models are close to the observations except for the

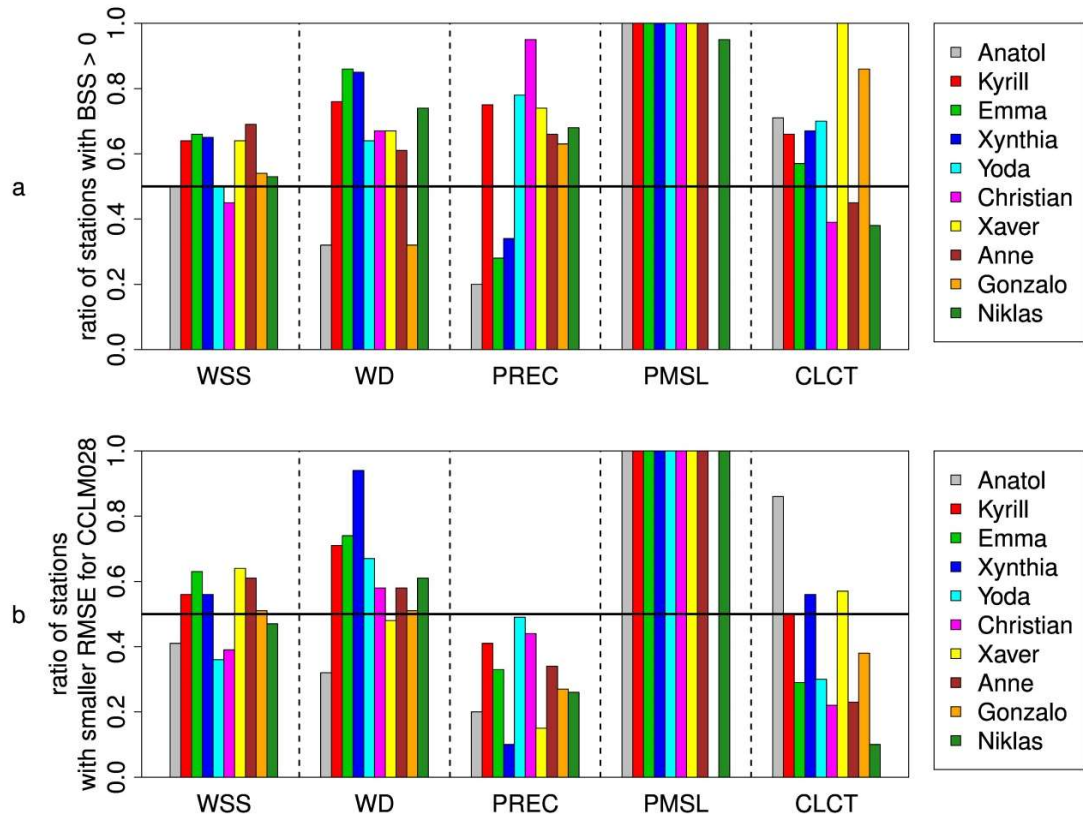


Figure 5.9: Ratio of stations with a Brier Skill Score larger than 0 (a) and smaller RMSE for CCLM028 than for CCLM240 (b) for all storm cases and variables: WSS: wind speed, WD: wind direction, PREC: precipitation, PMSL: mean sea level pressure, CLCT: total cloud cover.

highest wind speeds. For low wind speeds up to about 10 m/s, CCLM028 is closer to observed wind speeds than CCLM240, which shows slightly higher values. For wind speeds larger than 15 m/s, both models show smaller values than the observations. For CCLM028, the values are even smaller, and for the most extreme wind speeds, they converge towards CCLM240. This difference between both models for higher wind speeds will be examined in more detail in the following chapter, which takes a closer look at the roughness length of both simulations.

The 10 m wind speed RMSE between modelled and observed 10 m wind speed was analyzed for all 34 DWD stations available. For most storm cases, the majority of stations showed a smaller RMSE for CCLM028 and thus an added value for the high-resolution simulation (Figure 5.9). The 10 m wind

speed bias and time correlation in Table 5.4 show that there is an added value

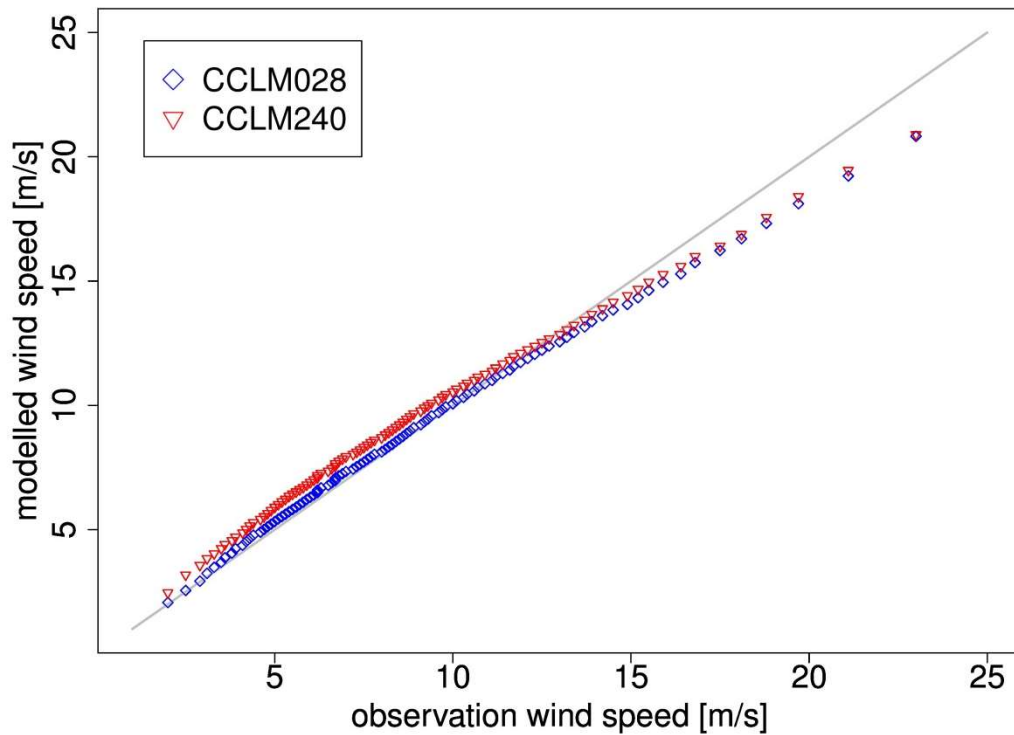


Figure 5.10: Mean percentile-percentile distribution of 10 m wind speed averaged across all DWD stations and grid points of the DWD stations for all ten storm cases. The 99 dots per color represent the wind speed percentiles in steps of 1 percent from the first to the 99th percentile of all storm events.

Table 5.4: 10 m wind speed bias [m/s] averaged over all stations and time correlation (T.C.) of CCLM028 and CCLM240 for the ten storm events.

	Anatol	Kyrill	Emma	Xynthia	Yoda	Christian	Xaver	Anne	Gonzalo	Niklas
Bias CCLM028	-1.05	0.17	0.98	0.38	0.20	0.06	-0.01	0.75	0.25	-0.47
Bias CCLM240	0.09	0.87	1.50	0.62	0.57	0.78	0.66	1.17	0.59	-0.20
T.C. CCLM028	0.75	0.77	0.82	0.69	0.83	0.34	0.90	0.64	0.26	0.17
T.C. CCLM240	0.79	0.77	0.83	0.67	0.86	0.50	0.91	0.65	0.30	0.18

for CCLM028 for the bias (mean over all stations) for most storm events. The time correlation is not improved with higher resolution except for storm Xynthia, but the values are close to the ones of CCLM240.

5.4.2 Impact of the roughness length

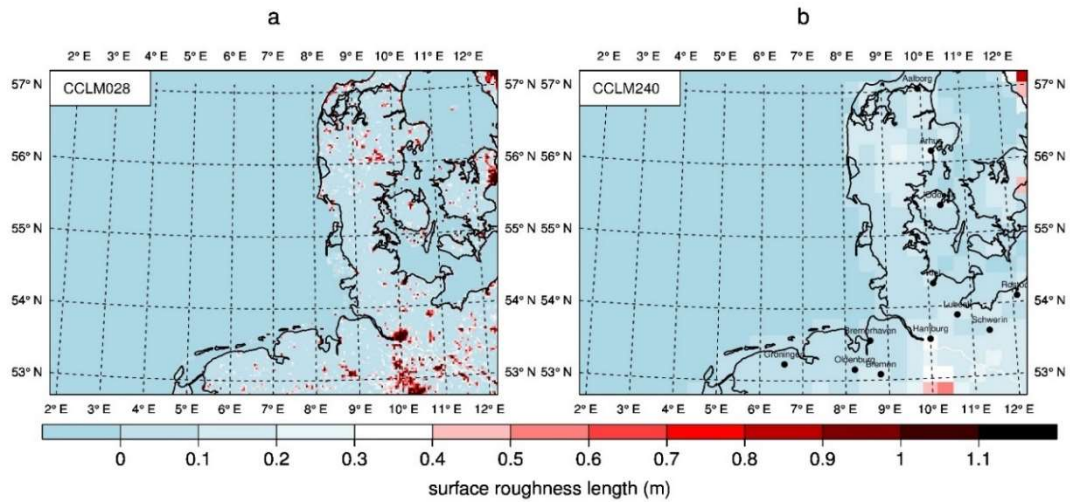


Figure 5.11: Roughness length [m] in a) the CCLM028 and b) the CCLM240 model domain. The 12 largest cities in the model domain are marked in Figure 5.11b.

Since both RCM simulations differ for the higher wind speeds (as presented in Figure 5.10), the roughness length in both models is examined, which is one of the main factors to influence modelled near-surface wind speed. As already presented in Chapter 5.3.2, Figure 5.6 shows the time series of wind speed during storm Christian (October 28 to 30, 2013) at a buoy in the North Sea and for the station Hamburg airport. Over the North Sea, both models are close to each other and to the observations, except for the largest peak on October 28, which is underestimated by the RCMs. However, the time series for the city of Hamburg (Figure 5.6) show systematically lower values for the high-resolution simulation. This different behavior of the RCMs at urban and sea stations can be explained by differing roughness length values. Figure 5.11 shows that the urban areas of CCLM028 feature larger roughness length values than CCLM240. In addition, the hilly area south of Hamburg and the hills in Denmark (Jutland) have larger roughness lengths. The 99th wind speed percentile difference between CCLM028 and CCLM240 (Figure 5.12) shows lower extreme wind speeds (selected from mean hourly wind speeds) over the cities for the CCLM028 simulation. The high roughness length values and according low near-surface wind speeds of the convection-permitting simulation pose a potential problem for comparison with observation data. Normally weather stations are built in open-space areas

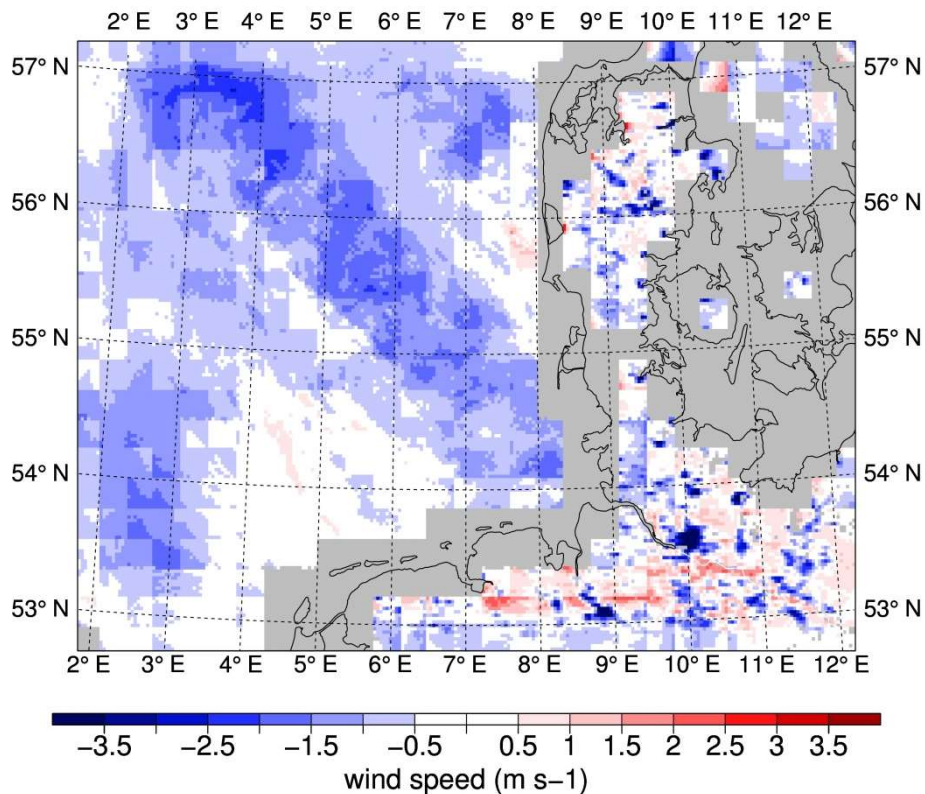


Figure 5.12: Difference of the 99th wind speed percentile between CCLM028 and CCLM240 for all ten storm events. Grey areas mark regions, which are land points in CCLM028, and sea points in CCLM240 or vice versa.

surrounded by as few obstacles as possible, but nevertheless close to the city center, e.g., at an airport. The roughness length in this flat countryside is not representative for the adjacent city areas, where more dense construction can be found and thus higher roughness length values prevail. The results therefore suggest an underestimation of the CCLM028 near-surface wind speeds in urban areas in comparison to observations, even though they are presumably more representative for cities than the coarser RCM simulation.

5.4.3 Conclusion

This study analyzed if convection-permitting high-resolution RCM simulations can provide an added value for strong storm and high wind conditions in comparison to RCM runs which use parameterized convection. The convective-permitting simulations were carried out with the RCM CCLM (Steppeler et al., 2003; Rockel et al., 2008) with a grid distance of 2.8 km (CCLM028) for Northern Germany and the German Bight, forced by a

coarser (about 24 km grid point distance) CCLM simulation (Geyer, 2014). Ten high-impact storm events between 1999 and 2013 were selected and examined for potential added value of CCLM028 in comparison to CCLM240.

Statistical analysis, such as the Brier Skill Score and a sign test of the 10 storm events, showed an added value for the high-resolution RCM simulation compared to the coarser simulation for many variables. Added value is apparent here for mean sea level pressure, wind speed, precipitation, wind direction, and cloud cover, but again the BSS values were small and therefore not as distinct to show added value as the synoptic comparisons.

A wind speed percentile-percentile distribution revealed an added value for lower wind speeds up to about 15 m/s for CCLM028 in comparison to CCLM240. For higher wind speeds, CCLM240 is slightly closer to the observations, while both RCMs show an underestimation of the most extreme wind speeds. These differences are most pronounced over urban areas, while both RCMs show very similar wind speeds over topographically flat regions like the North Sea. Such different behavior arises from varying roughness length values between both RCM runs. A more detailed roughness length, especially in urban areas, is a potential advantage of the higher resolution, but makes the comparison with meteorological weather stations more difficult. Many urban stations are not representative for densely built cities, even if they are located close to the city centers. However, the prescribed model roughness length of the convective-permitting simulation could still be improved. The whole city area shows high roughness length values greater than 1, even for areas that should have lower roughness lengths, like airports and fields, which should be resolved at this resolution.

This study revealed that convection-permitting RCM simulations can add value to coarser RCM simulations for high wind and storm conditions over the German Bight and Northern Germany in terms of synoptic comparisons such as the analysis of frontal systems. Here, the higher resolution gives more realistic results for frontal mesoscale precipitation patterns or post-frontal

cloud structures. More general statistical measures, such as the BSS or RMSE, provided less clear results in terms of added value for this study. This is in agreement with Li Delei (2016) and Di Luca et al. (2012) who suggest that exploring particular weather events may be more meaningful than statistical evaluations to detect added value. Long-term simulations covering more storm cases and using different model domains – in size and geographical location – would provide a valuable addition to our results and are planned as future work.

6 Long-term analysis

6.1 Introduction

Long-term changes of the global climate system have been observed. However, climatic long-term trends are also very important at regional scale. In particular, small-scale effects can influence the land use with respect to risk management, the calculation of renewable energies, agriculture and the attractiveness for tourism. Insurance companies need long-term homogeneous data sets at high spatial and temporal resolutions to calculate the risk for natural hazards as accurate as possible (Changnon and Changnon, 1990). Companies within the renewable energy sector, such as the wind energy or solar energy sector, need knowledge of local climatologies of wind speed and cloud cover. Agriculture benefits from the knowledge on the climate and extreme events at regional scale as agricultural production suffers from higher temperatures. In addition, agricultural systems are very sensitive to changes in rainfall. Higher rainfall intensities increase the risk of erosion and flood, whereas droughts increase the risk for reduced crop yield. Also protecting agricultural land from storms could be necessary with increasing storminess (IPCC, 2014). The influence of long-term climate trends and climate change on the local tourism is large. An increasing risk of storm surges can reduce beach tourism and inhibits further economic development of coastal areas. The time period with attractive conditions for

tourism can shift and the change in precipitation frequency and intensity may discourage tourists. Consequently, for all points mentioned, there is a multifaceted need for climatological knowledge. One approach to bridge this knowledge gap is the identification of possible climatological trends through the analysis of meteorological data of climate model simulations as well as through indices calculated from model results.

For instance, an often used index is the North-Atlantic-Oscillation (NAO) index, which describes the variable position and strength of the Azores high-pressure system and the Icelandic low-pressure-system. It is used to quantify long-term storminess, storm-track changes and also temperature changes in Europe (Dawson et al., 2002; Hurrell and Deser, 2010; Iles and Hegerl, 2017). However, the derived estimates are merely approximations. Several studies exist that deal with long-term trends of station measurements, which are good estimates of trends for a single point of measurement, yet they are often indifferent about the behavior in the close surrounding and between weather stations, especially for heterogeneous meteorological variables. For the region of Hamburg, a detailed overview over climate change is given by von Storch et al. (2017b).

Another example for an index-based analysis is provided by Roshan et al. (2016) who used the Tourism Climate Index of Perch-Nielsen et al. (2010) to investigate the effect of climate change on tourism for Iran for 1961-2010. They used meteorological station measurements and found that spring and summer seasons offer the best climatic conditions for tourism in Iran. A related study was done by Caloiero et al. (2017) for Southern Italy, where long-term trend analyses of the monthly mean temperatures based on 19 station-based time series for the period 1951–2010 were conducted. They found that the temperature showed a clear upward trend in warmer seasons over the years, while the trend analysis of the extreme indices revealed trends that were almost balanced between significant positive and negative.

The use of global or regional climate simulations or gridded observational data sets with relatively coarse grid distances of 15-20 km or more is another

approach used in many studies, which focus on climate trend analyses of the past. Using this method the whole area of interest is covered by pseudo-station data providing a better spatial and temporal coverage than station measurements. However, note that the coarse resolution of the model or gridded observation possibly lacks small-scale regional details. The following paragraph provides examples of recent analyses or applications of long-term trends for various regions in the world on the local scale.

For instance, such an analysis performed across the Caribbean using the gridded observational CRU data (resolution of 0.5°) from 1951-2012 shows no trends in precipitation, but a statistically significant warming everywhere in the Caribbean (Jones et al., 2016). A potential increase in thunderstorm occurrences and intensity is found in the Alps (Scheffczyk and Heinemann, 2017) showing the added value of highly resolved model simulations. Meinke et al. (2014) developed an information product for Northern Germany (Klimamonitor⁷), where station measurements and different hindcast simulations (e.g. coastDat II and CRU) can be combined to outweigh discrepancies between observational and modelled data. Here, all data sets show a warming of about 1.2°C in the recent six decades for northern Germany. For South America, Barkhordarian et al. (2017) present non-anthropogenic temperature trends by calculating trends of 30-year segments from a 20,000 years simulation. They concluded that the observed trends are consistent with the anthropogenic forcing. Suursaar et al. (2015) analyzed the storminess in Estonia using station data, but also a long-term wave hindcast. They could not confirm any increasing long-term trend for storminess. There are further high-resolution climate trend analysis studies with the necessary resolution for regional details. However, most do not focus on atmospheric meteorological aspects or consider only a time period of 10-20 years. Groll and Weisse (2017) evaluated a wind-wave hindcast for the North Sea for the period 1949-2014 and concluded that the hindcast provides useful data for assessing wave climate variability and risk analysis.

⁷ Klimamonitor (<http://www.klimamonitor.de>)

Summarizing, several studies exist, which evaluated the impact of anthropogenic climate change on regional and local meteorological parameters. However, they either lack the necessary spatial resolution, cover too short temporal periods, or do not include all relevant parameters. By means of a gridded high-resolution (say, less than 3 km) long-term data set, which currently is very rare, regional and local structures are resolved in contrast to point- or station-measurements or coarsely resolved model simulations. The simulation computed for this study is one of the first with a very high resolution of 2.8 km, which covers the past 67 years for Northern Germany and the German Bight.

In this part of the thesis meteorological parameters, which are important for the local tourism and also for agricultural cultivation, are analyzed. These are the 2 m temperature, the precipitation amount, the Convective Available Potential Energy (CAPE), the 10 m wind speed, and wind gusts. At first, the multidecadal trends and their regional impacts are investigated. In the second part, the extreme events, which could cause damages and have negative effects on tourism and agriculture, are examined, also for trends. The question, how the climate changed and how the regional changes are structured, is answered by analyzing a long-term high-resolution hindcast simulation.

6.2 Model configuration and methods

For the long-term evaluation one consistent and uninterrupted CCLM simulation is analyzed, which was calculated with the same settings and domain as in Chapter 5 (Schaaf, 2017). In the following, this high-resolution long-term simulation will be referred to as GBO028. The simulation was run from January 1948 to August 2015. This is exactly the time period of coastDat II, which was used as forcing data. Therefore, 67 whole years of homogenous meteorological data are available for the evaluation of long-term trends. This is one of the first of such long-term climate model simulations at a very high resolution of 2.8 km.

Annual mean values (annual sums for precipitation) and 99th percentiles were calculated. Linear trends of the considered variables were calculated through linear regression, using the least squares method. For the evaluation of temporal tendencies, the annual and extreme trend indices were tested with the non-parametric Mann-Kendall test (Mann, 1945; Kendall, 1975). The tests are carried out at the nominal 5% level of significance. The serial correlation was tested after Venables and Ripley (2002) and it was found that there is no autocorrelation for yearly values except for 2 m temperature and CAPE. In these cases the critical value corresponding to one value every three years, was used, as described in Chapter 4.2.2. Additionally, the trend over the area-averaged values was calculated to evaluate the interannual variability and significance of the trends. All trends were calculated for the time period 1948 – 2014 and are valid for this interval only as it is not possible to extrapolate the behavior of time series before or after this interval. Some trends of extreme events differed between land and sea area. In these situations, single grid points in Hamburg, Schwerin and over the North Sea were picked to compare the differing trends over the cities and the open ocean.

6.3 Comparison with QuikSCAT data

This section aims at a short validation of 10 m wind speed long-term data of the GBoo28 simulation with observations. Therefore, a comparison with the QuikSCAT dataset - a homogenous gridded data set of wind speeds described in Chapter 2.4.3- and with coastDat II (Chapter 2.3) was performed. The BSS was calculated as described in Chapter 5.2.3. It aims at showing an added value over a period of 10 years from 1999 until 2009 in 10 m wind speed and not only for strong storm events as done in Chapter 5. The evaluation is done quite similar as given in Chapter 5. For the calculation of the BSS, the GBoo28 data were used as forecast data and coastDat II as the reference. The error variances are calculated with QuikSCAT satellite data as observational data. The GBoo28 data were bilinearly interpolated to the same resolution for all data sets (grid distance of 12.5 km) in order to achieve a reasonable

comparison. The BSS could only be computed for time steps where the satellite data are available, which is up to once a day.

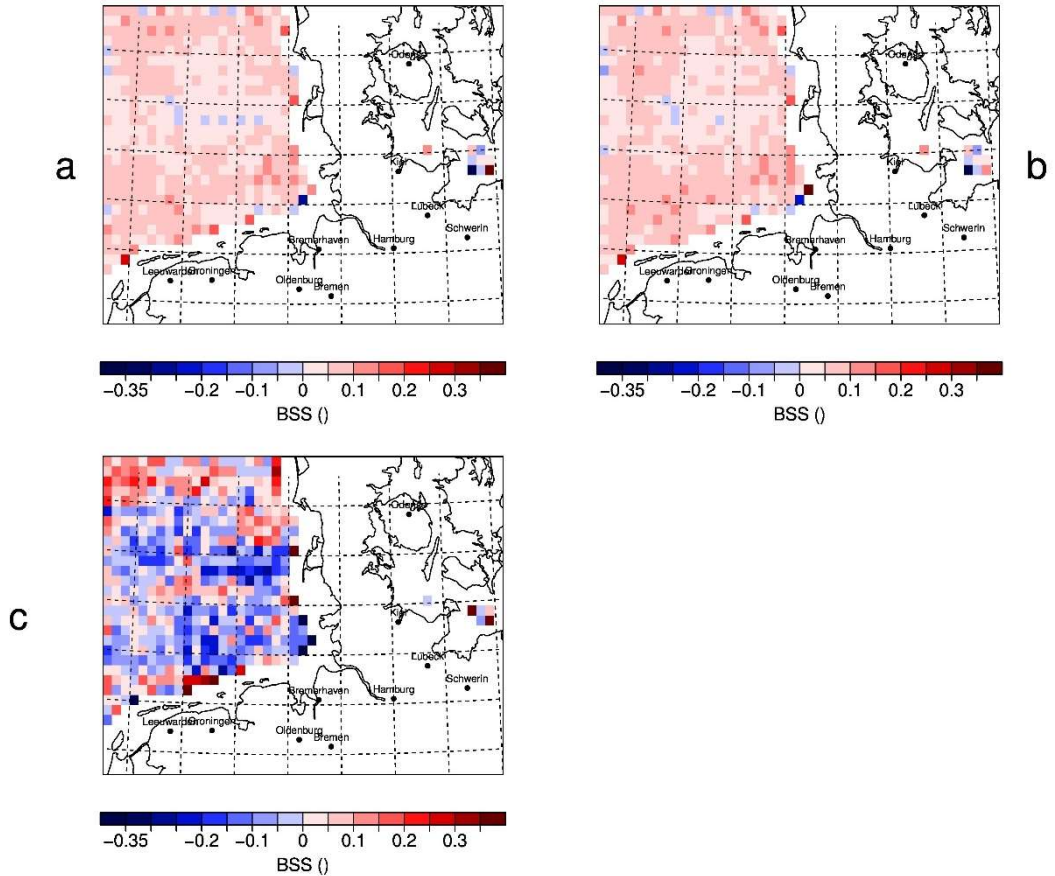


Figure 6.1: BSS between GBo028 and coastDat II in comparison to QuikSCAT satellite data for 10 m wind speeds between a) 3 and 25 m/s, b) 3 and 15 m/s and c) 15 and 25 m/s.

The BSS shows very low positive values between 0.1 and 0.2 (Figure 6.1a). All wind speeds measured by the satellite (from 3 m/s to 25 m/s) and all time steps (about 3500 during the 10 years of data) were considered. The BSS has small values, but is positive all over the North Sea. This indicates a weak added value for the 10 m wind speed in the GBo028 simulation compared to the coastDat II data set. Geyer et al. (2015) found for coastDat II a stronger added value for higher wind speeds in comparison to the forcing NCEP reanalysis. Strong added value was found for wind speeds higher than 12 m/s and even stronger added value for wind speeds higher than 17 m/s. Also for lower wind speeds smaller than 12 m/s a weak added value for coastal areas was found. In the case of high wind speeds, the added value is no more

limited to coastal areas, but also present for open ocean areas. This means that CoastDat II performs better for strong wind conditions than the NCEP reanalysis data with QuikSCAT as reference and is more advantageous to use. Now, the question arises whether the added value of GBO028 compared to coastDat II is also mainly due to the high wind speed conditions. Therefore, a classification into low and high wind speeds was done. The BSS was calculated separately for the interval from 3 to 15 m/s (Figure 6.1b) and for moderate to storm conditions from 15 to 25 m/s (Figure 6.1c). What needs to be taken into consideration is the resolution of the QuikSCAT data of 12.5 km, which is closer to coastDat II than to the convection-permitting GBO028 and may thus influence the results. In the convection permitting simulation, the opposite to the behavior of the comparison coastDat II to NCEP is found. The BSS analysis of GBO028 compared with coastDat II shows a positive signal for the low wind speed situations in the same magnitude as for all wind speeds (Figure 6.1a). However, there is no clear BSS signal for high wind speeds. There are more negative than positive BSS values for wind speeds higher than 15 m/s in the German Bight. At these points, no added value can be detected. This means that a resolution of 24 km (coastDat II) resulted already in high improvements for high wind speed conditions (Geyer et al., 2015), which could not be further improved by the convection permitting resolution of 2.8 km. The added value of the 2.8 km resolution compared to coastDat II lies in the low wind speed condition. For these low wind speeds, coastDat II did not add value compared to NCEP, except in coastal areas. The added value in coastal areas was a result of the more detailed coastline in the domain. In contrast, GBO028 shows an added value for the whole North Sea. These results confirm the results of Chapter 5.4.1 and Figure 5.10.

6.4 Trend analysis over Northern Germany 1948-2014

In this chapter, a long-term trend analysis was conducted for different variables, which are in interest of renewable energies, tourism or agriculture.

This section is divided into two parts. In the first part, annual mean values and total values for precipitation are presented. The second part contains extreme events with percentile calculations and maximum / minimum values.

6.4.1 Annual means

Figure 6.2 shows decadal trends of a set of variables, which are of particular interest and importance for renewable energies, tourism and agriculture. Presented are the decadal trends between 1948 and 2014 of the annual values. The value of the decadal trend denotes the average change of the linear trend in a time period of 10 years. Grid points are marked with small black dots, if the trend signal of a grid point is significant according to the Mann-Kendall-test. Shaded areas indicate a statistical significance at the nominal 5% level. The time series of the area-average (Figure 6.3) reveal the interannual variability, which may show the reasons for the lack of significance.

The trends of the 2 m temperature (Figure 6.2a and Figure 6.3a) and 10 m wind speed (Figure 6.2b and Figure 6.3b) show the strongest signals with the highest significance for the entire model domain. Both show a clearly positive signal. The 2 m temperature trend has a weak gradient from north to south. The highest trend with 0.17 °C decadal increase of the annual mean temperature can be found at the southern edge of the model domain, in Northern Germany. The weakest trend with 0.12 °C per decade occurs in Northern Denmark, at the Northern edge of the model domain. The trend values are relatively small for the period 1948-2014. This is a result of a slight cooling from the fifties until the eighties (see time series), which could be caused by increased aerosol concentrations (Schultze and Rockel, 2017), but that still needs to be clarified. The trend from the eighties until the present is much higher. The interannual variability has a maximum of 2 °C, which is strongly significant. The 10 m wind speed also shows a positive trend for the entire model domain with a clear land-sea-separation. There are decadal trends of 0.08 m/s in the annual mean wind speed over the North Sea, where the highest absolute wind speeds occur. The further inland, the weaker is the

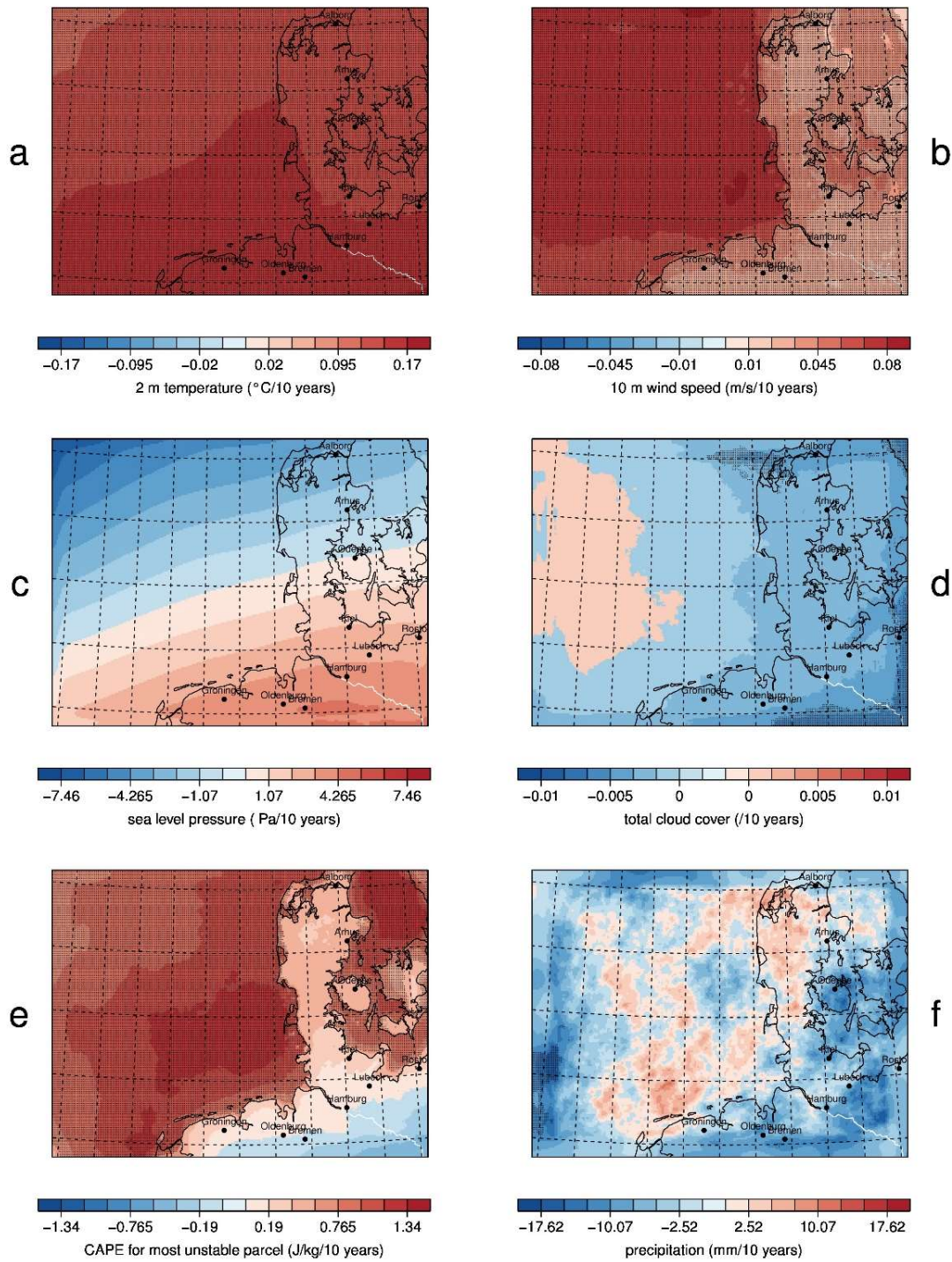


Figure 6.2: Decadal trend over 67 years of a) yearly mean 2 m temperature, b) yearly mean 10 m wind speed, c) yearly mean sea level pressure, d) yearly mean total cloud cover, e) yearly mean CAPE, f) yearly sum of precipitation. Shaded areas indicate a statistical significance at the nominal 5% level.

trend, but still positive with smallest values of 0.005 m/s. The patterns of the roughness length are visible in the trend, so that local effects of cities can be seen. In cities, where the absolute wind speed is reduced because of the high

roughness length, also the weakest trends are visible, compared with the surrounding areas. The positive trends mainly result from increasing mean wind speeds in the eighties and nineties, where a phase of high storm activity took place (Alexandersson et al., 2000). After that phase, a decrease in storminess can be observed until it increases again in the beginning of the 2010s.

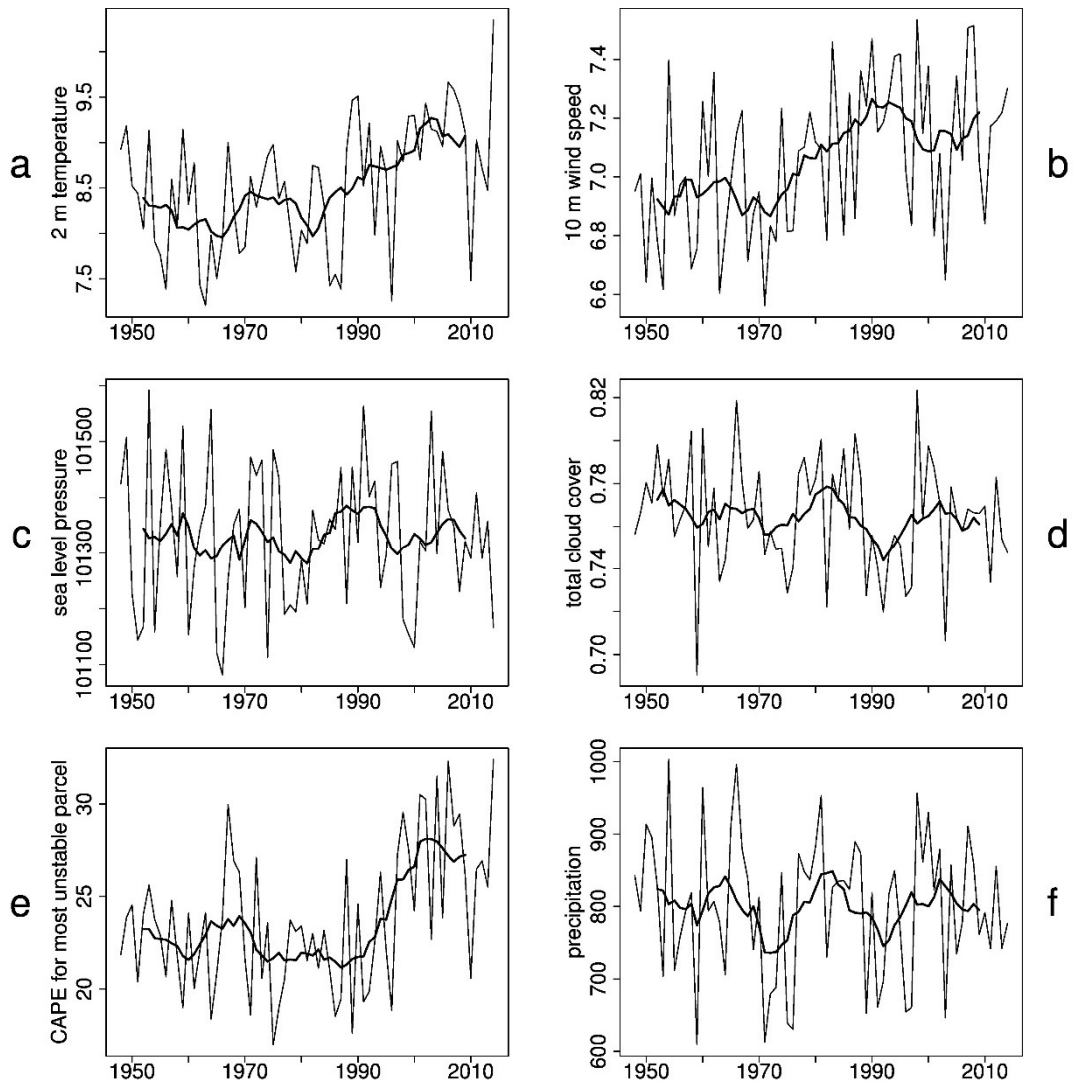


Figure 6.3: Time series over 67 years with 10 years running mean (bold line) of a) yearly mean 2 m temperature, b) yearly mean 10 m wind speed, c) yearly mean sea level pressure, d) yearly mean total cloud cover, e) yearly mean CAPE, f) yearly sum of precipitation.

The variability of wind speed and storminess in the model domain follows mostly the NAO index (Figure 6.4a) whereas the 2 m temperature trails the

secular temperature trend due to climate change as seen in the global temperature (Figure 6.4b). Many studies (Dawson et al., 2002; Matulla et al., 2008; Hurrell and Deser, 2010; Iles and Hegerl, 2017) use the NAO index for analyzing changes in wind speed and temperature. However, the 10 m wind speed is mainly influenced by the NAO index (Figure 6.4a) and not much by the climate change signal in the form of global temperature change. The time correlation between the NAO index and the 99th percentile of 10 m wind speed is 0.76 for the 10 years running mean and 0.32 for yearly values. Both curves in Figure 6.4a have a high correlation especially since the seventies, which confirms the findings of Matulla et al. (2008). The

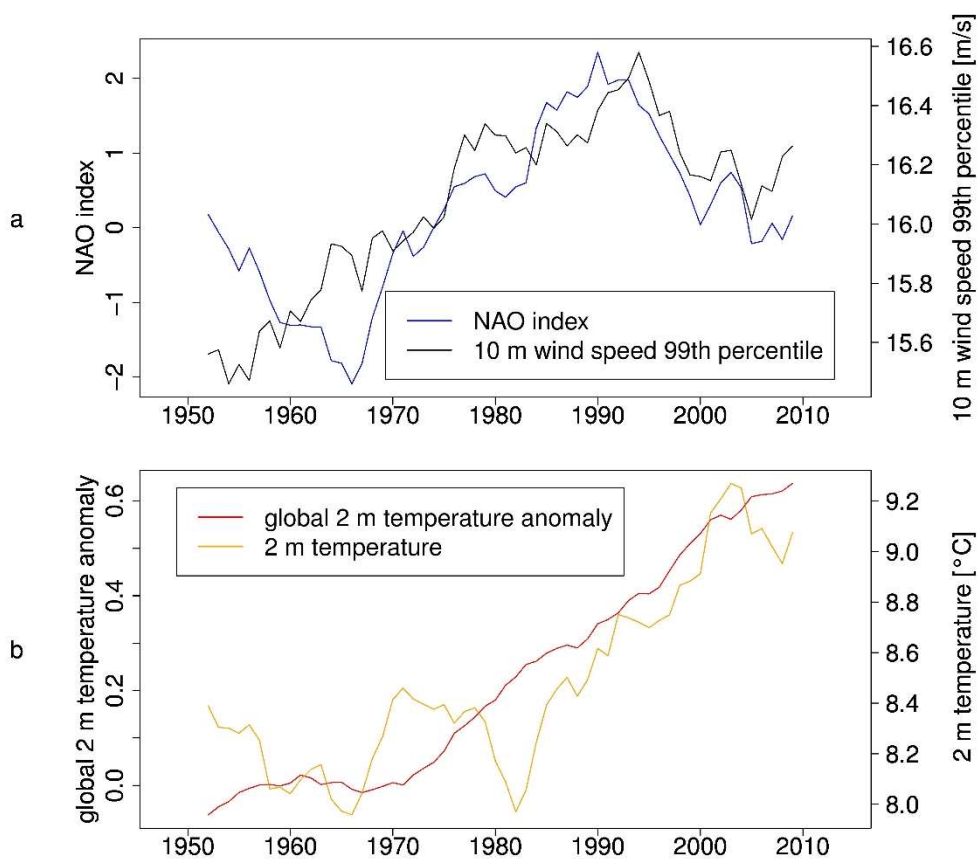


Figure 6.4: 10 years running mean between 1948 and 2014 of a) NAO index and 99th percentile of 10 m wind and b) global 2 m temperature anomaly (base period: 1901-2000) and 2 m temperature of GBo028.

correlation between the wind percentiles and the global temperature anomaly is low (0.2), which confirms that there is not a strong link between these variables. The 2 m temperature has a correlation of 0.87 with the global mean temperature anomaly (Figure 6.4b), which means that the behavior of the

temperature in Northern Germany is quite similar to the behavior of the global mean temperature. The temperature in Northern Germany starts to rise in the eighties, but global climate change already started in the middle of the 20th century.

Trends in the sea level pressure (Figure 6.2c and Figure 6.3c) and total cloud cover (Figure 6.2d and Figure 6.3d) are both weak and not significant. For sea level pressure a strong north-south gradient is visible with negative values in the north and positive values in the south, which could point to a northward shift of low-pressure systems, which would agree with (Barcikowska et al., 2017) or (Barcikowska et al., 2018). However, the trend values between +5 and -7 Pa per decade and the missing significance make the assumption very vague. For the total cloud cover one can see a slight reduction of the cloud cover, especially over land. However, it is not significant. The time series of both variables also show no clear trend, no clear decadal phases and high interannual variability.

The Convective Available Potential Energy (CAPE) for most unstable particles (MUCAPE) is the highest possible CAPE and not surface-based. Its value results from rising the most unstable air package regardless of its height. High MUCAPE values larger than about 800 J/kg imply a high potential for thunderstorms. If the MUCAPE values are higher, there is more energy “in the air” and thunderstorms become more likely. The MUCAPE mainly increased significantly over sea areas (Figure 6.2e), where the MUCAPE is normally relatively low and thunderstorms are rare also because of flat orography. The time series of the annual MUCAPE means (Figure 6.3e) shows that the positive trend over the sea originates from the last two decades of the analyzed time period.

The trend in the precipitation amount (Figure 6.2f and Figure 6.3f) is not significant for the whole model domain. The interannual variability is quite high and the model mean precipitation amount varies between 600 and 1000 mm per year. Nevertheless, the trend shows decreasing precipitation, especially Northern Germany becomes dryer, while no trend is present over

the North Sea and Denmark. The strong negative values at the boundaries has to be ignored. The boundary effect of the relaxation zone possibly extends further into the model domain than the sponge zone for precipitation as already assumed in Chapter 5.4.1.

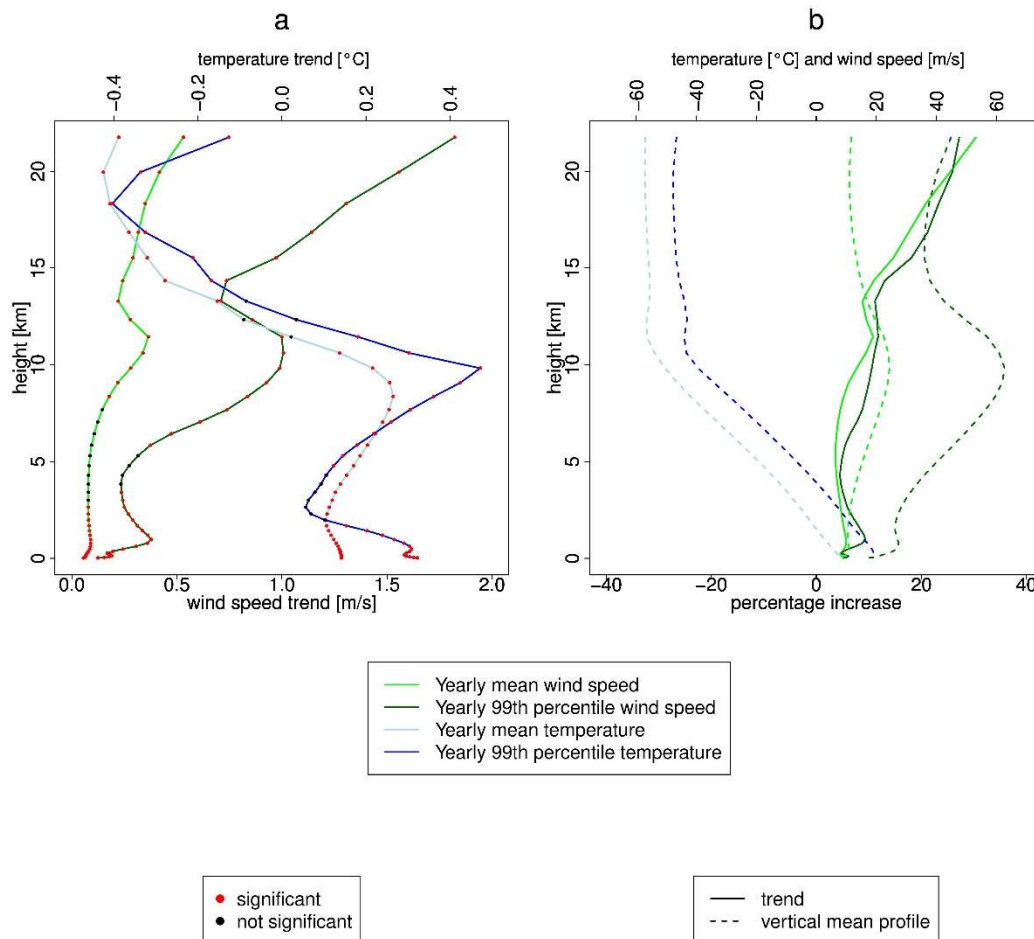


Figure 6.5: a) Trends of the domain mean and yearly mean (light colors) or yearly 99th percentile (strong colors) wind speed (green) and temperature (blue) for all 40 model levels. Every dot represents a model layer, a red dot shows that the trend is significant and a black dot indicates a non-significant trend. b) Percentage trends of wind speed of the domain mean and yearly mean (light colors) or yearly 99th percentile (strong colors) for all 40 model levels (solid lines) and the domain mean and 67 years mean wind speed (light colors) or 67 years mean of yearly 99th percentile (strong colors) (dotted lines).

Looking at the vertical trend of temperature and wind speed (Figure 6.5a) reveals a noticeable dependency of both trends on height. The positive trend of the wind speed increases with height. This increase is significant in all heights except for the height between 4 and 8 km. The temperature trend

decreases with increasing height and becomes negative at the top of the atmosphere at a height of about 13 km and above. This is the case as well for the mean temperature and for the extreme temperature trend (99th percentile). However, the 99th percentile of the wind speed shows a different behavior. The extreme wind speeds show a much more intense increase of the trend with increasing height. A trend of 2 m/s per decade is present at the top of the troposphere. The absolute values in this height are certainly higher than in the boundary layer. Further, the relative trend (Figure 6.5b) also shows that the trend increases with height for the mean and extreme wind speed at the same extent. However, it is not clear, as to whether the trends are caused by the regional climate model, or whether the forcing data (especially at the top of the model domain, where the Rayleigh damping takes place) affects the modelled variables and possibly induces artificial trends.

6.4.2 Extreme events

The occurrence of extreme events indicated by percentiles or the frequency of events beyond a certain threshold are also noteworthy and important for renewable energies, tourism and agriculture in addition to the annual mean values. Additionally, the question arises: Are there local effects in extreme events, which occur only in small and confined areas?

To get a general overview of the development of storminess in the last seven decades, different percentiles of the 10 m wind speed are evaluated (Figure 6.6). Additionally, the percentiles of the coastDat II simulation for the same area were added to the figures. One can see a similar behavior in the 90th, 95th and 99th percentile curves. There was a stormy phase in the nineties with high percentile values and a decrease of the extreme wind speeds afterwards. This result is similar to the result in Chapter 6.4.1 on the mean 10 m wind speed trend. The percentile values of coastDat II are systematically higher than the values of GBo028. The reason is presumably the different and higher spatially resolved roughness length in the GBo028 simulation. The differences in the roughness length are discussed in Chapter 5.4.2 in more detail. Looking at the percentiles in higher model levels (not shown), the GBo028 values get closer to the coastDat II values, and in the free

troposphere, the percentiles of GB0028 are even higher than the coastDat II percentiles (also not shown). This confirms the assumption that the lower

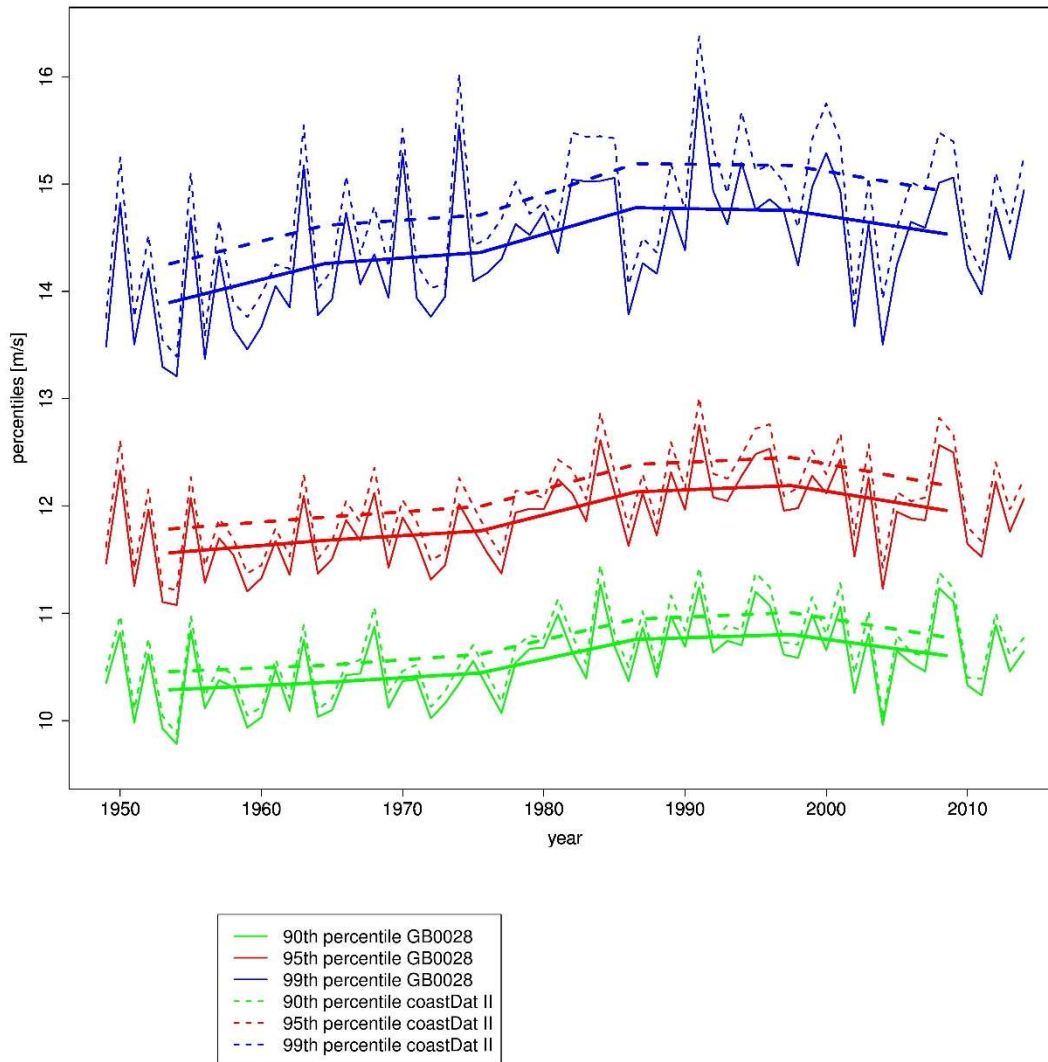


Figure 6.6: Time series of yearly 90th (green), 95th (red) and 99th (blue) percentile of 10 m wind speed of the domain mean. Solid lines represent the GB0028 simulation and dashed lines coastDat II. The 10 year running mean lines are added.

wind speeds at the surface are strongly influenced by the roughness length.

For evaluation of extreme events, it is suitable to evaluate annual percentiles of the considered variables in order to compare all years over the entire period of GB0028 devoid of intra-annual cycles. The 99.9th percentiles are calculated for hourly data, i. e. the values of only nine hours per year are more extreme than the shown value. The 99th percentiles are calculated for

daily data, which means that only on three days a year more extreme values can be found. The trend analysis of a set of meteorological variables is

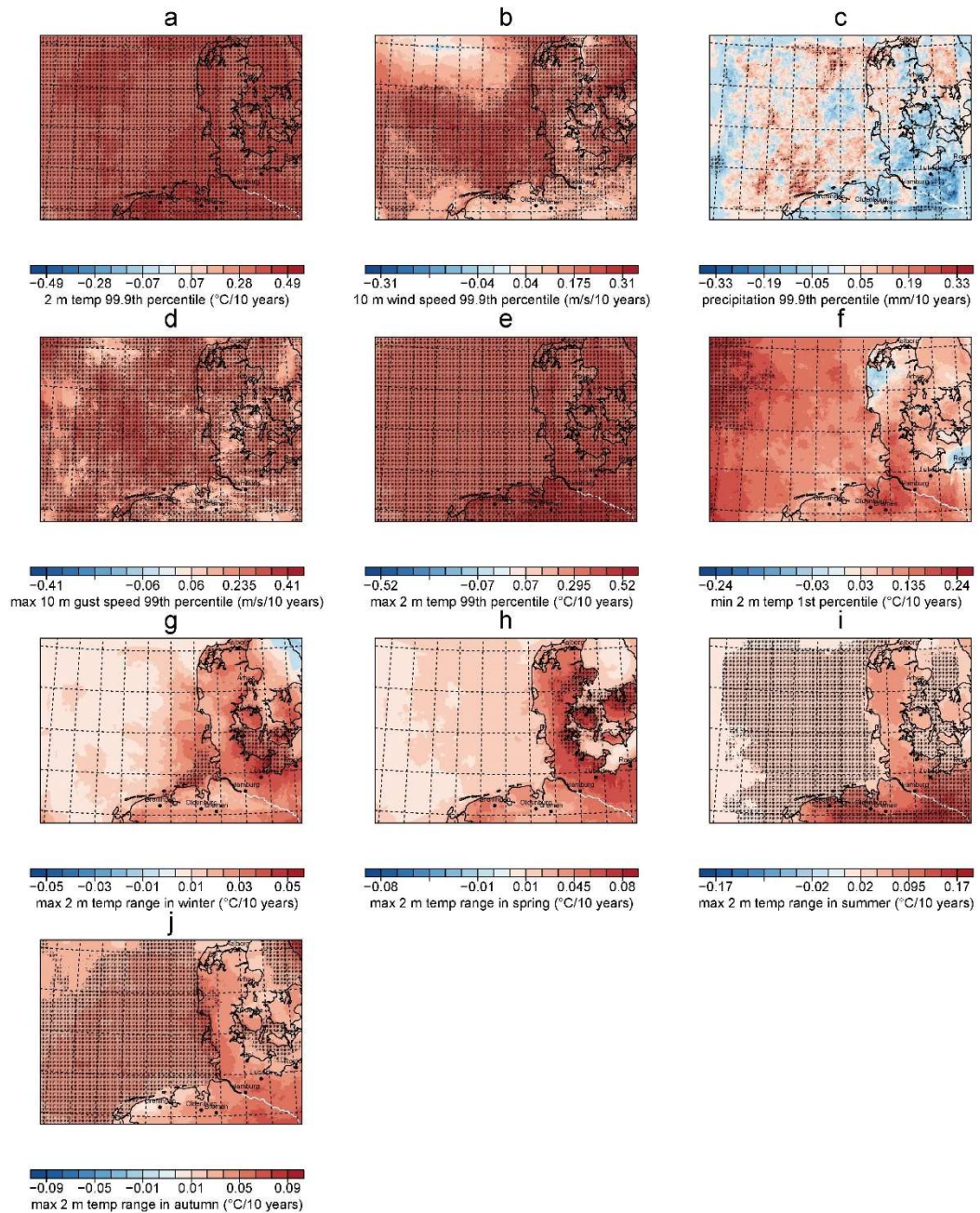


Figure 6.7: Decadal trends over 67 years of a) yearly 99.9th percentile of 2 m temperature, b) yearly 99.9th percentile of 10 m wind speed, c) yearly 99.9th percentile of precipitation, d) yearly 99th percentile of maximum 10 m gust speed, e) yearly 99th percentile maximum 2 m temperature, f) yearly 1st percentile of minimum 2 m temperature, g) maximum 2 m temperature range in winter, h) maximum 2 m temperature range in spring, i) maximum 2 m temperature range in summer, j) maximum 2 m temperature range in autumn. Shaded areas indicate a statistical significance at the nominal 5% level.

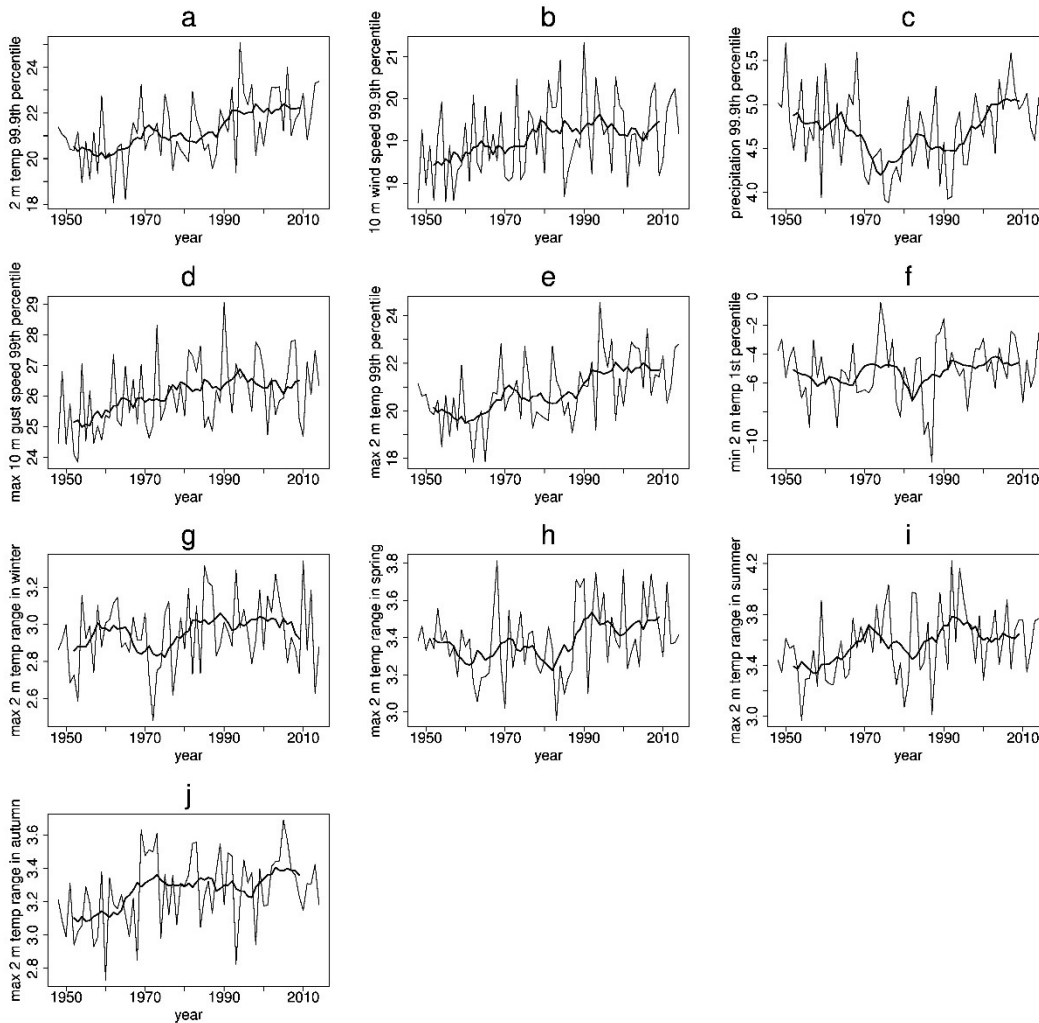


Figure 6.8: Time series for 67 years with 10 years running mean (bold line) of a) yearly 99.9th percentile of 2 m temperature, b) yearly 99.9th percentile of 10 m wind speed, c) yearly 99.9th percentile of precipitation, d) yearly 99th percentile of maximum 10 m gust speed, e) yearly 99th percentile maximum 2 m temperature, f) yearly 1st percentile of minimum 2 m temperature, g) maximum 2 m temperature range in winter, h) maximum 2 m temperature range in spring, i) maximum 2 m temperature range in summer, j) maximum 2 m temperature range in autumn.

presented in Figure 6.7 and Figure 6.8. Figure 6.7 shows the spatial pattern of the trends; Figure 6.8 associated pattern mean time series, corresponding to Chapter 6.4.1 for the annual means.

The 2 m temperature (Figure 6.7a and Figure 6.8a) shows, similar to the annual mean, an increase of the extreme values of about 0.5 °C per decade, which is statistically significant for the whole model domain. The 99.9th domain mean percentile increases from about 20°C in the fifties to about

23°C in the 2010s, which is dominated by the relatively cool temperature over the North Sea. The 10 m wind speed behaves similarly (Figure 6.7b and Figure 6.8b) with a significant positive signal especially over the German Bight region and over the North Sea where already the highest wind speeds occur. The interannual variability is very high with an intense phase of storminess in the nineties just like in the annual mean. The extreme precipitation trend (Figure 6.7c and Figure 6.8c) is quite indifferent and not significant, but it tends to be positive over the North Sea and Denmark and negative over Northern Germany. This means the highest hourly precipitation rates become lower in Northern Germany and the region of Hamburg. The time series of extreme precipitation show a less extreme phase in the seventies and eighties and more extreme precipitation before that and after that. This results in a neutral trend. The 99th percentile of the daily maximum 10 m gust speed (Figure 6.7d and Figure 6.8d) shows a significant positive trend of about 0.4 m/s per decade in the entire model domain, where the low-passed time series is very similar to the time series obtained for the annual 99th percentiles of wind speed. Quite a short period of time (regarding storminess) was examined, in which storminess generally increased even though there was a decrease in the 2000s. The trend for the entire 1948 to 2014 period is still positive. The values have the same magnitude over sea and land. There are some local structures in the trend, but no clear region, where the gust trend is favored. The stormy nineties in the time series are not so intensive for the gusts as for the wind speed without gusts. There is a continuous increase of the 99th percentile, which represents the minimum of the 3-4 windiest days (including gusts) per year.

A further important question is if the hottest (Figure 6.7e and Figure 6.8e) and coolest (Figure 6.7f and Figure 6.8f) days changed. The 99th percentiles of the daily maximum 2 m temperature show a strong significant increase of temperature with values of 0.5 °C per decade over the Northern German land areas. The trend of the first percentile of the daily minimum 2 m temperature is about three times smaller than the trend of the hottest days and is also not significant. It shows some hot spots at the North Sea Coast and in the regions

around Hamburg and Bremen. The interannual variability is higher than for the hottest days, which leads to a temperature signal being not significant.

The trend of the diurnal temperature range (DTR) is analyzed for seasonal time scales to show the different behavior of the seasons. Shown is the trend of the highest annual seasonal DTR ($T_{\max} - T_{\min}$), which is an important index of climate change (Jhajharia and Singh, 2011) and also relevant for local climatic studies in limited area domains (Schoetter et al., 2013) (Figure 6.7g-j and Figure 6.8g-j). In the winter and spring seasons there is a strong but not significant increase in the DTR over land areas. This is caused by the increasing T_{\max} . The DTR is not as strong over sea as over land, because of the temperature-dampening effect of the sea, which prevents a cooling of the air temperature at night. In the summer and autumn season, the positive trend is mainly significant and is highest as the extreme temperatures increase significantly (Figure 6.7e).

Looking at the number of days with threshold exceedances reduces inherent autocorrelation and avoids that consecutive time steps count multiple times as opposed to the 99.9th percentile of hourly data in the section before. Figure 6.9 shows the trend of the number of days of a set of climate indices and Figure 6.10 shows according time series for three different locations. Chosen were a location in the middle of the North Sea, a grid point in the center of Hamburg, and a grid point in Schwerin, a small city further inland about 100 km to the east of Hamburg located directly at a huge lake and more influenced by continental weather patterns. MUCAPE values larger than 850 J/kg imply a strong potential for thunderstorms. The number of these days (Figure 6.9a) is increasing over the North Sea with about 0.2 days per decade, but the total number of days is normally lower than 10 and therefore it is difficult to get a significant trend (Figure 6.10a). Interestingly, in Northern Germany there are decreasing numbers visible except for the area around Hamburg. This is also apparent in the time series for Hamburg, which shows a higher number of high MUCAPE days than in the one of Schwerin during the last 20 years. This results in the increasing trend. There is a large discrepancy in the number of days with 10 m wind gusts higher than

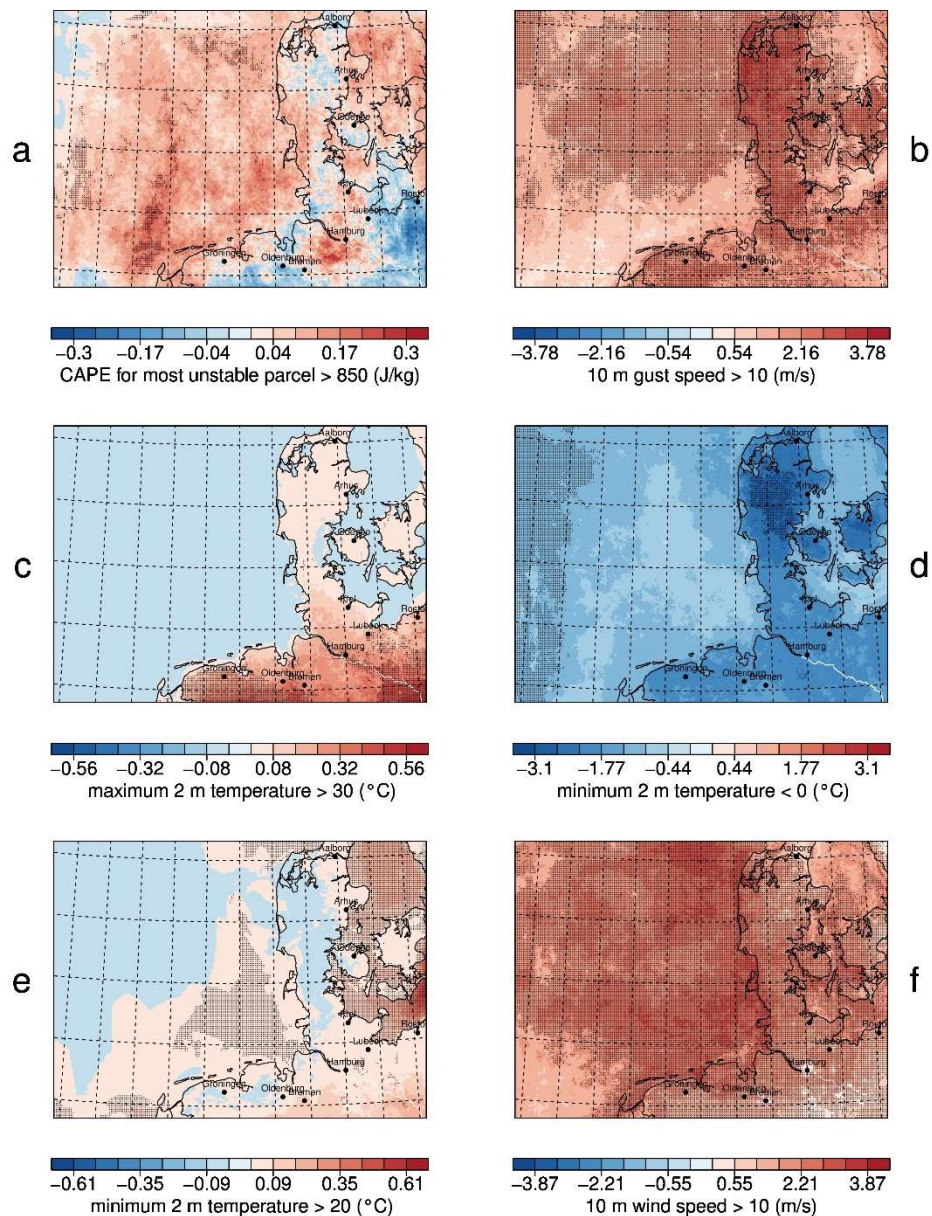


Figure 6.9: Decadal trend of yearly number of days with a) CAPE higher 850 J/kg, b) 10 m gust speed higher than 10 m/s, c) maximum 2 m temperature higher than 30 °C (hot days), d) minimum 2 m temperature lower than 0 °C (frost days), e) minimum 2 m temperature higher than 20 °C (tropical nights), f) 10 m wind speed higher than 10 m/s. Shaded areas indicate a statistical significance at the nominal 5% level.

10 m/s between the North Sea and Hamburg (Figure 6.10b). Over the North Sea there are gusts with intensities over 10 m/s almost every day, while for Hamburg such gusts happen every second day only. Although the number over the North Sea is high, the trend is not significant everywhere as the trend is weak. In Hamburg, the number of days is even lower than in

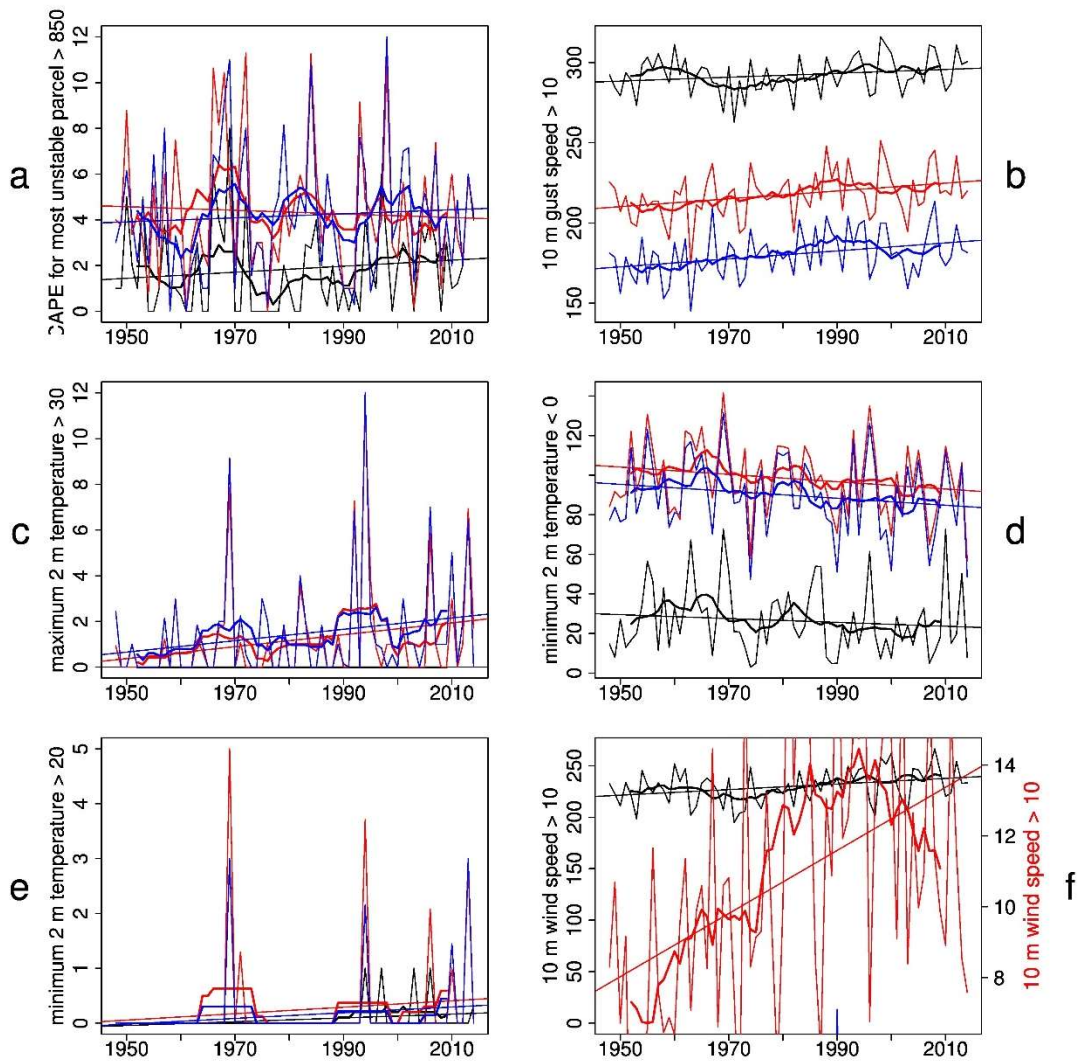


Figure 6.10: Time series of yearly numbers of days over the North Sea (black), in the city Schwerin (red) and in the city of Hamburg (blue) with a) CAPE higher 850 J/kg, b) 10 m gust speed higher than 10 m/s, c) maximum 2 m temperature higher than 30 °C (hot days), d) minimum 2 m temperature lower than 0 °C (frost days), e) minimum 2 m temperature higher than 20 °C (tropical nights), f) 10 m wind speed higher than 10 m/s.

Schwerin. However, the trend is positive in both cities (Figure 6.9b). For hot days (maximum 2 m temperature higher than 30 °C), only a trend over the Northern German mainland is visible as there are no temperatures above 30 °C in Denmark and over the sea (Figure 6.9c) due to a stronger warming of landmasses in summer times. The trend is clearly positive with an increase of 0.5 hot days per decade and is partly significant. In the first decade of the analyzed period, there is a maximum of two hot days in Hamburg and Schwerin. In more recent periods, hot days often occur more than 5 times per

year (Figure 6.10c). The number of frost days (lowest 2 m temperature below 0 °C) decreases in the entire model domain (Figure 6.9d). The magnitude of the trend is quite large with 3 frost days less per decade in Denmark, 2 days less in Northern Germany and 1 day less over the ocean. Considering the number of 20-30 frost days over the ocean and around 90 days over land, the trend is quite robust (Figure 6.10d).

Tropical nights (lowest 2 m temperature higher than 20 °C) do not occur often in the model domain, but are very important for human well-being. Over the North Sea and the adjacent land area, the number of tropical nights is increasing. From the nineties onwards they occur every year at least once (Figure 6.10e). Over the Baltic Sea the trend is stronger and significant (Figure 6.9e). Here, they occur more often due to the warmer sea surface temperature of the Baltic Sea compared to the North Sea. Also lower wind speeds and related reduced cooling over the Baltic Sea contribute to the increase. Days with 10 m wind speeds greater than 10 m/s occur less often than gust speeds exceeding 10 m/s. In Hamburg, there was only one day in the analyzed period of 67 years (in the year 1990) with a wind speed greater than 10 m/s. This is a consequence of the high roughness length in Hamburg (Chapter 5.4.2). Therefore, no trend evaluation for Hamburg is possible (Figure 6.10f). For all other regions there is a clear positive and significant trend (Figure 6.9f), likewise found for the annual mean wind speed and the 99.9th wind speed percentiles before.

6.5 Summary and discussion

The question whether and to what extent regional effects occur in the trends of the model domain of 2.8 km grid distance was answered. For this purpose, a very high-resolution simulation was carried out with the regional climate model COSMO-CLM at a grid distance of 2.8 km for this region from 1948 – 2014. Climatologies of annual mean values and extreme events of variables relevant for tourism and agricultural activities were created for Northern Germany and the German Bight.

A comparison of the new high-resolution model data with satellite wind measurements and with the coastDat II data set (24 km resolution) over a 10 years period showed an improvement in the Brier Skill Score of lower wind speeds between 3 and 15 m/s. On the contrary, the high-resolution simulation did not add any value compared to coastDat II for high wind speeds between 15 and 25 m/s.

The trend analysis revealed that CCLM provides the most distinct and significant trends for 2 m temperature, 10 m wind speed and 10 m gust velocity in the 2.8 km simulation. These variables showed an increase in the last seven decades in all of the following cases: There is an increase for annual mean values as well as for extreme events like 99th percentiles, hot days or number of windy days. The increase of the annual mean 2 m temperature of about 0.17 °C in the model domain agrees with the trend in Hamburg of 0.19 °C analyzed by von Storch et al. (2017b). The trend in temperature especially in summer is important for agricultural activities and for the crop yields (Franzaring et al., 2007). They found decreasing yields by 5-10 % for every degree temperature increase in southern Germany. Wind speeds remained mostly unchanged until the eighties confirming the findings of Schmidt and von Storch (1993), who found a stationary annual distribution of geostrophic wind speeds over the German Bight between 1880 and 1990. Thereafter, there was an intense phase of storm activity during the 1990s resulting in an overall increasing wind. The trend of the wind speed is decreasing since the end of the nineties.

No clear and no significant trend is detectable for the annual sum of precipitation and for extreme precipitation. However, there tends to be less precipitation over Northern Germany and no change in the intensity with decadal variability present, which was confirmed by Casty et al. (2007). The cloud cover seems to have been slightly reduced in the past seven decades - but not significantly. The trend of CAPE for the most unstable parcel and the number of days with potential thunderstorms slightly increased. The number of frost days became less and the coldest nights became warmer. The daily

temperature range, which is an important index of climate change, increased mainly over land areas and mainly in the summer time.

The 2 m temperature as a large-scale variable did not show any notable spatial structures. However, increasing temperatures and relatively constant precipitation intensities are favorable conditions for touristic activities. In addition, the trends in cloud cover, sea level pressure and CAPE for most unstable parcels did not show regional effects, for which the high resolution of 2.8 km is necessary. For wind speed, some local effects like lower trends in the cities are visible as the absolute wind speed is lower over areas with increased (and increasing) surface roughness. In addition, many regional small-scale details in the precipitation trends are present. However, as they are not significant at all, such details can be considered to be randomly distributed with no significant impact on the trends of precipitation. In contrast, the wind speed shows significant and reliable regional details like the city effect with lower trends in the mean wind speed, but not in the gust speed. This knowledge could be a huge advantage for the wind energy industry, knowing where to build wind farms most effectively.

7 Summary and conclusions

This thesis focused on the study of long-term trends of a very highly resolved (2.8 km) regional climate model (RCM) simulation over Northern Germany and its added value compared to RCM simulations with coarser resolution. Therefore, an ensemble of hindcast simulations using dynamical downscaling with the RCM COSMO-CLM was analyzed for this purpose. A simulation between 1948 and 2015 revealed the regional long-term trends. The area of interest was the North Sea, particularly the German Bight and the North Sea coast from the Netherlands and Germany until Northern Denmark. The model domain also covered Denmark and Northern Germany including Hamburg and Fehmarn at the Eastern boundary. A double nesting was used to increase the coarse NCEP/NCAR reanalysis of 1.875° up to a very high resolution of 2.8 km (0.025°). The simulation was performed for the time

period from 1948 until August 2015 so that 67 full years could be analyzed with this high resolution.

The major findings of this thesis can be summarized by giving answers to the following three research questions:

Does spectral nudging have an effect on dynamical downscaling applied in geographically comparatively small regional climate model domains (such as the domain size of 500 km x 700 km used for this study)?

The effect of spectral nudging on regional climate model results when using very small model domains was examined. The results show that spectral nudging is not necessary for small RCM domain sizes of only several hundred kilometers in extent over geographical flat and homogeneous terrain.

Comparing the ensemble variability of simulations with and without spectral nudging for the surface variables 10 m wind speed and precipitation on a domain size of about 700 km x 500 km showed the same negligible magnitude over sea as well as over flat terrain. The ensemble variability of the runs without spectral nudging for wind speed at 500 hPa and for sea level pressure is slightly higher. This is reasonable because at 500 hPa spectral nudging takes place in the runs with spectral nudging and the sea level pressure is a height-integrated variable. The temporal and spatial states of the ensembles with and without spectral nudging are also nearly identical for all the investigated variables.

Simulations without spectral nudging produced very similar states and fields, independently of the initialization date for the domain size chosen in this study. This is not the case for larger domain sizes (Alexandru et al., 2009). Even though the high-resolution RCM features a high number of grid points, the region is still small in absolute dimensions. At those local scales, the number of grid points is not crucial for the variability: An air parcel crosses a small model domain quickly and it will only slightly diverge from its condition at the inflowing model boundaries. This implies that the size of the domain in this study was too small to allow for internal large-scale variations.

Therefore, the lateral boundary conditions are sufficient to force the atmospheric state into a similar state for both setups.

Is there added value of convection-permitting very high resolved regional climate model simulations for simulating storms over the German Bight and Northern Germany?

The very high-resolution simulation with a grid distance of 2.8 km was compared with a simulation of 24 km grid distance for Northern Germany and the German Bight. It was found that convection-permitting RCM simulations can add value to coarser RCM simulations for high wind and storm conditions in terms of synoptic comparisons, i.e. related to the analysis of frontal systems. The higher resolution provides more realistic results for frontal mesoscale precipitation patterns or post-frontal cloud structures. More general statistical measures, such as the Brier Skill Score (BSS) or root mean square error, provided less clear results in terms of added value. This is in agreement with (Di Luca et al., 2012) who suggest that exploring particular weather events may be more meaningful than statistical evaluation for detecting added value.

The winter storm Christian of October 2013 was analyzed in detail to show small-scale meteorological features of the high-resolution simulation. For this storm, the 2.8 km simulation shows more convective and more intense precipitation at its cold front in comparison to the 24 km simulation. Behind the cold front, post-frontal subsidence and partly clear skies were simulated by the 2.8 km simulation. In contrast, the 24 km simulation did not show this small band of cloud-free area because of too locally restricted descending motion of the air mass. That result shows that the grid distance of the 24 km simulation is still too coarse to resolve those small-scale patterns. The Brier Skill Score analysis for storm Christian between the regional simulations and DWD station data as a reference showed the largest added value for mean sea level pressure and precipitation, followed by wind direction. However, generally the added value is weak because the BSS values were small.

The BSS and a sign test of ten high-impact storm events between 1999 and 2013 showed an added value for the high-resolution RCM simulation compared to the coarser simulation for mean sea level pressure, wind speed, precipitation, wind direction, and cloud cover. Again, the BSS values were small and, therefore, not as distinct to show added value as the synoptic comparisons.

An added value of the higher resolved simulation was found for lower wind speeds of up to about 15 m/s. The most extreme wind speeds higher than 18 m/s are underestimated in both, the 2.8 km and 24 km simulation, respectively. These underestimations are most pronounced over urban areas, while the underestimation of wind speeds in both RCMs is very similar over topographically flat regions like the North Sea. This arises from varying roughness length values between both RCM runs. A more detailed roughness length, particularly in urban areas, is a potential advantage of the higher resolution. However, it complicates the comparison with meteorological weather stations. Many urban stations are not representative for densely built cities, even if they are located close to the city centers.

The study therefore shows that regional climate modelling including very high resolved RCM simulations do not per se resolve all issues related to added values for various aspects. This is for instance shown by the comparison between the 2.8 km and 24 km simulations. Moreover, for certain synoptic detailed analysis, especially in the context of storms and the structure of cyclones, it is important to aim for the highest possible resolution to simulate some of the key features of storm systems, such as the frontal sectors, wind direction changes and maximum wind gusts.

Are there regional effects in the multidecadal trends of annual mean values and extreme events in Northern Germany and the German Bight?

This question was addressed in Chapter 6 for the period from 1948 to 2014. The trend analysis revealed that CCLM shows the most distinct and significant trends for 2 m temperature, 10 m wind speed and 10 m gust speed. These variables showed an increase in the last seven decades for several

metrics: For annual mean values as well as for extreme events like 99th percentiles, hot days or number of windy days. No clear and no statistically significant trend is discernible for the annual sum and extreme precipitation, but there tends to be less precipitation over Northern Germany, albeit no change in the intensity. The cloud cover seems to be slightly reduced in the past seven decades, but not statistically significantly. The trend of CAPE for the most unstable parcel and the number of days with potential thunderstorms slightly increased. The number of frost days became less and the coldest nights became warmer. The daily temperature range, which is an important index of climate change, increased mainly over land areas and mainly in the summer time.

Near-surface air temperatures, usually reflecting large-scale characteristics did not show any spatial structures. In addition, the trends in cloud cover, sea level pressure and CAPE for most unstable parcels did not show regional effects. In the wind speed, some local effects like lower trends in the cities (urban areas) are visible, because the absolute wind speed is lower there. In addition, many regional small-scale details in the precipitation trends are present. However, they are not statistically significant at all, which indicates a random distribution of these details. In contrast, the wind speed shows significant and reliable regional details like the city effects with lower trends in the mean wind speed but not in the gust speed: Generally, cities increase the wind gusts and do not lead to a decrease, as it is the case for the mean wind speed.

Bibliography

- Alexandersson, H., H. Tuomenvirta, T. Schmith, and K. Iden, 2000: Trends of storms in NW Europe derived from an updated pressure data set. *Clim Res*, **14**, 71–73.
- Alexandru, A., R. de Elia, R. Laprise, L. Separovic, and S. Biner, 2009: Sensitivity Study of Regional Climate Model Simulations to Large-Scale Nudging Parameters. *Mon. Weather Rev.*, doi:10.1175/2008MWR2620.1.
- Anders, I., and B. Rockel, 2009: The influence of prescribed soil type distribution on the representation of present climate in a regional climate model. *Clim. Dyn.*, **33**, 177–186.
- Baldauf, M., A. Seifert, J. Förstner, D. Majewski, M. Raschendorfer, and T. Reinhardt, 2011: Operational Convective-Scale Numerical Weather Prediction with the COSMO Model: Description and Sensitivities. *Mon. Weather Rev.*, **139**, 3887–3905, doi:10.1175/MWR-D-10-05013.1.
- Barcikowska, M., F. Feser, W. Zhang, and W. Mei, 2017: Changes in intense tropical cyclone activity for the western North Pacific during the last decades derived from a regional climate model simulation. *Clim. Dyn.*, **49**, 2931–2949, doi:10.1007/s00382-016-3420-0.
- Barcikowska, M. J., S. J. Weaver, F. Feser, S. Russo, F. Schenk, D. A. Stone, and M. Zahn, 2018: Euro-Atlantic winter storminess and precipitation extremes under 1.5 °C versus 2 °C warming scenarios. *Earth Syst Dynam Discuss*, doi:10.5194/esd-2017-106. <https://www.earth-syst-dynam-discuss.net/esd-2017-106/>.
- Barkhordarian, A., H. von Storch, E. Zorita, P. C. Loikith, and C. R. Mechoso, 2017: Observed warming over northern South America has an

- anthropogenic origin. *Clim. Dyn.*, doi:10.1007/s00382-017-3988-z.
<https://doi.org/10.1007/s00382-017-3988-z>.
- Caloiero, T., R. Coscarelli, E. Ferrari, and B. Sirangelo, 2017: Trend analysis of monthly mean values and extreme indices of daily temperature in a region of southern Italy. *Int. J. Climatol.*, **37**, 284–297, doi:10.1002/joc.5003.
- Castro, C. L., R. A. Pielke, and G. Leoncini, 2005: Dynamical downscaling: Assessment of value retained and added using the Regional Atmospheric Modeling System (RAMS). *J. Geophys Res*, **110**, D05108, doi:10.1029/2004JD004721.
- Casty, C., C. C. Raible, T. F. Stocker, H. Wanner, and J. Luterbacher, 2007: A European pattern climatology 1766–2000. *Clim. Dyn.*, **29**, 791–805, doi:10.1007/s00382-007-0257-6.
- Chan, S. C., E. J. Kendon, H. J. Fowler, S. Blenkinsop, N. M. Roberts, and C. A. Ferro, 2014: The Value of High-Resolution Met Office Regional Climate Models in the Simulation of Multihourly Precipitation Extremes. *J. Clim.*, **27**, 6155–6174, doi:10.1175/JCLI-D-13-00723.1.
- Changnon, S. A., and J. M. Changnon, 1990: Use of Climatological Data in Weather Insurance. *J. Clim.*, **3**, 568–576, doi:10.1175/1520-0442(1990)003<0568:UOCDIW>2.0.CO;2.
- Cholette, M., R. Laprise, and J. M. Thériault, 2015: Perspectives for Very High-Resolution Climate Simulations with Nested Models: Illustration of Potential in Simulating St. Lawrence River Valley Channelling Winds with the Fifth-Generation Canadian Regional Climate Model. *Climate*, **3**, 283–307, doi:10.3390/cli3020283.
- Christensen, O. B., M. A. Gaertner, J. A. Prego, and J. Polcher, 2001: Internal variability of regional climate models. *Clim Dyn*, **17**, 875–887.

-
- Davies, H. C., 1976: A lateral boundary formulation for multi-level prediction models. *Q. J. R. Meteorol. Soc.*, **102**, 405–418, doi:10.1002/qj.49710243210.
- Dawson, A. G., and Coauthors, 2002: Complex North Atlantic Oscillation (NAO) Index signal of historic North Atlantic storm-track changes. *The Holocene*, **12**, 363–369, doi:10.1191/0959683602hl552rr.
- Dee, D. P., and Coauthors, 2011: The ERA-Interim reanalysis: configuration and performance of the data assimilation system. *Q. J. R. Meteorol. Soc.*, **137**, 553–597, doi:10.1002/qj.828.
- Deque, M., S. Somot, E. Sanchez-Gomez, C. M. Goodess, D. Jacob, G. Lenderink, and O. B. Christensen, 2012: The spread amongst ENSEMBLES regional scenarios: regional climate models, driving general circulation models and interannual variability. *Clim. Dyn.*, **38**, 951–964, doi:10.1007/s00382-011-1053-x.
- Di Luca, A., R. de Elía, and R. Laprise, 2012: Potential for added value in precipitation simulated by high-resolution nested Regional Climate Models and observations. *Clim. Dyn.*, **38**, 1229–1247, doi:10.1007/s00382-011-1068-3.
- , R. de Elía, and R. Laprise, 2015: Challenges in the Quest for Added Value of Regional Climate Dynamical Downscaling. *Curr. Clim. Change Rep.*, **1**, 10–21.
- , D. Argüeso, J. P. Evans, R. de Elía, and R. Laprise, 2016: Quantifying the overall added value of dynamical downscaling and the contribution from different spatial scales. *J. Geophysical Res.*, **121**, doi:10.1002/2015JD024009.
- Dieng, D., G. Smiatek, J. Bliefernicht, D. Heinzeller, A. Sarr, A. T. Gaye, and H. Kunstmann, 2017: Evaluation of the COSMO-CLM high-resolution climate simulations over West Africa. *J. Geophys. Res. Atmospheres*, **122**, 1437–1455, doi:10.1002/2016JD025457.

- Doms, G., and Coauthors, 2011: *A Description of the Nonhydrostatic Regional COSMO Model. Part II: Physical Parameterization*. Deutscher Wetterdienst, <http://www.cosmo-model.org/content/model/documentation/core/cosmoPhysParamtr.pdf>.
- DWD Climate Data Center (CDC), Raster der Monatsmittel der Lufttemperatur (2m) für Deutschland, Version v1.0. ftp://ftp-cdc.dwd.de/pub/CDC/grids_germany/monthly/air_temperature_mean/ (Accessed June 27, 2018).
- Feser, F., and H. von Storch, 2005: A spatial two-dimensional discrete filter for limited-area-model evaluation purposes. *Mon. Weather Rev.*, **133**, 1774–1786.
- Feser, F., and H. von Storch, 2008a: A dynamical downscaling case study for typhoons in SE Asia using a regional climate model. *Mon. Weather Rev.*, **136**, 1806–1815.
- , and —, 2008b: A dynamical downscaling case study for typhoons in SE Asia using a regional climate model. *Mon. Weather Rev.*, **136**, 1806–1815.
- Feser, F., and M. Barcikowska, 2012: The Influence of Spectral Nudging on Typhoon Formation in Regional Climate Models. *Env. Res Lett*, **7**, doi:10.1088/1748-9326/7/1/014024.
- , B. Rockel, H. von Storch, J. Winterfeldt, and M. Zahn, 2011: Regional Climate Models add Value to Global Model Data: A Review and selected Examples. *Bull Amer Meteor Soc*, **92**, 1181–1192, doi:10.1175/2011BAMS3061.1.
- , M. Barcikowska, O. Krueger, F. Schenk, R. Weisse, and L. Xia, 2015: Storminess over the North Atlantic and Northwestern Europe - A Review. *Q J R Meteorol Soc*, **141**, 350–382, doi:10.1002/qj.2364.

-
- Fischer-Bruns, I., H. von Storch, J. F. González-Rouco, and E. Zorita, 2005: Modelling the variability of midlatitude storm activity on decadal to century time scales. *Clim Dynam*, doi:10.1007/s00382-005-0036-1.
- Franzaring, J., I. Henning-Müller, R. Funk, W. Hermann, V. Wulfmeyer, W. Claupein, and A. Fangmeier, 2007: Effects of solar, climatic and atmospheric components on historical crop yields. *Gefahrstoffe-Reinhalt. Luft*, **67**, 251–258.
- Gallagher, S., R. Tiron, E. Whelan, E. Gleeson, F. Dias, and R. McGrath, 2016: The nearshore wind and wave energy potential of Ireland: A high resolution assessment of availability and accessibility. *Renew. Energy*, **88**, 494–516, doi:10.1016/j.renene.2015.11.010.
- Gentry, M. S., and G. S. Lackmann, 2010: Sensitivity of Simulated Tropical Cyclone Structure and Intensity to Horizontal Resolution. *Mon. Weather Rev.*, **138**, 688–704, doi:10.1175/2009MWR2976.1.
- Geyer, B., 2014: High-resolution atmospheric reconstruction for Europe 1948–2012: coastDat2. *Earth Syst Sci Data*, **6**, 147–164, doi:10.5194/essd-6-147-2014.
- , and B. Rockel, 2013: *coastDat-2 COSMO-CLM*. http://cera-www.dkrz.de/WDCC/ui/Compact.jsp?acronym=coastDat-2_COSMO-CLM.
- , R. Weisse, P. Bisling, and J. Winterfeldt, 2015: Climatology of North Sea wind energy derived from a model hindcast for 1958–2012. *J. Wind Eng. Ind. Aerodyn.*, **147**, 18–29, doi:10.1016/j.jweia.2015.09.005.
- Giorgi, F., and B. Xunqiang, 2000: A study of internal variability of a regional climate model. *J. Geophys Res*, **105**, 29,503–29,521.
- Groll, N., and R. Weisse, 2017: A multi-decadal wind-wave hindcast for the North Sea 1949–2014: coastDat2. *Earth Syst Sci Data*, **9**, 955–968, doi:10.5194/essd-9-955-2017.

- Guo, D., and H. Wang, 2016: Comparison of a very-fine-resolution GCM with RCM dynamical downscaling in simulating climate in China. *Adv. Atmospheric Sci.*, **33**, 559–570, doi:10.1007/s00376-015-5147-y.
- Haeseler, B., and C. Lefebvre, 2013: *Heavy storm CHRISTIAN on 28 October 2013*. http://www.dwd.de/bvbw/generator/DWDWWW/Content/Oeffentlichkeit/KU/KU2/KU24/besondere__ereignisse__global/stuerme/englischeberichte/20131028__CHRISTIAN__europe,templateId=raw,property=publicationFile.pdf/20131028__CHRISTIAN__europe.pdf.
- Hurrell, J. W., and C. Deser, 2010: North Atlantic climate variability: The role of the North Atlantic Oscillation. *Impact Clim. Var. Mar. Ecosyst. Comp. Approach*, **79**, 231–244, doi:10.1016/j.jmarsys.2009.11.002.
- Iles, C., and G. Hegerl, 2017: Role of the North Atlantic Oscillation in decadal temperature trends. *Environ. Res. Lett.*, **12**, 114010.
- IPCC, 2013: *Climate Change 2013: The Physical Science Basis. Contribution of Working Group I to the Fifth Assessment Report of the Intergovernmental Panel on Climate Change*. Cambridge University Press, Cambridge, United Kingdom and New York, NY, USA, 1535 pp. www.climatechange2013.org.
- , 2014: *Climate Change 2014: Mitigation of Climate Change: Working Group III Contribution to the IPCC Fifth Assessment Report*.
- Jhajharia, D., and V. P. Singh, 2011: Trends in temperature, diurnal temperature range and sunshine duration in Northeast India. *Int. J. Climatol.*, **31**, 1353–1367, doi:10.1002/joc.2164.
- Jones, P. D., and Coauthors, 2016: Long-term trends in precipitation and temperature across the Caribbean. *Int. J. Climatol.*, **36**, 3314–3333, doi:10.1002/joc.4557.

-
- Kain, J. S., S. J. Weiss, J. J. Levit, M. E. Baldwin, and D. R. Bright, 2006: Examination of Convection-Allowing Configurations of the WRF Model for the Prediction of Severe Convective Weather: The SPC/NSSL Spring Program 2004. *Weather Forecast.*, **21**, 167–181, doi:10.1175/WAF906.1.
- Kalnay, E., and Coauthors, 1996: The NCEP/NCAR 40-year reanalysis project. *Bull. Am. Meteorol. Soc.*, **77**, 437–471.
- Kendall, M. G., 1975: Rank Correlation Methods. *Charles Griffin*,.
- Kitoh, A., T. Ose, and I. Takayabu, 2016: Dynamical Downscaling for Climate Projection with High-Resolution MRI AGCM-RCM. *J. Meteorol. Soc. Jpn.*, **94A**, 1–16, doi:10.2151/jmsj.2015-022.
- Klawa, M., and U. Ulbrich, 2003: A model for the estimation of storm losses and the identification of severe winter storms in Germany. *Nat. Hazards Earth Syst. Sci.*, 725–732.
- Klimamonitor, Norddeutscher Klimamonitor. <http://www.norddeutscher-klimamonitor.de/> (Accessed January 21, 2018).
- Krueger, O., and H. von Storch, 2011: Evaluation of an Air Pressure–Based Proxy for Storm Activity. *J. Clim.*, **24**, 2612–2619.
- Lange, I., 2014: Wind- und Temperaturdaten vom Wettermast Hamburg des Meteorologischen Instituts der Universität Hamburg. *Com.*,
- Laprise, R., and Coauthors, 2012: Considerations of Domain Size and Large-Scale Driving for Nested Regional Climate Models: Impact on Internal Variability and Ability at Developing Small-Scale Details. *Clim. Change*, 181–199, doi:10.1007/978-3-7091-0973-1_14.
- Leutwyler, D., D. Lüthi, N. Ban, O. Fuhrer, and C. Schär, 2017: Evaluation of the convection-resolving climate modeling approach on continental scales. *J. Geophys. Res. Atmospheres*, **122**, 5237–5258, doi:10.1002/2016JD026013.

- Li, D., H. Von Storch, and B. Geyer, 2016: High-resolution wind hindcast over the Bohai Sea and the Yellow Sea in East Asia: Evaluation and wind climatology analysis. *J. Geophys Res*, **92**, 121, doi:10.1002/2015JDO24177.
- Li Delei, 2016: Added value of high-resolution regional climate model: selected cases over the Bohai Sea and the Yellow Sea areas. *Int. J. Climatol.*, **37**, 169–179, doi:10.1002/joc.4695.
- Liberato, M. L. R., J. G. Pinto, R. M. Trigo, P. Ludwig, P. Ordóñez, D. Yuen, and I. F. Trigo, 2013: Explosive development of winter storm Xynthia over the Southeastern North Atlantic Ocean. *Hazards Earth Syst Sci*, **13**, 2239–2251, doi:10.5194/nhess-13-2239-2013.
- Lucas-Picher, P., D. Caya, R. de Elia, and R. Laprise, 2008: Investigation of regional climate models' internal variability with a ten-member ensemble of 10-year simulations over a large domain. *Clim Dyn*, **21**, 927–940, doi:10.1007/s00382-008-0384-8.
- Ludwig, P., J. G. Pinto, S. A. Hoeppe, A. H. Fink, and S. L. Gray, 2015: Secondary Cyclogenesis along an Occluded Front Leading to Damaging Wind Gusts: Windstorm Kyrill, January 2007. *Mon. Weather Rev.*, **143**, 1417–1437, doi:dx.doi.org/10.1175/MWR-D-14-00304.1.
- Ma, Y., Y. Yang, X. Mai, C. Qiu, X. Long, and C. Wang, 2016: Comparison of Analysis and Spectral Nudging Techniques for Dynamical Downscaling with the WRF Model over China. *Adv. Meteorol.*, **2016**, 16.
- Mann, H. B., 1945: Nonparametric Tests Against Trend. *Econometrica*, **13**, 245–259, doi:10.2307/1907187.
- Matulla, C., W. Schöner, H. Alexandersson, H. von Storch, and X. L. Wang, 2008: European storminess: late nineteenth century to present. *Clim. Dyn.*, **31**, 125–130, doi:10.1007/s00382-007-0333-y.

-
- Meinke, I., M. Maneke, W. Riecke, and B. Tinz, 2014: Norddeutscher Klimamonitor – Klimazustand und Klimaentwicklung in Norddeutschland innerhalb der letzten 60 Jahre (1951-2010). *Mitteilungen DMG* 012014, https://www.hzg.de/imperia/md/content/klimabuero/norddeutscher_klimamonitor.pdf (Accessed January 8, 2018).
- Neumayer, E., and F. Barthel, 2011: Normalizing economic loss from natural disasters: A global analysis. *Glob. Environ. Change*, **21**, 13–24.
- Nilsson, C., S. Goyette, and L. Barring, 2007: Relating forest damage data to the wind field from high-resolution RCM simulations: Case study of Anatol striking Sweden in December 1999. *Glob. Planet. Change*, **57**, 161–176, doi:10.1016/j.gloplacha.2006.11.011.
- Oouchi, K., J. Yoshimura, H. Yoshimura, R. Mizuta, S. Kusunoki, and A. Noda, 2006: Tropical cyclone climatology in a global warming climate as simulated in a 20 km-mesh global atmospheric model: frequency and wind intensity analyses. *J. Meteorol. Soc. Jpn.*, **84**, 259–276, doi:doi.org/10.2151/jmsj.84.259.
- Park, J., and S.-O. Hwang, 2017: Impacts of spectral nudging on the simulated surface air temperature in summer compared with the selection of shortwave radiation and land surface model physics parameterization in a high-resolution regional atmospheric model. *J. Atmospheric Sol.-Terr. Phys.*, **164**, 259–267, doi:10.1016/j.jastp.2017.09.001.
- Parker, R. J., B. J. Reich, and S. R. Sain, 2015: A Multiresolution Approach to Estimating the Value Added by Regional Climate Models. *J. Clim.*, doi:10.1175/JCLI-D-14-00557.1.
- Perch-Nielsen, S. L., B. Amelung, and R. Knutti, 2010: Future climate resources for tourism in Europe based on the daily Tourism Climatic Index. *Clim. Change*, **103**, 363–381, doi:10.1007/s10584-009-9772-2.

- Pinto, J. G., E. L. Fröhlich, G. C. Leckebusch, and U. Ulbrich, 2007: Changing European storm loss potentials under modified climate conditions according to ensemble simulations of the ECHAM5/MPI-OM1 GCM. *Nat. Hazards Earth Syst. Sci.*, 165–175.
- Prein, A. F., A. Gobiet, M. Suklitsch, H. Truhetz, N. K. Awan, K. Keuler, and G. Georgievski, 2013: Added value of convection permitting seasonal simulations. *Clim. Dyn.*, **41**, 26555–2677, doi:10.1007/s00382-013-1744-6.
- , and Coauthors, 2015: A review on regional convection-permitting climate modeling: demonstrations, prospects, and challenges. *Rev. Geophys.*, **52**, 323–361, doi:10.1002/2014RG000475.
- Rockel, B., C. L. Castro, R. A. Pielke, H. von Storch, and G. Leoncini, 2008: Dynamical downscaling: Assessment of model system dependent retained and added variability for two different regional climate models. *J. Geophys Res*, **113**, D21103.
- Roeckner, E., 2003: Allgemeine Zirkulationsmodelle, Atmosphäre, Numerische Klimamodelle, Teil II: Modellierung natürlicher Klimaschwankungen. **29**, 6–14.
- Roshan, G., R. Yousefi, and J. M. Fitchett, 2016: Long-term trends in tourism climate index scores for 40 stations across Iran: the role of climate change and influence on tourism sustainability. *Int. J. Biometeorol.*, **60**, 33–52, doi:10.1007/s00484-015-1003-0.
- Rummukainen, M., 2010: State-of-the-art with regional climate models. *Wiley Interdiscip. Rev. Clim. Change*, **1**, 82–96, doi:10.1002/wcc.8.
- Schaaf, B., 2017: coastDat_COSMO-CLM_GBoo28. http://cera-www.dkrz.de/WDCC/ui/Compact.jsp?acronym=coastDat_COSMO-CLM_GBoo28.

-
- , and F. Feser, 2018: Is there added value of convection-permitting regional climate model simulations for storms over the German Bight and Northern Germany? *Meteorol. Hydrol. Water Manag.*, doi:10.26491/mhwm/85507.
<http://dx.doi.org/10.26491/mhwm/85507>.
- , H. von Storch, and F. Feser, 2017: Does Spectral Nudging Have an Effect on Dynamical Downscaling Applied in Small Regional Model Domains? *Mon. Weather Rev.*, **145**, 4303–4311, doi:10.1175/MWR-D-17-0087.1.
- Schaettler, U., G. Doms, and C. Schraff, 2008: *A Description of the Nonhydrostatic Regional COSMO-Model Part VII: User's Guide*. Deutscher Wetterdienst,.
- Schefczyk, L., and G. Heinemann, 2017: Climate change impact on thunderstorms: Analysis of thunderstorm indices using high-resolution regional climate simulations. *Meteorol. Z.*, **26**, 409–419, doi:10.1127/metz/2017/0749.
- Schmidt, H., and H. von Storch, 1993: German Bight storms analysed. *Nature*, **365**, 791.
- Schoetter, R., D. Grawe, P. Hoffmann, P. Kirschner, A. Grätz, and K. H. Schlünzen, 2013: Impact of local adaptation measures and regional climate change on perceived temperature. *Meteorol. Z.*, **22**, 117–130, doi:10.1127/0941-2948/2013/0381.
- Schultze, M., and B. Rockel, 2017: Direct and semi-direct effects of aerosol climatologies on long-term climate simulations over Europe. *Clim. Dyn.*, doi:10.1007/s00382-017-3808-5.
<https://doi.org/10.1007/s00382-017-3808-5>.
- Schulz, J.-P., 2008: Revision of the turbulent gust diagnostic in the COSMO model. *COSMO Newsl.*, **8**, 17–22.

- , and E. Heise, 2003: A new scheme for diagnosing near-surface convective gusts. *COSMO Newsl.*, **3**, 221–225.
- , and U. Schaettler, 2009: *Kurze Beschreibung des Lokal-Modells Europa COSMO-EU (LME) und seiner Datenbanken auf dem Datenserver des DWD.* Deutscher Wetterdienst, http://www.dwd.de/bvbw/generator/Sites/DWDWWW/Content/Forschung/FE1/Veroeffentlichungen/Download/LME__DBbeschr__0901,templateId=raw,property=publicationFile.pdf/LME_DBbeschr_0901.pdf.
- Separovic, L., S. Z. Husain, and W. Yu, 2015: Internal variability of fine-scale components of meteorological fields in extended-range limited-area model simulations with atmospheric and surface nudging. *J. Geophys Res.*, **120**, 8621–8641, doi:10.1002/2015JD023350.
- Shapiro, M. A., and D. Keyser, 1990: Fronts, jet streams and the tropopause. *Amer Meteor Soc*, 167–191.
- Steppeler, J., G. Doms, U. Schättler, H. W. Bitzer, A. Gassmann, U. Damrath, and G. Gregoric, 2003: Meso-gamma scale forecasts using the nonhydrostatic model LM. *Meteorol. Atmospheric Phys.*, **82**, 75–96, doi:10.1007/s00703-001-0592-9.
- von Storch, H., and F. W. Zwiers, 1999: *Statistical Analysis in Climate Research.* Cambridge University Press, Cambridge,.
- , H. Langenberg, and F. Feser, 2000: A Spectral Nudging Technique for Dynamical Downscaling Purposes. *Mon. Weather Rev.*, **128**, 3664–3673, doi:10.1175/1520-0493(2000)128<3664:ASNTFD>2.0.CO;2.
- , F. Feser, S. Haeseler, C. Lefebvre, and M. Stendel, 2014: A violent midlatitude storm in Northern Germany and Denmark, 28 October 2013. *Bull Amer Meteor Soc*, **95**, 76–78.

-
- , and Coauthors, 2017a: Regional reanalysis without local data: Exploiting the downscaling paradigm. *J. Geophys. Res. Atmospheres*, **122**, 8631–8649, doi:10.1002/2016JD026332.
- , I. Meinke, and M. Claussen, 2017b: *Hamburger Klimabericht – Wissen über Klima, Klimawandel und Auswirkungen in Hamburg und Norddeutschland*. <https://doi.org/10.1007/978-3-662-55379-4>.
- Suursaar, Ü., J. Jaagus, and H. Tõnisson, 2015: How to quantify long-term changes in coastal sea storminess? *Chang. Process. Estuaries Coast. Waters Due Intense Mult. Press.*, **156**, 31–41, doi:10.1016/j.ecss.2014.08.001.
- Taraphdar, S., P. Mukhopadhyay, L. R. Leung, F. Zhang, S. Abhilash, and B. N. Goswami, 2014: The role of moist processes in the intrinsic predictability of Indian Ocean cyclones. *J. Geophys. Res.-Atmospheres*, **119**, 8032–8048, doi:10.1002/2013JD021265.
- Tiedtke, M., 1989: A Comprehensive Mass Flux Scheme For Cumulus Parameterization In Large-scale Models. *Mon. Weather Rev.*, **117**, 1779–1800.
- Usbeck, W., and Coauthors, 2012: Relating remotely sensed forest damage data to wind data: storms Lothar (1999) and Vivian (1990) in Switzerland. *Theor. Appl. Climatol.*, **108**, 451–462, doi:10.1007/s00704-011-0526-5.
- Venables, W. N., and B. D. Ripley, 2002: *Modern Applied Statistics with S*. *Modern Applied Statistics with S*, Springer-Verlag, New York.
- Waldron, K. M., J. Peagle, and J. D. Horel, 1996: Sensitivity of a spectrally filtered and nudged limited area model to outer model options. *Mon Wea Rev*, **124**, 529–547.

- Weisse, R., and F. Feser, 2003: Evaluation of a method to reduce uncertainty in wind hindcasts performed with regional atmosphere models. *Coast Eng*, **48**, 211–225.
- , H. Heyen, and H. von Storch, 2000: Sensitivity of a regional atmospheric model to a sea state-dependent roughness and the need for ensemble calculations. *Mon. Weather Rev.*, **128**, 3631–3642.
- , H. von Storch, and F. Feser, 2005: Northeast Atlantic and North Sea Storminess as Simulated by a Regional Climate Model during 1958–2001 and Comparison with Observations. *J Clim.*, **18**, 465–479.
- , and Coauthors, 2009: Regional Meteorological-Marine Reanalyses and Climate Change Projections. *Bull. Am. Meteorol. Soc.*, **90**, 849–860, doi:10.1175/2008BAMS2713.1.
- , L. Gaslikova, B. Geyer, N. Groll, and E. Meyer, 2014: coastDat - Model Data for Science and Industry. *Küste*, **81**, 5–18.
- Winterfeldt, J., and R. Weisse, 2009: Assessment of value added for surface marine wind speed obtained from two regional climate models. *Mon Wea Rev*, **137**, 2955–2965, doi:10.1175/2009MWR2704.1.
- , B. Geyer, and R. Weisse, 2010: Using QuikSCAT in the added value assessment of dynamically downscaled wind speed. *Int J Clim.*, **3**, 1028–1039, doi:10.1002/joc.2105.
- Xia, L., H. von Storch, F. Feser, and J. Wu, 2016: A study of quasi-millennial extratropical winter cyclone activity over the Southern Hemisphere. *Clim. Dyn.*, **47**, 2121–2138, doi:10.1007/s00382-015-2954-x.
- Xue, M., J. Schreif, F. Kong, K. W. Thomas, Y. Wang, and F. Zhu, 2013: Track and Intensity Forecasting of Hurricanes: Impact of Convection-Permitting Resolution and Global Ensemble Kalman Filter Analysis on 2010 Atlantic Season Forecasts. *Weather Forecast.*, **28**, 1366–1384, doi:http://dx.doi.org/10.1175/WAF-D-12-00063.1.

Zhao, Y., D. Wang, Z. Liang, and J. Xu, 2016: Improving numerical experiments on persistent severe rainfall events in southern China using spectral nudging and filtering schemes. *Q J R Meteorol Soc*, doi:10.1002/qj.2892.

—, —, and X. Jianjun, 2017: Improving the regional model forecasting of persistent severe rainfall over the Yangtze River Valley using the spectral nudging and update cycle methods: a case study. *Atmos Sci Let*, doi:10.1002/asl.731.

Zwiers, F., and H. von Storch, 1995: Taking Serial Correlation into Account in Tests of the Mean. *J. Clim.*, **8**, 336–351, doi:10.1175/1520-0442(1995)008<0336:TSCIAI>2.0.CO;2.

List of Figures

Figure 3.1: Model domain of the simulations and according topography of the a) “high tide” state and b) “low tide” state.....	14
Figure 3.2: Difference of the seasonal mean 2 m temperature between low and high tide state for a) winter, b) spring, c) summer, and d) autumn.....	15
Figure 3.3: Difference of the seasonal mean 10 m wind speed between low and high tide state for a) winter, b) spring, c) summer, and d) autumn.....	16
Figure 3.4: Model domain of the simulations and according topography of the a) CCLMo28large and b) CCLMo28small domain.	17
Figure 3.5: Difference of the a) maximum 10 m gust speed b) maximum 10 m wind speed c) lowest mean sea level pressure d) precipitation sum during storm Christian (28 th – 29 th of October 2013) between large and small domain (CCLMo28large – CCLMo28small) for the common domain area.	18
Figure 3.6: 10 m wind speed (shaded areas) in combination with isobars (black lines) for storm Christian on October 28, 2013, 11 UTC. a) large domain, b) small domain.....	19
Figure 3.7: Model domain for the high-resolution simulations	20
Figure 4.1: Model domain of the high-resolution simulation with tracks of storm Verena of January 1993 for SN (red) and NN (blue) simulations.	23
Figure 4.2: Distribution function of the RMSE between SN ₁ and SN ₂ (light color) and between NN ₁ and NN ₂ (dark color) for 10 m wind speed (red, WSS_10M), sea level pressure (black, PMSL), and wind speed in 500 hPa (blue, WSS_500hPa).	26

Figure 4.3: Time series of the hourly pattern correlation between SN ₁ and NN ₁ (except for “TOT_PREC day sum” daily values are shown) of sea level pressure (PMSL), 2 m temperature (T_2M), 10 m wind speed (WSS_10M), 500 hPa wind speed (WSS_500hPa), and the daily sum of precipitation (TOT_PREC day sum).	28
Figure 4.4: Pressure isobars (NN ₁ (top left), NN ₂ (bottom left), SN ₁ (top right), SN ₂ (bottom right)) for the (a) 11 th of July 1993, 17UTC, (b) 11 th of March 1993, 00UTC, with shaded wind speed fields; (c) 23 rd of May 1993, 04UTC, with shaded precipitation fields.	29
Figure 4.5: Distribution function of the RMSE between SN and observations (light colors) and between NN and observations (dark colors) for 10 m wind speed (WSS_10M), total precipitation (TOT_PREC), 2 m temperature (T_2M), and sea level pressure (PMSL).	31
Figure 5.1: Model domain of a) the high-resolution simulation CCLMo28 and b) CCLM240 and related topographies. The locations of the weather stations used for most comparisons in the study are shown as red dots. Storm tracks of storm Christian of CCLMo28 (blue), CCLM240 (green) and the German Weather Service (DWD) analysis (red) are shown as well.	38
Figure 5.2: Precipitation rate (shaded areas) in combination with wind vectors and isobars (black lines) for storm Christian on October 28, 2013, 12 UTC. a) CCLMo28, b) CCLM240.....	44
Figure 5.3: Ceilometer backscatter intensity at Hamburg weather mast (see Figure 5.1) for storm Christian on October 28, 2013, 00 UTC – October 29, 2013 00 UTC in 1/10000 sr rad km. The lines represent the time series of total cloud cover at weather mast Hamburg (see Figure 5.1) for CCLM240 (red) and CCLMo28 (blue).	45

Figure 5.4: Total cloud cover for storm Christian on October 28, 2013, 13 and 14 UTC for CCLMo28 (a, c) and CCLM240 (b, d) at 13 UTC (a, b), 14 UTC (c, d). Grey shows a high backscatter signal and consequently clouds or precipitation. White areas represent cloud-free skies. Satellite image of October 28, 2013, 13 UTC © DLR (e) White represents clouds, green represents visible land areas and blue represents visible sea areas. This means that areas with blue and green have cloud-free skies.....46

Figure 5.5: Vertical wind profile at the Schleswig station in Northern Germany (see Figure 5.1a) for CCLM240 (red) and CCLMo28 (blue) compared with sounding measurements (green) on the 28th of October 2013 at 12 UTC (solid lines). Vertical wind profile at weather mast Hamburg in CCLM240 (red) and CCLMo28 (blue) in comparison with the weather mast Hamburg measurements (green, for its location see Figure 5.1a) for the maximum mean wind speed during storm Christian on the 28th of October, 2013 (dashed lines).47

Figure 5.6: Time series of storm Christian in CCLM240 (red), CCLMo28 (blue) and observations (green) for the Hamburg airport station (strong colors) in Northern Germany (see Figure 5.1a) and for a buoy in the North Sea (light colors). Shown is 10 m wind speed (solid lines) and sea level pressure (dotted lines).....48

Figure 5.7: Brier Skill Score between CCLMo28 and CCLM240 in comparison to DWD station data for storm Christian at all available DWD stations for the variables: a) wind speed (WSS), b) wind direction (WD), c) total cloud cover (CLCT), d) mean sea level pressure (PMSL), and e) total precipitation (TOT_PREC). BSS values larger than 0 (green) indicate an added value for CCLMo28 compared with CCLM240. Negative BSS values (added value for CCLM240) are plotted in orange to red. White dots show BSS values around 0

(CCLM028 and CCLM240 have similar quality) and black dots represent missing values..... 49

Figure 5.8: Sign test for BSS between CCLM028 and CCLM240 in comparison to DWD station data for all 10 storms at all available DWD stations for the variables: a) wind speed (WSS), b) wind direction (WD), c) total cloud cover (CLCT), d) mean sea level pressure (PMSL), and e) total precipitation (TOT_PREC). Shown is the percentage of storm cases with a BSS larger than 0, which indicates an added value of CCLM028 compared with CCLM240. Green dots show that more than 50% of all storm cases, which were measured at an individual station, have a positive BSS, white dots illustrate that 50% of the storm cases have a positive BSS, and red dots represent values of less than 50%. The numbers in the dots give the percentage of positive BSS values. Light colors indicate that the sign test at a station is not significant according to a significance test. Thereby very light colors represent stations where the sign test was not significant at the 10% significance level. Medium-light colors show stations where the sign test was significant at the 10% level, but not at the 5% significance level. 52

Figure 5.9: Ratio of stations with a Brier Skill Score larger than 0 (a) and smaller RMSE for CCLM028 than for CCLM240 (b) for all storm cases and variables: WSS: wind speed, WD: wind direction, PREC: precipitation, PMSL: mean sea level pressure, CLCT: total cloud cover. 55

Figure 5.10: Mean percentile-percentile distribution of 10 m wind speed averaged across all DWD stations and grid points of the DWD stations for all ten storm cases. The 99 dots per color represent the wind speed percentiles in steps of 1 percent from the first to the 99th percentile of all storm events. 56

Figure 5.11: Roughness length [m] in a) the CCLM028 and b) the CCLM240 model domain. The 12 largest cities in the model domain are marked in Figure 5.11b. 57

Figure 5.12: Difference of the 99th wind speed percentile between CCLM028 and CCLM240 for all ten storm events. Grey areas mark regions, which are land points in CCLM028, and sea points in CCLM240 or vice versa. 58

Figure 6.1: BSS between GBO028 and coastDat II in comparison to QuikSCAT satellite data for 10 m wind speeds between a) 3 and 25 m/s, b) 3 and 15 m/s and c) 15 and 25 m/s. 65

Figure 6.2: Decadal trend over 67 years of a) yearly mean 2 m temperature, b) yearly mean 10 m wind speed, c) yearly mean sea level pressure, d) yearly mean total cloud cover, e) yearly mean CAPE, f) yearly sum of precipitation. Shaded areas indicate a statistical significance at the nominal 5% level. 68

Figure 6.3: Time series over 67 years with 10 years running mean (bold line) of a) yearly mean 2 m temperature, b) yearly mean 10 m wind speed, c) yearly mean sea level pressure, d) yearly mean total cloud cover, e) yearly mean CAPE, f) yearly sum of precipitation. 69

Figure 6.4: 10 years running mean between 1948 and 2014 of a) NAO index and 99th percentile of 10 m wind and b) global 2 m temperature anomaly (base period: 1901-2000) and 2 m temperature of GBO028. 70

Figure 6.5: a) Trends of the domain mean and yearly mean (light colors) or yearly 99th percentile (strong colors) wind speed (green) and temperature (blue) for all 40 model levels. Every dot represents a model layer, a red dot shows that the trend is significant and a black dot indicates a non-significant trend. b) Percentage trends of wind speed of the domain mean and yearly mean (light colors) or yearly 99th percentile (strong

colors) for all 40 model levels (solid lines) and the domain mean and 67 years mean wind speed (light colors) or 67 years mean of yearly 99th percentile (strong colors) (dotted lines). 72

Figure 6.6: Time series of yearly 90th (green), 95th (red) and 99th (blue) percentile of 10 m wind speed of the domain mean. Solid lines represent the GBO028 simulation and dashed lines coastDat II. The 10 year running mean lines are added. 74

Figure 6.7: Decadal trends over 67 years of a) yearly 99.9th percentile of 2 m temperature, b) yearly 99.9th percentile of 10 m wind speed, c) yearly 99.9th percentile of precipitation, d) yearly 99th percentile of maximum 10 m gust speed, e) yearly 99th percentile maximum 2 m temperature, f) yearly 1st percentile of minimum 2 m temperature, g) maximum 2 m temperature range in winter, h) maximum 2 m temperature range in spring, i) maximum 2 m temperature range in summer, j) maximum 2 m temperature range in autumn. Shaded areas indicate a statistical significance at the nominal 5% level.75

Figure 6.8: Time series for 67 years with 10 years running mean (bold line) of a) yearly 99.9th percentile of 2 m temperature, b) yearly 99.9th percentile of 10 m wind speed, c) yearly 99.9th percentile of precipitation, d) yearly 99th percentile of maximum 10 m gust speed, e) yearly 99th percentile maximum 2 m temperature, f) yearly 1st percentile of minimum 2 m temperature, g) maximum 2 m temperature range in winter, h) maximum 2 m temperature range in spring, i) maximum 2 m temperature range in summer, j) maximum 2 m temperature range in autumn..... 76

Figure 6.9: Decadal trend of yearly number of days with a) CAPE higher 850 J/kg, b) 10 m gust speed higher than 10 m/s, c) maximum 2 m temperature higher than 30 °C (hot days), d) minimum 2 m temperature lower than 0 °C (frost days), e)

minimum 2 m temperature higher than 20 °C (tropical nights), f) 10 m wind speed higher than 10 m/s. Shaded areas indicate a statistical significance at the nominal 5% level. 79

Figure 6.10: Time series of yearly numbers of days over the North Sea (black), in the city Schwerin (red) and in the city of Hamburg (blue) with a) CAPE higher 850 J/kg, b) 10 m gust speed higher than 10 m/s, c) maximum 2 m temperature higher than 30 °C (hot days), d) minimum 2 m temperature lower than 0°C (frost days), e) minimum 2 m temperature higher than 20 °C (tropical nights), f) 10 m wind speed higher than 10 m/s..... 80

List of Tables

Table 4.1: Statistical values of hourly data differences SN_1 - NN_1 (upper value), NN_1 - NN_2 (middle value) and SN_1 - SN_2 (lower value) for 1993 for 10 m wind speed (WSS_10M), total precipitation (TOT_PREC), sea level pressure (PMSL), wind speed in 500 hPa (WSS_500hPa) and 2 m temperature (T_2M). For precipitation only hourly precipitation sums are considered, which are different from zero. Shown is the absolute maximum difference, the mean difference, the standard deviation and the 99 th percentile of the difference. In addition, the values and dates of the minimal pattern correlation between SN_1 and NN_1 (upper value), NN_1 and NN_2 (middle value) and SN_1 and SN_2 (lower value) are shown. Also the 10 th percentiles of the pattern correlation and the values of the minimum time correlations are listed.....	27
Table 5.1: Analysis period and number of hourly values used for the calculation of the BSS for each of the ten storm events investigated.....	36
Table 5.2: Number of stations, which show a positive or negative BSS, corresponding to Figure 5.7.....	50
Table 5.3: Number of stations which show a positive, neutral, or negative sign test (with 5%, 10%, or no significance), corresponding to Figure 5.8. The positive/negative sign test is defined as a positive BSS for more/less than 50% of all storm cases available at a station. Neutral sign test means that 50% of all storm cases show a negative BSS and 50% a positive BSS.	53
Table 5.4: 10 m wind speed bias [m/s] averaged over all stations and time correlation (T.C.) of CCLM028 and CCLM240 for the ten storm events.....	56

List of publications

Schaaf, B. and F. Feser, 2017: The effect of the Wadden Sea for very high resolution atmospheric regional climate models, *Research Activities in Atmospheric and Oceanic Modelling (WGNE Blue Book)*, 7.13.

Schaaf, B., H. von Storch, and F. Feser, 2017: Does Spectral Nudging Have an Effect on Dynamical Downscaling Applied in Small Regional Model Domains? *Mon. Weather Rev.*, **145**, 4303–4311, doi:10.1175/MWR-D-17-0087.1.

Schaaf, B. and F. Feser, 2018: Is there added value of convection-permitting regional climate model simulations for storms over the German Bight and Northern Germany? *Meteorology Hydrology and Water Management*, doi:10.26491/mhwm/85507.

Schaaf, B., F. Feser and I. Meinke, 2018: Long-term atmospheric changes in a convection-permitting regional climate model hindcast simulation over Northern Germany and the German Bight *Natural Hazards*, submitted.

Acknowledgements

First of all, I would like to thank Dr. Frauke Feser and Prof. Hans von Storch for giving me the possibility to work on this interesting topic.

Special thanks go to Prof. Hans von Storch, Dr. Frauke Feser and Prof. Felix Ament for their valuable comments and suggestions regarding this thesis.

In particular, I have to thank my supervisor Dr. Frauke Feser for a very good and productive collaboration. I have always been able to come to you for questions, and you have been very supportive in writing my first publications.

I would like to thank my office mate Markus Schultze for scientific discussions and having fun in everyday work.

The work was supported through the Cluster of Excellence 'CliSAP' (EXC177), Universität Hamburg, funded through the German Research Foundation (DFG). Furthermore, I am thankful for being a PhD student at the School of Integrated Climate System Sciences (SICSS) of CliSAP in Hamburg.

Many thanks go to Dr. Oliver Krüger, Dr. Daniel Neumann, Selina Titel and Dr. Sebastian Wagner for proofreading and improving this work.

I am grateful to Dr. Beate Geyer, Dr. Delei Li, Dr. Ronny Petrik, Dr. Burkhard Rockel, colleagues of the 'Coordination of Storm Themes' and 'KSR' group and all these many people I have not mentioned here for a nice working atmosphere and technical and scientific assistance.

Special thanks go to my parents, my family and friends for their belief in me and to Selina for every day support.

Eidesstattliche Versicherung

Hiermit versichere ich an Eides statt, die vorliegende Dissertation selbst verfasst und keine anderen als die angegebenen Hilfsmittel benutzt zu haben.

Die eingereichte schriftliche Fassung entspricht der auf dem elektronischen Speichermedium. Ich versichere, dass diese Dissertation nicht in einem früheren Promotionsverfahren eingereicht wurde.

Unterschrift: _____

Datum: _____